A Precise Underwater Acoustic Positioning Method Based on Phase Measurement

by

Li Zhou
B. Eng., Northwestern Polytechnical University, 1996
M. Eng., Northwestern Polytechnical University, 1999

A Thesis Submitted in Partial Fulfillment
of the Requirements for the Degree of

MASTER OF APPLIED SCIENCE

in the Department of Electrical and Computer Engineering

Supervisory Committee

A Precise Underwater Acoustic Positioning Method Based on Phase Measurement

by

Li Zhou
B. Eng., Northwestern Polytechnical University, 1996
M. Eng., Northwestern Polytechnical University, 1999

Supervisory Committee

Dr. Adam Zielinski, (Department of Electrical and Computer Engineering)
Co-Supervisor

Dr. Paul Kraeutner, (Department of Electrical and Computer Engineering)
Co-Supervisor

Dr. Aaron Gulliver, (Department of Electrical and Computer Engineering)
Departmental Member

Abstract

Supervisory Committee

Dr. Adam Zielinski, (Department of Electrical and Computer Engineering)
Co-Supervisor

Dr. Paul Kraeutner, (Department of Electrical and Computer Engineering)
Co-Supervisor

Dr. Aaron Gulliver, (Department of Electrical and Computer Engineering)
Departmental Member

Positioning an underwater object with respect to a reference point is required in diverse areas in ocean scientific and engineering undertakings, such as marine habitat monitoring, study of sedimentation processes, underwater searching and mapping, data collection, instrument placement and retrieval, and so on.

Underwater acoustic positioning systems, including long baseline (LBL) systems, short baseline (SBL) systems, and ultra-short baseline (USBL) systems, are designed to operate from a reference point and employ external transducers or transducer arrays as aids for positioning. Traditional positioning methods rely on measuring of time-of-flight of an acoustic signal travelling from the target to the reference platform by means of the cross-correlation method. The positioning accuracy of LBL systems varies from a few centimeters to a few meters, depending on the operating range and working frequency. LBL systems provide a uniform positioning accuracy for a given transponder array setup, but they suffer the time-consuming instrument deployment on the seafloor, as well as the complicated operating procedures. SBL and USBL systems have relatively simple configurations. But their positioning accuracy is a function of water depth and operating

range. To obtain absolute position accuracy, additional sensors such as the ship's gyro or a surface navigation system are needed.

In this thesis, a novel positioning method is proposed which takes advantages of a tether cable between the reference platform and the target. This method conducts positioning via continuous phase measurement between a reference signal and the acoustic signal transmitted by the target to the reference platform. It is named the **P**ositioning-based-on-**PH**ase-**M**easurement method or PPHM method in short. Every 2π change in the phase difference between these two signals corresponds to a one-wavelength range increment along the radial direction from the target's initial position to its new position. If a receiver array is used, with at least two hydrophones, the target's bearing information can be also calculated by measuring the phases of the output signals from each of the array hydrophones. Under ideal conditions, the positioning error of the PPHM method is proportional to the phase measurement error.

The PPHM method is very sensitive to changes in the underwater medium, such as sound speed variations, ocean currents and multipath interferences. Environmental fluctuations will degrade the positioning performance. These problems will be investigated and solutions will be proposed to minimize their effects.

The PPHM method can be used to position an underwater moving object such as a remotely operated vehicle (ROV) or a bottom crawler. Also, it can be used to monitor the ocean currents speed variations over a path, or to monitor the movements of tectonic plates. The last two applications will be addressed in detail in this thesis, whereas the first one is very challenging and needs more work.

Table of Contents

List of Tables

List of Figures

List of Acronyms

GPS	Global Positioning System
LBL	Long Baseline
SBL	Short Baseline
USBL	Ultra-short Baseline
ROV	Remotely Operated Vehicle
AUV	Autonomous Underwater Vehicle
GIB	GPS Intelligent Buoys
GAPS	Global Acoustic Positioning System
VRU	Vertical Reference Unit
TOA	Time-of-Arrival
DOA	Direction-of-Arrival
CW	Continuous Wave
SNR	Signal-to-Noise Ratio
MA	Moving Averaging
MORVEL	Mid-Ocean Ridge Velocities
VLBI	Very Long Baseline Interferometry
SLR	Satellite Laser Ranging
GPS/A	GPS/Acoustic
ADCP	Acoustic Doppler Current Profiler
NEPTUNE	North-East Pacific Time-Series Undersea Networked Experiments
ORION	Ocean Research Interactive Observatory Networks
UWSN	Underwater Acoustic Sensor Network
A/D	Analog/Digital
NEB	Noise Equivalent Bandwidth
PSD	Power Spectral Density
PDF	Probability Density Function
LTI	Linear Time Invariant

Acknowledgments

Many people contributed to the success of this effort and I would like to express my appreciation to them here.

First of all, I would like to thank my supervisor, Professor Adam Zielinski. His expertise, understanding, and patience, added considerably to my graduate experience. He has made available his support all the ways I can ask for. I would like to express my gratitude to my co-supervisor, Dr. Paul Kraeutner. His inspiration and ideas made the thesis work a more enjoyable journey. I would like to thank Marek Butowski for his generous help and inspiring discussions. I am indebted to Paul Fedrigo, Rob Fichtner and Lynn Palmer for their technical support. Financial assistance was provided by Natural Sciences and Engineering Research Council of Canada and the Department of Electrical and Computer Engineering, University of Victoria. This is gratefully acknowledged.

I owe my deepest gratitude to my family. My husband, Yan, has been very supportive throughout my lengthy graduate program, as he has always been for the past twelve years. This thesis would not have been possible without his love, care and patience. I wish to thank my parents, who have been a constant source of support throughout my life. Last, I would like to thank my son, Samuel, who brings endless joy to every single day.

Dedication

To my father.

To my mother, Yan, and Samuel.

Chapter 1 Introduction

In many terrestrial and submerged applications, the location of a mobile object must be tracked. The process of acquiring the location of an object of interest is called positioning. One of the best known positioning systems is the Global Positioning System, or GPS in short. GPS is operating on a set of 24 satellites that are continuously orbiting the earth. These satellites are equipped with atomic clocks and send out radio signals as to the exact time and their location. The radio signals from the satellites are picked up by the GPS receiver. Once the GPS receiver locks on to four or more of these satellites, it can triangulate its location from the known positions of the satellites [1].

The signal used in GPS is an electromagnetic signal, which propagates well in air but can only travel for a very short distance underwater because of its high absorption rate in water. Seventy percent of the Earth is covered under sea. In these areas where GPS cannot work, alternative underwater positioning systems play an important role. Positioning an underwater target with respect to a reference platform is required in diverse areas in ocean scientific research, industry engineering tasks and military activities. Examples include marine habitat monitoring, study of sedimentation processes, underwater searching and mapping, data collection, marine archaeology, instrument placement and retrieval for oil and gas exploration, mine hunting, and so on.

Underwater acoustic positioning systems, including long baseline (LBL) systems, short baseline (SBL) systems, and ultra-short baseline (USBL) systems, are designed to operate from a reference platform and employ external transducers or transducer arrays as aids for positioning [2, 3]. Traditional positioning methods have been employed in these systems, which rely on measuring of time-of-flight of an acoustic signal travelling from the observing target to the reference platform, by means of the cross-correlation method. Most LBL systems work at a frequency of approximately 10 kHz and the position accuracy is within a few meters for a maximum operation range on the order of a few kilometers [3]. When the operating range is short, the system works at a higher frequency and a positioning repeatability down to a few centimeters' accuracy is achievable [3]. For a given transponder array set up, LBL positioning accuracy will not be affected when

the range from the target to the transponder array is changing, which is called a uniform positioning accuracy. This is because the target's range to the transponders is very small as compared to the size of the LBL baseline. Although LBL systems provide a uniform positioning accuracy, they suffer time-consuming instrument deployment on the seafloor, as well as complicated operating procedures. For SBL and USBL systems, there is no need of transducer deployment and calibration on the seafloor. Their system configurations are simpler as compared to that of an LBL system. But their positioning accuracies depend on additional sensors such as the ship's gyro or a surface navigation system [4].

Measurement accuracy of conventional underwater acoustic positioning systems is limited by the difficult underwater acoustic environment in presence of varying sound speed in time and space, medium inhomogeneities, ocean current, multipath interferences, and so on. Another source of error comes from the uncertainties of the reference platform or the transducer array geometry [3, 4]. The major disadvantage of an LBL system is the complexity of system deployment and operation. For SBL and USBL systems, their performances undergo serious degradation in deep water or large area applications. For reasons of versatility, most of the commercially available underwater acoustic positioning systems are autonomous in the sense that there is no communication link over a tether cable connecting the target to the reference platform. However, in some cases, a tether cable is presented and connects a reference platform and a moving target such as an ROV or a crawler. This tether cable is the link for power and data transmission. It can be utilized as an aid for target positioning.

Motivated by these facts, a novel positioning method is proposed which takes advantages of a tethered cable linking the target and the reference platform [5, 6]. Unlike traditional positioning methods based on time-of-flight measurement, the proposed method conducts positioning via continuous phase measurement between a zero-phase reference signal and an acoustic signal transmitted by the target. This method is named the Positioning-based-on-Phase-Measurement method, or PPHM method in short. In the PPHM method, the initial position of the target with respect to the reference platform is assumed known. Then the target starts to moves away from this initial position for its mission. While moving, the target continuously transmits an acoustic signal back to the

reference platform. This signal arrives at the receiver in the reference platform with a phase shift, which is due to the range changes from the target to the reference platform. This phase shift is then measured by a phase detector. Every 2π change in the measured phase corresponds to a one-wavelength range increment along the radial direction from the target's initial position to its new position. The slant range from the target to the reference platform is thus obtained by counting how many 2π-flips in the measured phase have occurred, and then converting them into a range increment using the known sound velocity. If a receiver array is used, with at least two receivers (hydrophones), the target's bearing angle can also be obtained by measuring the phases of the output signals from each of the array hydrophones. The positioning error of the PPHM method depends on how accurately the received signal's phase will be measured. The method is based on continuous phase measurement. It is very sensitive to changes in the underwater medium. Degradation of positioning accuracy due to environmental fluctuations will be investigated. Solutions will be proposed to minimize their effects. The goal of this project is to develop a robust positioning system which works with high measurement accuracy in complicated underwater environment.

The PPHM method was initially designed for tracking an underwater moving target. A simpler application is to measure the ocean currents speed and perturbations over a path. Also, it finds application in monitoring the movements of tectonic plates. The second and the third applications will be addressed in details in this thesis, whereas the first one is more challenging and needs more exploration.

This thesis is organized as following:

- Chapter 2 surveys underwater acoustic positioning techniques, including conventional methods and newly developed GPS-involved methods. Following topics will be presented: methods of operation, system configurations, positioning accuracies and applicable areas. Also, their advantages and disadvantages will be discussed in this chapter.

- Chapter 3 introduces the theoretical background and positioning principle of the PPHM method. The system configuration for positioning a moving target will be presented. Estimations of a target's slant range and bearing angle using phase

measurement will be addressed. Computer simulations are conducted to verify the theoretical analysis.

- Chapter 4 discusses the signal processing issues of the PPHM method. Firstly two transmission patterns are evaluated: continuous wave and pulsed signal. Then, four solutions for phase estimation will be presented. The estimated phase needs to be unwrapped to reflect the correct range increment. A phase unwrapping method will be introduced that can compensate for false phase jumps caused by noisy input signals.

- In Chapter 5, the sources of error from the propagation medium are investigated, with emphasis on sound speed variations, ocean currents, and multipath interference from the seafloor. Their effects on the PPHM method are described. Solutions are proposed to minimize these effects. In addition to the three major error sources, other influence factors, including noise, acoustic scintillation, and water turbulences, will be briefly discussed.

- Chapter 6 presents three potential applications for the PPHM method: trajectory tracking of an ROV; measurement of ocean current speed and perturbations over a path; and monitoring of tectonic plate movements. For each case, the background knowledge will be introduced, followed by the descriptions for system configuration and operation pattern, performance evaluation, and finally environmental influences analysis.

- To verify the concepts, a scale-down air-prototype experiment using ultrasonic transmission has been designed and implemented. In Chapter 7, the experiment setup will be presented at first. Two experiments are conducted. The first experiment is the trajectory tracking of a moving target using slant range measurement. The second experiment is the monitoring of an air flow (in analogy to an ocean current) speed. Data collection and processing method are presented. Experimental results will be evaluated. The practical issues that arise during the experiments will also be discussed.

- A summary of work done is given in Chapter 8. In this chapter, problems that have not been solved in this thesis will be addressed. Recommendations for future research and development are given at the end.

Chapter 2 Underwater Positioning Systems

Over recent years, there is increasing interest in underwater acoustic positioning systems. Underwater acoustic positioning systems have found their applications in diverse areas in ocean scientific and engineering tasks, such as marine habitat monitoring, bottom and water column surveys along a precise and repeatable trajectory to monitor the chemical and physical variables and to study the sedimentation processes, underwater searching and mapping, high-resolution synthetic sonar observations, instrument placement and retrieval for oil and gas industry, mine hunting, among others [2~11].

An underwater acoustic positioning system tracks and navigates underwater vehicles or divers by means of acoustic distance and direction measurements, and subsequent position triangulation. Unlike the in-land positioning systems such as the GPS, which use electromagnetic signals, the underwater positioning systems use acoustic signals, because acoustic signals have a lower absorption rate by sea water, as compared to that of electromagnetic signals. As a result, acoustic wave can propagate a much longer distance.

Basic components of an acoustic positioning system include a transceiver and an array of transponders (or a transponder and an array of transceivers), a processing unit and a display unit [3]. The transceivers and the transponders transmit and receive acoustic signals for distance and direction measurements. The spacing between transponders (or transceivers) in the array is called baseline. Underwater acoustic positioning systems are categorized into three major groups according to the size of their baselines, as given in Table 2.1. More recently, triggered by the fast development in GPS technology, new underwater acoustic positioning systems have arisen that utilize buoys equipped with GPS receivers and acoustic communication techniques [12~16]. Examples of those systems include the so-called GPS Intelligent Buoys (GIB) system [12, 13] and the Global Acoustic Positioning System (GAPS) [14].

Table 2.1: Three Major Groups of Underwater Acoustic Positioning Systems

System Type	*Baseline Length*	*Positioning Strategy*
Long Baseline (LBL)	50m~6000m	range measurements only
Short Baseline (SBL)	10m~50m	range and bearing measurements
Ultra Short Baseline (USBL)	<10cm	range and bearing measurements

In this chapter, a brief review for classical positioning approaches as well as the newly developed methods will be given. Following topics will be presented: general methods of operation, system configurations, positioning accuracies and applicable areas. Common problems associated with acoustic positioning systems will be discussed and solutions are outlined. Advantages and limitations for each group of systems will be presented and compared.

2.1 Long Baseline (LBL) Positioning Systems

A typical LBL positioning system consists of one transceiver and at least three transponders. The transceiver is mounted on a submersible or a surface vessel, which is the target to be positioned. The transponders are installed on the seafloor to form an array. Before positioning the target, transponders will be deployed on the seafloor. Their positions (or at least the distances between each other) need to be known precisely. The deployment and retrieval of transponders on the seafloor are performed by a surface ship, or by divers or an underwater automatic vehicle. The spacing between transponders (i.e. the LBL baseline) is 50~2000m in an LBL system. The transceiver on the target pings each transponder on the seafloor. The travelling time of the transmitted signal from the target to the transponders and backwards is measured. Knowing the sound velocity at the site allows this measurement to be converted directly to the travelling distances. Once the distances from all transponders to the transceiver are obtained, a unique point where all these distances intersect is obtained via calculations and this point is the position of the transceiver. This method is called “trilateration” [17, 18]. The calculated transceiver’s position is within and referenced to the transponders array.

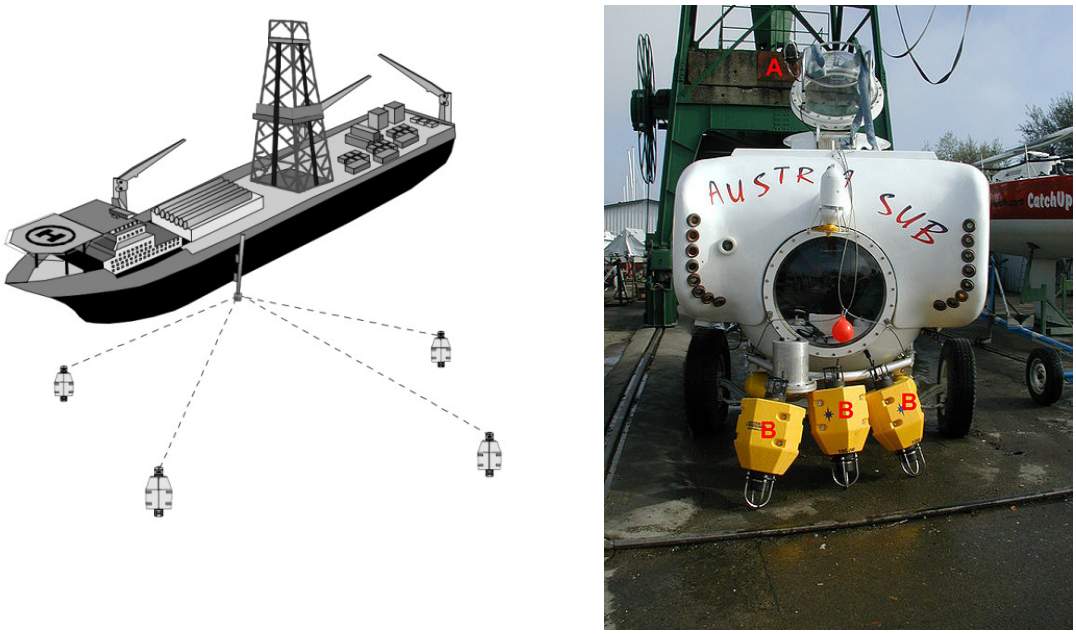

(a) (b)

Figure 2.1: (a) LBL System Configuration for a Surface Platform Localization [3];
(b) Submersible with an LBL Positioning System including Baseline Transponders (B) and Submersible Mounted Transceiver (A) [19]

Most LBL systems work at a frequency of approximately 10 kHz and the positioning accuracy is within several meters for a maximum operation range on the order of a few kilometers [2]. The positioning accuracy is a function of the operating frequency. At 8~16 kHz the accuracy could achieve 2~5m and at 18~36 kHz it could achieve 0.25~1m. In a near distance application where the operating area is a triangular with 100 meters a side, and the working frequency is 300 kHz, a positioning repeatability could be created with 1 centimeter resolution [2].

In general, LBL positioning accuracy is in the order of decimeters to a few meters over a range up to several kilometers [20], which is much more accurate than USBL or SBL positioning methods for a large area application. More importantly, the positioning accuracy is uniform and independent of the water depth. This gives LBL systems more advantages in deep water surveys. LBL systems have good repeatability, high reliability and are extremely robust. The transponders installed on the seafloor provide observation redundancy. LBL systems also have disadvantages. They can only provide high accuracy positioning over the area which the seafloor transponder array covers. The system itself is

complicated. It requires expert operators as well as time-consuming deployment of transponders array on the seafloor. Besides, LBL systems require comprehensive calibrations at each deployment. Large arrays of transponders installed on the seafloor also cost a lot of money.

LBL systems are commonly used for precisely locating a surface ship which is installing the drilling equipment in gas and oil industry. They are also used to positioning a submersible (autonomous underwater vehicle (AUV), ROV, crawler or diver) with respect to the seafloor transponder array. Examples of commercially available LBL systems include the SIMRAD HPR408 SUBSEA LBL System by Kongsberg Maritime [20], and the Fusion LBL System by Sonardyne [21].

An LBL system can work in a reverse manner; i.e., the transponders are located on the sea surface. One example is the GPS Intelligent Buoy (GIB) system [12, 13]. The transponders are installed on GPS equipped buoys that are either drifting or moored and form an array on the sea surface. A GIB system may be used in conjunction with an active underwater device such as a pinger equipped torpedo, or with a passive acoustic sound source such as an inert bomb striking the surface of the water. The position of the sound source or impact event is obtained using range measurement and trilateration. Positions of transponders on sea surface are measured by GPS using radio electromagnetic signal. To combine the measured data and get an absolute position of the target, good time synchronization is essential in a GIB system.

2.2 Short Baseline (SBL) Positioning Systems

SBL systems do not require any seafloor mounted instruments. In an SBL system, three or more transceivers are installed on the hull of a ship or a surface platform. A transponder is attached to the submersible to be positioned. One of the transceivers sends out an acoustic signal. The transponder responds it with another acoustic signal on a different frequency. This signal is received by the transceiver array. The two–way time-of-flight from the transponder to the transceiver array is measured and converted into slant range if the sound speed at the site is known. The submersible's position is obtained by using the trilateration method.

The SBL positioning accuracy improves with the operating range and the spacing between the transceivers on the surface platform. Thus, where space permits, such as when operating from larger vessels or a dock, the SBL system can achieve a precision and position robustness that is similar to that of seafloor mounted LBL systems, making the system suitable for high-accuracy survey work. When operating from a smaller vessel where transducer spacing is limited, the SBL system will exhibit reduced positioning accuracy.

The range derived from an SBL system is with respect to the transceivers which are mounted on the ship or the platform. The ship or the platform are floating on the sea surface and are subject to pitch, roll and raw movements. As such, an SBL system needs additional sensors such as a ship's gyro, a vertical reference unit (VRU), or sometimes a surface navigation system, to correct the derived range.

As compared to LBL systems, the low system complexity makes SBL easy to use. It is a ship based system so there is no need to deploy transponders on the seafloor, which saves time and money. SBL systems are mainly used to track a submersible with respect to a surface platform such as an oil drilling platform. It also can be used for searching a crashed airplane in the sea. Examples of commercial available SBL models are the SHARPS SBL system by Marine Sonic Technology [22] and the RS5D SBL system by Nautronix [3].

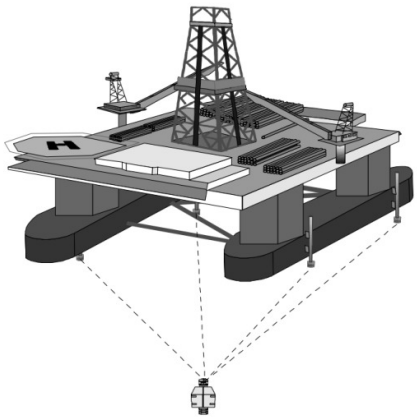

Figure 2.2: SBL Positioning System [3]

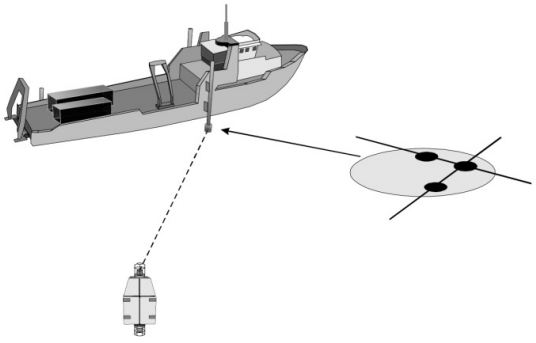

Figure 2.3: USBL Positioning System [3]

2.3 Ultra Short Baseline (USBL) Positioning Systems

Ultra Short Base Line system (USBL) is sometimes called Super Short Base Line (SSBL) system. Similar to the SBL system, an array of transceivers (three or more) is fixed to a surface vessel. A transponder is attached to a submerged target, which could be an ROV, an AUV, a crawler or a diver. An acoustic pulse is transmitted by the transceiver and detected by the transponder on the target, which replies with its own acoustic pulse. This return pulse is detected by the shipboard transceivers array. The time from the transmission of the initial acoustic pulse until the reply is detected is measured and converted into a range.

Instead of using the trilateration to calculate a subsea position, the USBL measures both the range and the angle from the subsea target to the transceiver array. An important assumption is that the wavefront of the acoustic signal is planar at the transceiver array. To avoid ambiguity in phase angle measurement, transceivers in the array are separated by only half of the wavelength (usually 10 cm or less) of the acoustic signal. To determine the azimuth angle θ, the phase difference of the signal from the target between two receivers in the array is measured relative to the array's baseline. Here the azimuth angle is defined as the angle between the positive X-axis and the target position vector (the line points out to the target from the coordinate origin) projected onto the horizontal X-Y plane. If a third receiver is used, orthogonal to the first two, the elevation angle ψ, which is the angle between the positive Z-axis and the target position vector, can be determined. The distance from the transceiver to the target, r, is the amplitude of the target vector. It is obtained by measuring the time of arrival, as in LBL and SBL systems. A complete figure is shown in Figure 2.4 and the Cartesian coordinate (x, y, z) of this target is given by:

$$x = r \sin\psi \cos\theta \tag{2.1a}$$

$$y = r \sin\psi \sin\theta \tag{2.1b}$$

$$z = r \cos\psi \,. \tag{2.1c}$$

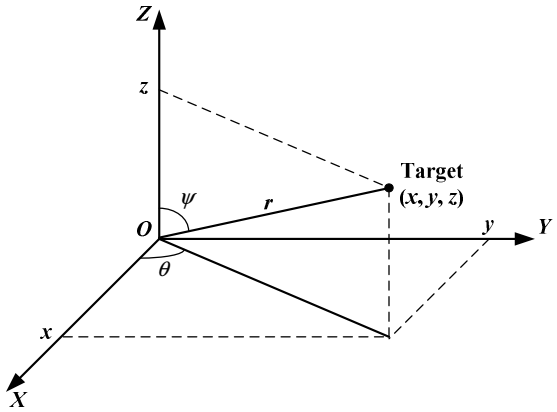

Figure 2.4: USBL Range and Angle Measurements

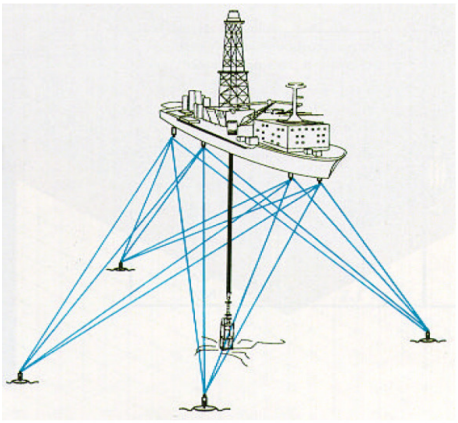

Figure 2.5: Combined Positioning Systems [3]

The transceivers in a USBL system are typically built into a single assembly in close proximity, which makes USBL systems more compatible and easily be deployed. So in an USBL system there is no need of deployment and calibration of transponders array on the seafloor. Since the range and bearing measured in an USBL system is referenced to the transceivers mounted to the surface vessel, additional sensors are needed to provide a position that is seafloor referenced, as similar to the SBL systems. Positioning accuracy of an USBL system is related to the slant range and water depth. It has better performance within short range or in shallow water. The positioning performance depends on the accuracy of additional sensors for vessel self-motions. A representative of commercial available USBL systems is the HiPAP Family (HiPAP 500/450/350/350p/100) by Kongsberg [20]. A detailed comparison made between the positioning products from six worldwide leading manufacturers is listed in Table 2.2.

Table 2.2: Examples of Underwater Acoustic Positioning Systems

Company	*System*	*Type*	*Operating Range (m)*	*Operating Depth (m)*	*Operating Frequency (kHz)*	*Positioning Accuracy*	*Features*
IXSEA	Posidonia	USBL	8,000	6,000	12~18	0.3% of slant range	MFSK chirp modulation
IXSEA	GAPS	USBL	4,000	N/A	20~30	0.2% of slant range	MFSK chirp modulation
LinkQuest	PinPoint 1500	LBL	1,000	4,000	26~45	0.05~0.5m	Broadband acoustic spread spectrum technology
LinkQuest	PinPoint 10000	LBL	10000	7,000	7.5~12.5	0.3~2.0m	Broadband acoustic spread spectrum technology
LinkQuest	TrackLink 5000	USBL	5,000	7,000	12~22	0.3% of slant range	
Sonardyne	Fusion LBL	USBL	7,000	3,000	18~36	0.2% of slant range	
Nautronix	NasPOS	USBL	4,500	3,000	8.5~11.5	0.25% of slant range	Nautronix acoustic digital spread spectrum technology
Kongsberg	HiPAP 100	USBL	10,000	6,500	10~15.5	0.2% of slant range	
Kongsberg	HiPAP 350	USBL	3,000	N/A	21~30.5	0.3% of slant range	
Kongsberg	HiPAP 500	USBL	4,000	N/A	21~30.5	0.2% of slant range	

There are also many varieties of combined positioning systems, such as L/USBL, L/SBL, S/USBL and L/S/USBL [3]. As indicated by their names, these systems combine the benefits from all of the above classical systems and provide very reliable and redundant positions. However, with these benefits come more complicated systems.

2.4 Time-of-flight Measurement

In conventional acoustic positioning systems, the target's slant range is obtained via measuring the time-of-flight of an acoustic signal. The traditional solution for time-of-flight measurement is the matched filter, in which the time taken from sending an interrogation signal to receiving its reply has been found by locating the cross correlation peak of the received signal with a reference signal. Specifically, the reference signal and the received signal are multiplied and integrated, for a range of hypothesized time delays or time shifts until the peak is obtained. The time shift corresponding to this peak value is the estimated time-of-flight or time-of-arrival (TOA). This value is then converted into range based on the sound velocity at the site. The target's bearing is derived by comparing the small differences in the TOA of the reply signal at each hydrophone within the array. Matched filtering method achieves better performance when the signal-to-noise ratio (SNR) is high. A higher SNR can be achieved by means of a narrowband filter. This requires a longer transmission pulse, which in turn reduces the battery powered transponder's life. Furthermore, the resolution of the matched filtering method is limited by the sampling frequency. The true location of the cross correlation's peak value may fall in between two samples when the sampling frequency is insufficient. The performance can be improved by increasing the sampling frequency. But a higher sampling frequency limits the capability for real-time processing of the data. Sub-sample resolution is a common solution, which uses either interpolation of the input signals or interpolation between points on the correlation function.

2.5 Common Issues Associated with Acoustic Positioning Systems

Major problems associated with the commercially available underwater acoustic positioning systems include positioning accuracy, system complexity and cost [3].

Acoustic positioning systems can yield an accuracy of a few centimeters to tens of meters and can be used over operating distance from tens of meters to tens of kilometers. Performance depends strongly on the type and model of the positioning system, its configuration for a particular job, and the characteristics of the underwater acoustic environment at the work site. Factors that reduce the system performance include sound velocity variations, noise, multipath, and the inhomogeneities of the sea water.

When the measured time-of-flight is converted into slant range, the sound speed at the site needs to be known. The sound speed in water is a function of water temperature, salinity and depth. Variations in sound speed will bring a systematic error. The sound speed must be monitored in different areas and at different times throughout the positioning task within the required accuracy of the survey to maintain the positioning accuracy. The ambient noise in water and the self noise from the surface platform will degrade the matched filtering for the time-of-flight estimation, and consequently the positioning accuracy. Another factor that reduces the positioning accuracy is the multipath interferences. Multipath interferences degrade positioning accuracy because of the highly coherency. They can cause total destructive interference with the direct path signal from the target. The consequences can be minimized by correct choice of mounting location, frequency band and array geometry. The ocean current and turbulence can also degrade the positioning accuracy to a certain degree. A detailed study on the underwater environmental factors that degrade an acoustic positioning system will be given in Chapter 5.

LBL systems have uniform positioning accuracy for a large area survey. The biggest concern is its system complexity and deployment. SBL and USBL systems have low system complexity. There is no need of transponders deployment on the seafloor in these systems. This merit makes SBL and USBL systems very attractive in many applications. The disadvantage is that the positioning accuracy is a function of the water depth and operation range. The absolute position of the target depends on additional sensors.

The conventional systems usually involve a surface ship and multiple transducers. This type of configuration is not economic for long term observations of underwater activities such as the monitoring of the marine habitat at a certain spot. The costs of individual equipments, plus the expense on system components deployment in each of the research trial, should also be taken into account. For example, the price of the Tracklink 5000 system, a USBL system from LinkQuest Inc., starts from 34,900 US dollars [3].

All above listed systems are autonomous in the sense that no cable connects the reference platform with the target. In many situations, however, the target is an ROV or a towed body and a tethered cable is presented. This cable serves as a communication link

between the reference platform and the target. It could be utilized as an aid for target positioning.

Chapter 3 Underwater Positioning using Phase Measurement

In this chapter, an acoustic positioning method is proposed which is based on continuous phase measurement and is called the PPHM method. Firstly, its background theory will be introduced. Then the system configuration will be presented for positioning a moving target. Next, estimation accuracy of the PPHM method is investigated and compared with conventional positioning systems. Computer simulation results are given to support the theoretical analysis.

Following topics will be covered in this chapter:

1. Background theory and general working principle of the PPHM method.
2. Slant range estimation. This is a simple application of the PPHM method. The measurement accuracy is determined by the phase measurement accuracy.
3. Bearing angle estimation. The PPHM method can be used to measure the bearing angle of the target. A receiver array with at least two hydrophones is needed.
4. Positioning a moving target within a horizontal plane. The strategy is to combine the slant range measurement and the bearing angle estimation plus trigonometry knowledge.

3.1 General Working Principle

A novel precise underwater positioning method based on phase measurement of acoustic signals has been proposed [5]. The motivations are

- to design a positioning system with less complexity and can be easily operated;
- to improve the positioning accuracy;
- to reduce the instruments deployment time and cost; and
- to establish a platform for long-term observation.

The proposed PPHM method has the following features:

- Unlike conventional positioning systems which estimate the target's position by measuring the time-of-flight of the target's signal, the proposed method is based on continuous phase monitoring of acoustic signals.

- The PPHM method measures the relative range increment between the reference platform and the target, instead of the target's absolute coordinates.
- The PPHM method takes advantages of the tethered cable connecting a reference platform and a target.
- The PPHM method can track the trajectory of a moving target continuously in real-time.

When an acoustic sinusoidal signal propagates in water with speed c, its wavelength λ is defined as the distance over which the wave travels during one period T, i.e. $\lambda = cT$. As shown in Figure 3.1, one period is equivalent to one 2π-phase flip in the sinusoidal waveform.

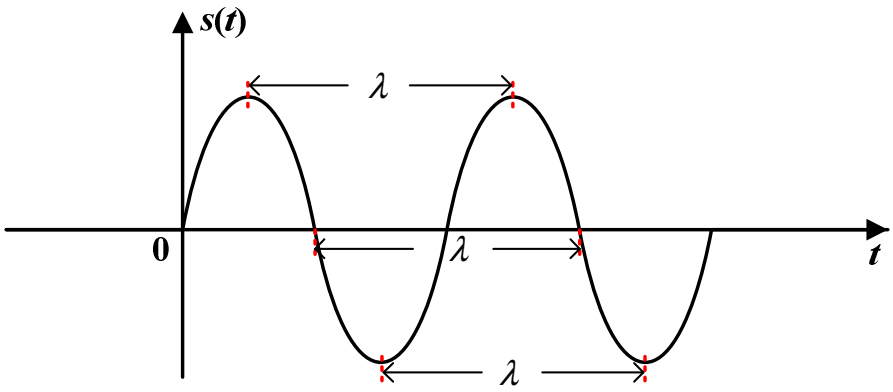

Figure 3.1: Relationship of the Wavelength and the Phase Change in a Sinusoidal Waveform

Each 2π-phase flip in the received waveform in the time domain corresponds to one wavelength in distance in the spatial domain, which means that the distance estimation can be done by phase measurement, providing that the number of phase flips is counted continuously and precisely. Assume there is a receiver at Point A and a transmitter at Point B. The distance between A and B is r_0. A sinusoidal signal given in Equation (3.1) is sent out from B to A,

$$s_0(t) = \cos(2\pi f_0 t), \tag{3.1}$$

where f_0 is the signal's frequency. The signal received at A is given by

$$s(t) = s_0(t-\tau) = s_0(t-\frac{r_0}{c}) = \cos\left[2\pi f_0(t-\frac{r_0}{c})\right]$$
$$= \cos\left[2\pi f_0 t - 2\pi f_0 \cdot \frac{r_0}{c}\right] = \cos(2\pi f_0 t - \phi_0) \quad , \tag{3.2}$$

where

$$\phi_0 = 2\pi f_0 \cdot \frac{r_0}{c} \tag{3.3}$$

is the phase delay caused by r_0. ϕ_0 is a constant value if r_0 and the sound speed c are fixed. As the transmitter at B starts to move to a new position B_1, r_0 has an increment Δr. For simplicity, it is assumed that the transmitter is moving away from B along a straight line in the radial direction of AB with a constant speed v, as shown in Figure 3.2. The range increment $\Delta r = AB_1 - AB$ will cause a phase shift $\Delta\phi$ (or $\Delta\phi(t)$ if the target's speed is not constant) in the received signal at A as below:

$$s_1(t) = s\left(t - \frac{(r_0 + \Delta r)}{c}\right) = \cos(2\pi f_0 t - \phi_0 - \Delta\phi) \quad , \tag{3.4}$$

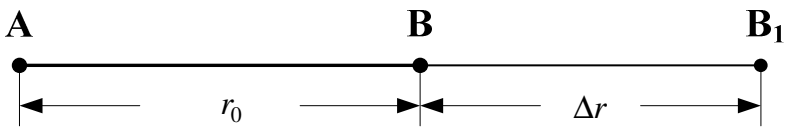

Figure 3.2: Target's Movement in the Radial Direction of AB

where

$$\Delta\phi = 2\pi f_0 \frac{\Delta r}{c} \quad . \tag{3.5}$$

Figure 3.3 plots the received signals from its initial position B (the dashed line) and from the new position B_1 (the dot-dashed line), respectively. The transmitted signal was plotted in the same figure (the solid line). It serves as the reference for phase comparison. As demonstrated, any range increment Δr induces the phase shift $\Delta\phi$ in the received signal. To estimate Δr, firstly an estimate of the phase shift, $\Delta\hat{\phi}$, is obtained using a phase detector, and then converted into $\Delta\hat{r}$ based on Equation (3.5) as

$$\Delta\hat{r} = \frac{\Delta\hat{\phi}\cdot c}{2\pi f_0} = \frac{\Delta\hat{\phi}}{2\pi}\cdot\frac{c}{f_0} = n\cdot\lambda, \tag{3.6}$$

where

$$n = \frac{\Delta\hat{\phi}}{2\pi} \tag{3.7}$$

is the number of 2π-phase flips in $\Delta\hat{r}$, and $\lambda = c/f_0$ is the wavelength. Equation (3.6) essentially counts the number of 2π-phase flips in $\Delta\hat{\phi}$. This number multiplying the wavelength gives the estimate of the range increment, $\Delta\hat{r}$.

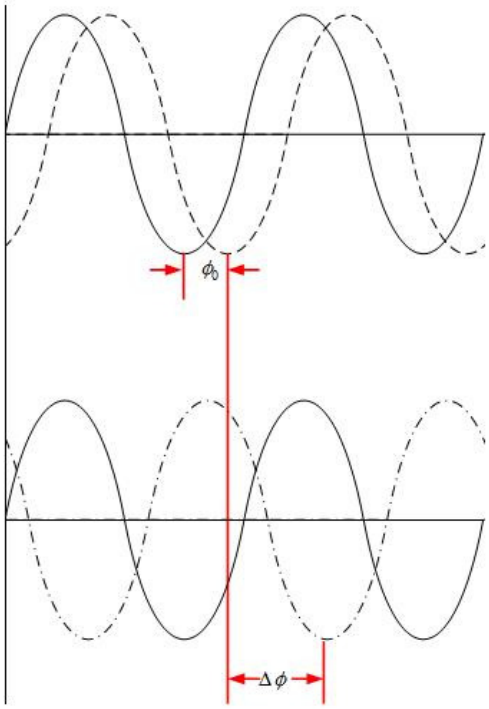

Figure 3.3: Received signals from B (dash line) and B_1 (dot-dash line) with reference signal (solid line). Only two periods of the signals are shown for demonstration.

The received signal's phase is measured with error in a practical system due to the system errors and influences from the underwater medium. As an illustration, let's assume the measurement error of $\Delta\hat{\phi}$ be $e_{\Delta\hat{\phi}}$. From Equation (3.3), the range increment estimation error is

$$e_{\Delta\hat{r}} = \frac{\lambda}{2\pi} e_{\Delta\hat{\phi}} \ . \tag{3.8}$$

So the range estimation error is a fraction of the phase measurement error. Assuming the frequency of the sinusoidal signal is f_0=20 kHz, which corresponds to a wavelength λ = 0.075m at c = 1500 m/s. If the phase is measured with ±10° error, the distance estimation error will be $e_{\Delta\hat{r}}$ = ±12.5mm. This potential accuracy is much higher than most of existing commercial underwater acoustic positioning systems.

3.2 System Configuration for Positioning a Moving Target

The proposed system configuration for positioning a moving target is depicted in Figure 3.4. A reference platform has been installed on the top of a tower. It is fixed at a few meters above the seafloor, and is denoted as A. To get power supply and to transfer collected data, the reference platform is connected to an observatory node [23], an offshore station or a surface vessel via an electric cable. In some case, it can also be connected to a surface buoy. A bottom unit which consists of an oscillator, a receiver (or a receivers array) and signal processors is mounted on the reference platform. The target being located could be a diver or submerged vehicles such as an AUV or ROV. It is connected to the reference platform with an electrical tethered cable. This cable is used for power supply and data transmission between the target and the reference platform. A transponder is clamped on the target for signal transmission. The seafloor is assumed to be flat and smooth.

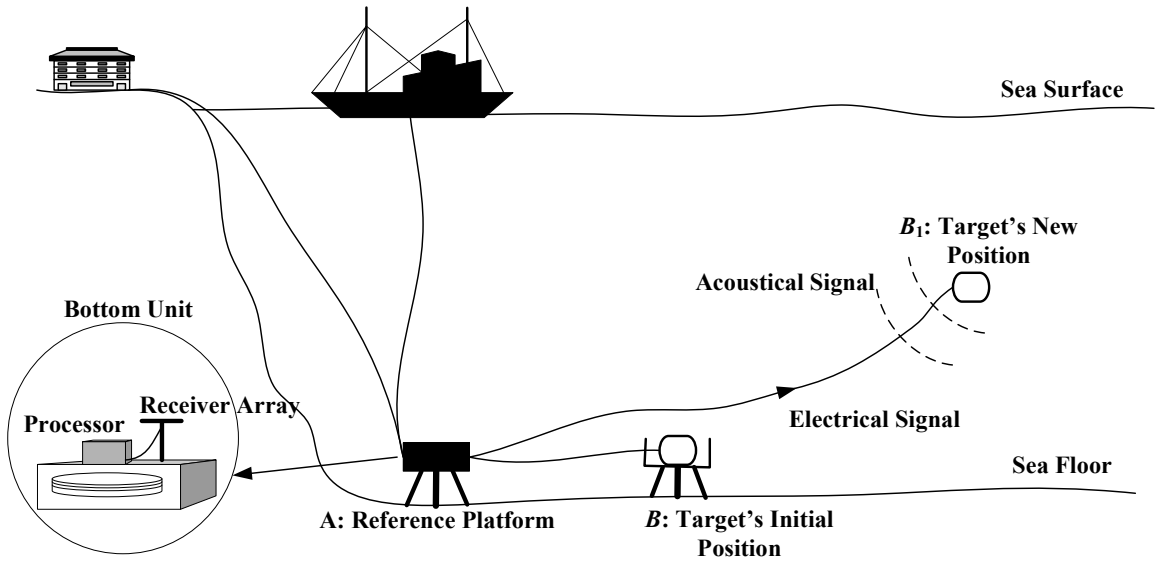

Figure 3.4: System Configuration to Position a Moving Target

Point A is assigned as the coordinate origin in the measurement. Assuming at $t<0$, the target rests at its dock and its position is known as $\mathbf{B}=\{r_0,\theta_0,\psi_0\}^T$, where r_0 is the initial slant range, θ_0 is the initial azimuth angle and ψ_0 is the initial elevation angle (as defined in Section 2.3 and Figure 2.4). At $t=0$, the target receives the command signal from the reference platform at A through the tethered cable, and leaves its initial position B for the intended mission. The new position of the target is denoted as $\mathbf{B}_1=\{r,\theta,\psi\}^T$. The task of the positioning system is to estimate r, θ and ψ.

3.3 Slant Range Measurement

As the target rests at the initial position B, a continuous electrical signal $s_0(t)$ as given in Equation (3.1) is generated by the oscillator at the reference platform and then sent to the target through the tethered cable. This electrical signal is the reference signal for later phase detection. Upon receiving the electrical signal, the transponder on the target responds $s_0(t)$ in an acoustic form toward A. This acoustic signal propagates in the water and arrives A after a time delay τ, as given in Equation (3.2). τ is caused by r_0, the initial distance between A and B. It is a fixed value and assumed known. If displayed on an

oscilloscope, the received electrical and acoustic signals will have the waveforms as shown in Figure 3.3 (the top waveforms).

At $t = 0$, the target starts moving away from B in the radial direction as shown in Figure 3.2. For simplicity, the transmitter and the receiver are at the same height H as measured from the seafloor throughout the entire measurement. There will be a range increment Δr from the target's initial position B to its new position B_1. This range increment causes an additional phase shift $\Delta\phi$ in the received acoustic signal which was given in Equation (3.5). In a practical system, the received signal contains the acoustic signal from the target and the noise, as shown below

$$x(t) = s_1(t) + n(t) = s\left(t - \frac{(r_0 + \Delta r)}{c}\right) + n(t) = \cos(2\pi f_0 t - \phi_0 - \Delta\phi) + n(t) \quad , \quad (3.11)$$

where $n(t)$ is the noise coming from the environment and the system itself. $\Delta\hat{\phi}$ is recovered using a phase detector, then converted into the estimate of the slant range increment $\Delta\hat{r}$ using Equation (3.6). The target's new position in terms of range will be

$$\hat{r} = r_0 + \Delta\hat{r} \quad . \quad (3.12)$$

Conventional phase detectors usually require the inverse tangent computation to get $\Delta\hat{\phi}$. The inverse tangent function is a many-to-one function. All values of $\Delta\hat{\phi}$ outside the interval $(-\pi, \pi)$ will be mapped back into this interval. However, as Δr increases, $\Delta\phi$ will go beyond $(-\pi, \pi)$. The phase obtained from the phase detector cannot correctly reflect the range increment. This is called the phase ambiguity. To resolve it, one straightforward solution is to monitor $\Delta\hat{\phi}$ continuously to detect any jumps bigger than 2π. It requires a sufficiently high sampling rate. These jumps are then corrected by adding a factor of 2π to all subsequent terms in the sequence. This procedure is called phase unwrapping. The unwrapped phase is

$$\Phi = 2\pi n + \Delta\hat{\phi} \quad , \quad (3.13)$$

where n is the number of phase jumps.

Figure 3.5 presents the PPHM system's block diagram. A sine signal is generated by an oscillator located at the reference platform and is transmitted to the target through a tethered cable in the electrical form. It is also fed into the phase detector at the reference platform. When the electrical signal arrives at the target, the transponder clamped on the target responds with an acoustic replica to the reference platform through water. This signal arrives at the reference platform and will be passed into a signal amplifier and a narrowband filter to reduce the noise, and then fed into a phase detector. So the two input signals of the phase detector are the reference signal from the tethered cable, and the acoustic signal from the target. The phase detector will measure the phase difference between these two input signals and produce an output waveform. The magnitude of the output waveform directly reflects the phase difference. To track the phase changes beyond the interval $(-\pi, \pi)$, the number of jumps are counted and a phase unwrapping is performed. Using the readings from a sound velocimeter at the reference platform, the unwrapped phase is converted into the range increment, and therefore the target's position is obtained. This system monitors the target's position in real-time.

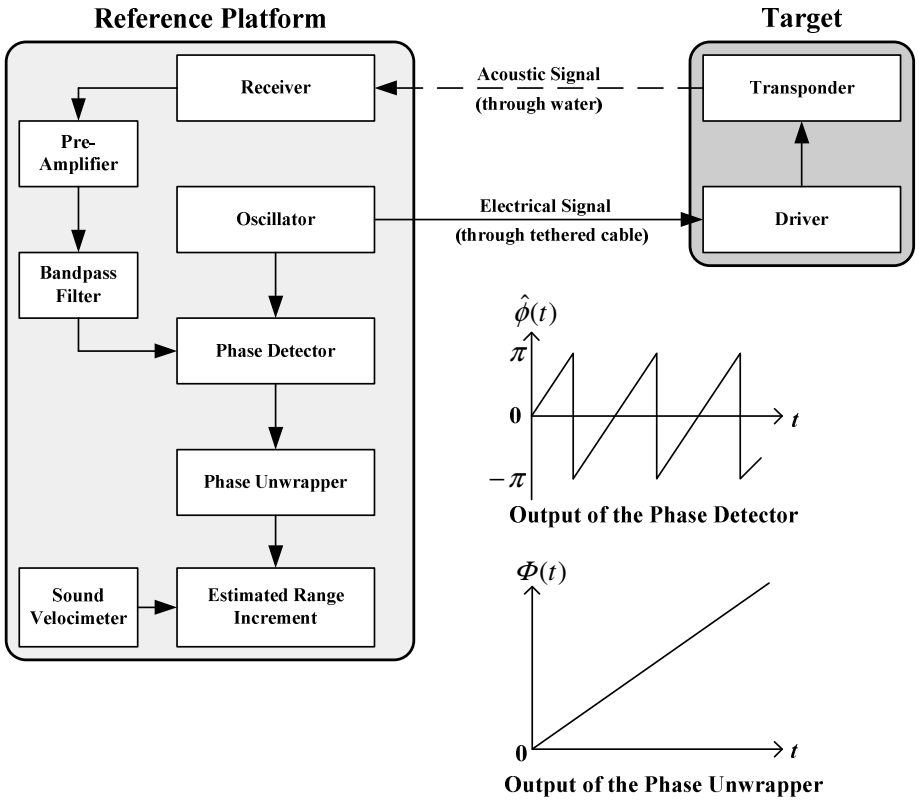

Figure 3.5: Block Diagram for Tracking a Moving Target

3.4 Signal-to-Noise Ratio

The received signal at the reference platform is contaminated by ambient noise, turbulences, and other environmental factors. As a result, its amplitude has small oscillations. In this thesis, these oscillations are modeled as a white noise $n(t)$ with Gaussian distribution. Its probability density function (PDF) is given as

$$p(n) = \frac{1}{\sigma\sqrt{2\pi}} e^{\left(-\frac{(n-\mu)^2}{2\sigma^2}\right)}, \tag{3.14}$$

where μ and σ^2 are the mean and variance of $n(t)$, respectively. The quantity "signal-to-noise ratio (SNR)" is used to evaluate the strength of the desired signal as compared to the noise. SNR is defined as the ratio of the signal power to the noise power, and is given as below,

$$SNR = 10\log\frac{\frac{1}{T_t}\int_0^{T_t} s^2(t)dt}{\sigma^2}, \tag{3.15}$$

where T_t is the signal's duration. To improve the SNR, a bandpass filter is used before phase detection. The bandwidth of the filter is determined by the drifting of the oscillator, as well as the frequency change in the received signal, which is mainly due to the Doppler effect [7]. In the proposed system, the operation frequency is tens of kilohertz and the target's speed is a few meters per second. So the system bandwidth is very narrow as compared to the operation frequency. This type of system is called a narrowband system. Most of the noise will be filtered out when pass through it. A detailed study on noise passing through a narrowband system has been given in Appendix A.

3.5 Simulation Results

Performance of the PPHM method is evaluated using a simulated noisy sinusoidal signal. Table 3.1 summarizes the parameters for computer simulations.

Table 3.1: Parameters for Computer Simulations

Parameters	***Values***
Transmitter Height H_T (m)	5
Receiver Height H_R (m)	5
Initial Range from Transmitter to Receiver r_0 (m)	5
Target Speed v_t (m/s)	2
Sound Speed in Water c (m/s)	1500
Observing Time T_t (s)	5
Carrier Frequency f_0 (Hz)	20000
Sampling Frequency f_s (Hz)	$4 f_0$

Simulations are conducted in a simplified scenario, in which the acoustic signal from the target travels to the receiver only along the direct path. Figure 3.6 shows the target's estimated range increment as the function of time, at SNR = 45dB and 55dB (as measured at the front of the receiver), respectively. The solid line is the measured range increment $\Delta\hat{r}(t)$ The dashed line represents the true value $\Delta r(t)$. The phase estimation is performed using a conventional quadrature phase detector, which will be described in Chapter 4. At SNR = 45dB, $\Delta\hat{r}(t)$ has small offsets from $\Delta r(t)$. At SNR = 55dB, $\Delta\hat{r}(t)$ fits the true value very well. Figure 3.7 shows a small section of the measured phase $\Delta\hat{\phi}(t)$ before and after unwrapping at SNR = 45dB and 55 dB, respectively.

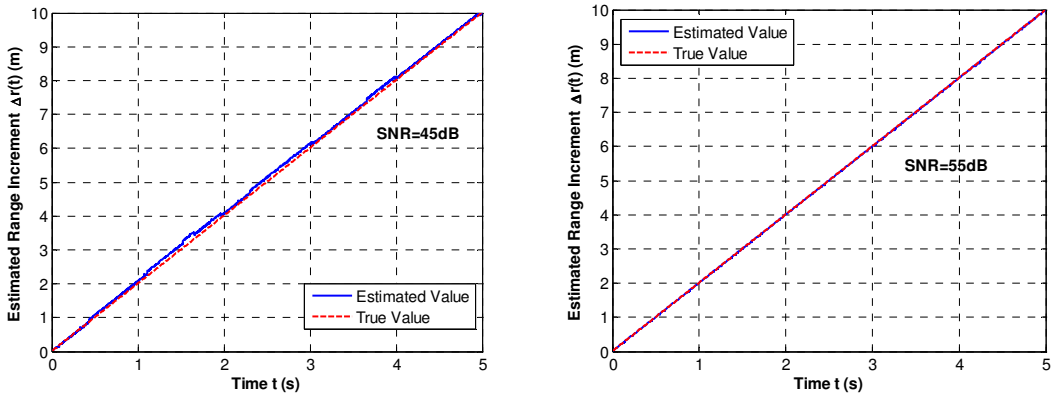

(a) (b)

Figure 3.6: Estimated Range Increment vs. True Range Increment at (a) SNR = 45dB and (b) SNR = 55dB

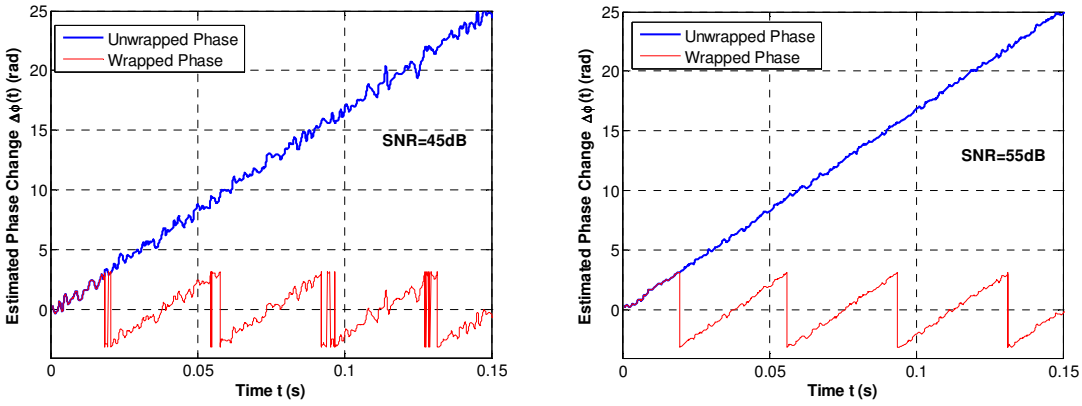

(a) (b)

Figure 3.7: Measured Phase before and after Unwrapping at (a) SNR = 45dB and (b) SNR = 55dB

The standard deviation of $\Delta\hat{r}(t)$ is used here to evaluate the positioning accuracy. It is defined as the root-mean-square (RMS) value of the difference between the estimated value $\Delta\hat{r}(t)$ and the true value $\Delta r(t)$, as given below:

$$\sigma_{\Delta\hat{r}} = \sqrt{\lim_{T\to\infty}\frac{1}{T_t}\int_0^{T_t}(\Delta\hat{r}(t)-\Delta r(t))^2\,dt}\ , \tag{3.16}$$

where T_t is the observation time. Figure 3.8 depicts $\sigma_{\Delta\hat{r}(t)}$ as a function of SNR. At SNR = 55 dB, the positioning accuracy attains 1mm.

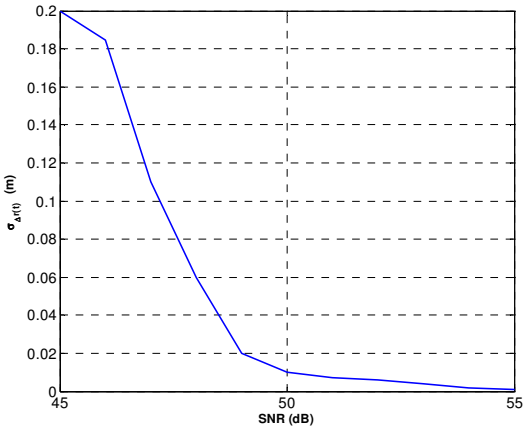

Figure 3.8: Standard Deviation of Estimated Range Increment vs. SNR, 100 Trials

In above simulations, the target's speed is a constant. For a target moving with a non-uniform speed, the PPHM method can still track the target's trajectory with high accuracy, as shown in Figure 3.9.

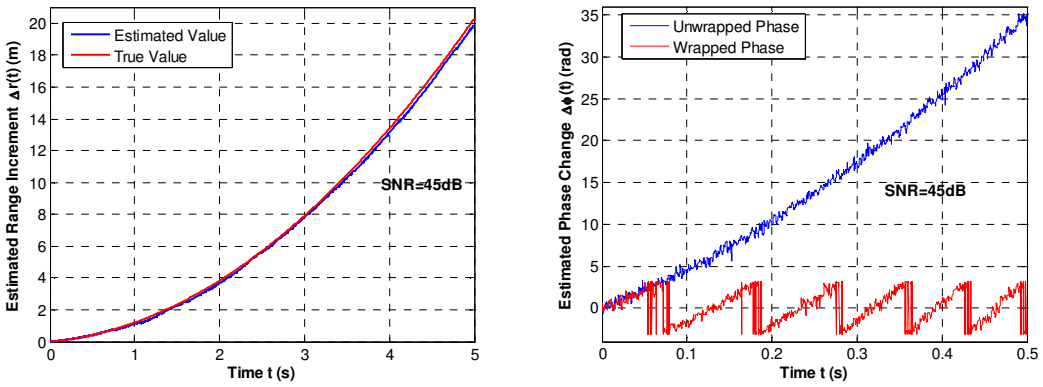

Figure 3.9: Tracking of a Moving Target with non-uniform speed

3.6 Bearing Angle Measurement

Above strategy of slant range measurement based on phase monitoring can be expanded for bearing angle estimation. An array with two receivers is needed at the reference platform, as shown in Figure 3.10. L is the receiver spacing. L is chosen to satisfy $L << r_0 + \Delta r$, so that the signal from the target has a planar wavefront when it arrives the receivers array (i.e. the far-field assumption is satisfied) [24]. The arriving angle of the received signal with respect to the array's broadside is θ degree, which is also called the direction-of-arrival (DOA) of the target's signal.

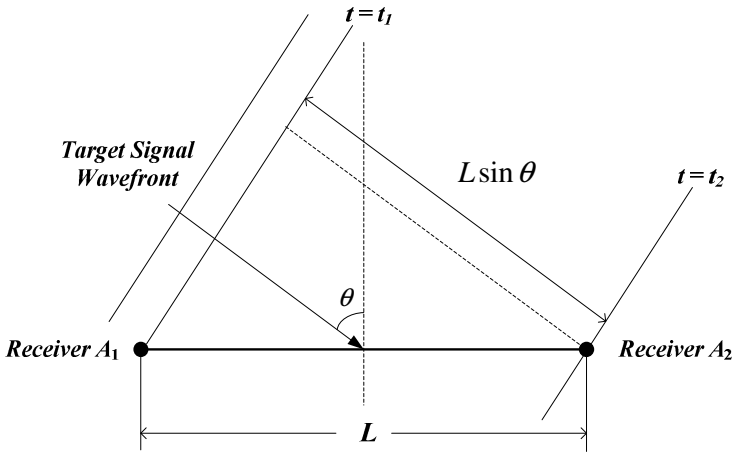

Figure 3.10: Geometry of the Receiver Array for Bearing Angle Measurement

At $t=t_1$, the target signal hits Receiver A_1 and at $t=t_2$ it hits Receiver A_2. From the geometry of the receive array shown in Figure 3.10, the difference in signals' arrival times, $\Delta t = t_1 - t_2$, is related to θ as

$$\Delta t = \frac{L}{c}\sin\theta\,. \tag{3.17}$$

From Equation (3.2),

$$\Delta t = \frac{\Delta\phi}{2\pi f_0} == \frac{\Delta\phi_1 - \Delta\phi_2}{2\pi f_0}\,, \tag{3.18}$$

where $\Delta\phi_1$ and $\Delta\phi_2$ are the phases of the signals received at Receiver A_1 and A_2 as compared to the reference signal, respectively. Combining Equation (3.17) and Equation (3.18), the estimated azimuth angle $\hat{\theta}$ is obtained as

$$\hat{\theta} = \sin^{-1}\left(\frac{\lambda}{2\pi L}\Delta\hat{\phi}\right) = \sin^{-1}\left(\frac{\lambda}{2\pi L}(\Delta\hat{\phi}_1 - \Delta\hat{\phi}_2)\right). \tag{3.19}$$

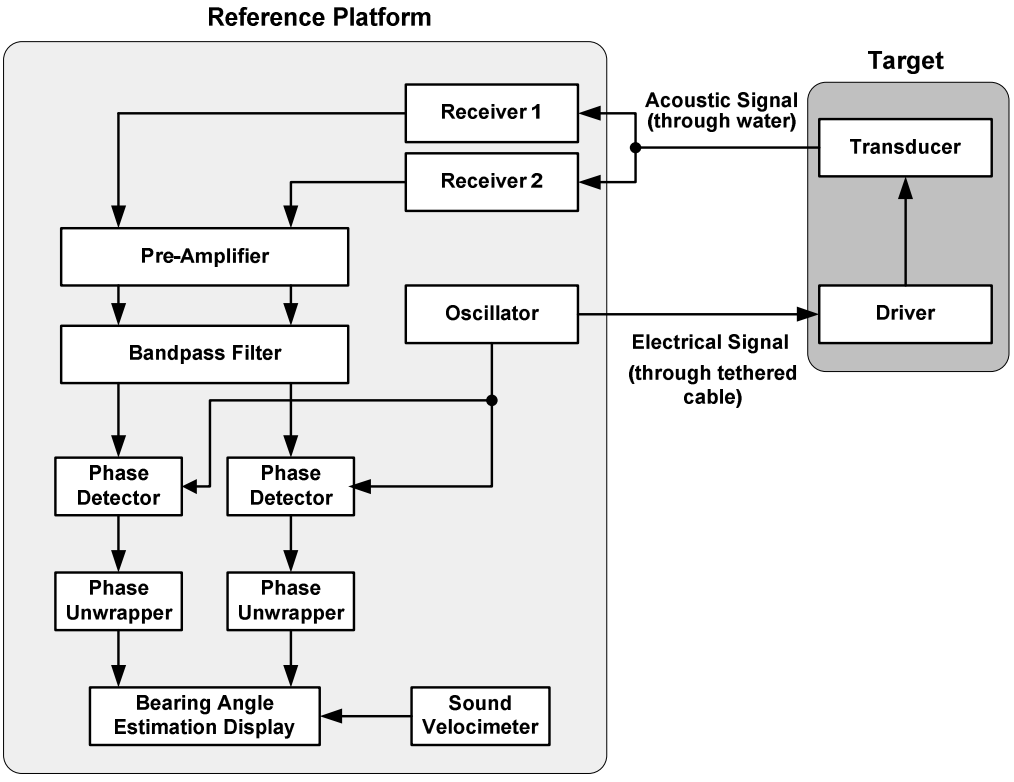

Figure 3.11: Block Diagram for Bearing Angle Measurement

Figure 3.11 is the block diagram for bearing angle measurement. The signals from both receivers passed through the pre-amplifier and bandpass filter to remove the noise. Their phases were measured separately using the same reference signal. After unwrapping, the two phases are subtracted. With Equation (3.17), $\hat{\theta}$ is obtained. In Equation (3.19), $\Delta\phi$ can be measured by feeding the two receivers' outputs into the phase detector and comparing their difference directly. But there will not be a stable reference for phase detection.

The same concept can be used to measure the elevation angle ψ. For this purpose, another receiver array with at least two receivers is need. This array should be perpendicular to the array for azimuth angle measurement.

3.7 Positioning a Moving Target in a Horizontal Plane

Having the strategies of estimating slant range and bearing angle using phase measurement in Section 3.4 and 3.5, respectively, we can expand the target's movement to an arbitrary direction, as long as this movement is along a straight line and within a horizontal plane. As shown in Figure 3.12, the target's initial position is B. Its new position is B_1. The range increment in the radial direction is $\Delta r = r_{CB_1}$ and can be estimated using the method in Section 3.4. The angle θ is estimated using the method in Section 3.5. From the cosine formula, the distance from B to B_1 is calculated as

$$r_{BB_1} = \sqrt{r_0^{\,2} + (r_0 + \Delta\hat{r})^2 - 2r_0(r_0 + \Delta\hat{r})\cos\hat{\theta}} \quad , \tag{3.20}$$

and its bearing angle

$$\angle B_1BA_1 = \cos^{-1}\left(\frac{r_0^{\,2} + r_{BB_1}^{\,2} - (r_0 + \Delta\hat{r})^2}{2 \cdot r_0 r_{BB_1}}\right) . \tag{3.21}$$

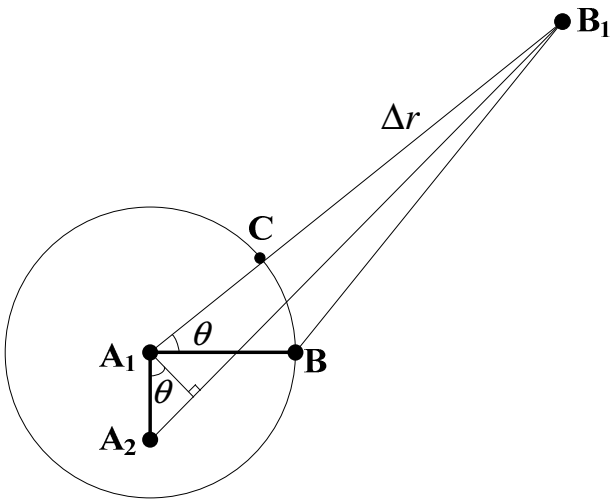

Figure 3.12: Tracking a Target's Movement within a Horizontal Plane

When the target starts moving toward a different direction from B_1, the measurement resumes, which means it takes B_1 as the initial position. An electrical signal will be generated at A and sent to B_1 through the cable. Upon receiving it, the transponder on B_1 transmits an acoustic signal in the same form through water back to A while it's moving.

Chapter 4 Signal Transmission and Phase Detection

The concept of target positioning using phase measurement relies on continuous phase monitoring. This chapter firstly discusses the signal transmission mode. The signal that is going to be used is a sinusoidal signal with its frequency at tens of kilohertz. For continuous monitoring of the target's position, the transmission should be a continuous wave and its duration equals to the observation time. The transmitted signal travels along the direct path, which is desired, and along the multiple paths (from boundaries such as sea surface and seafloor), which are unwanted interferences. The direct path signal and the multipath signals are mixed up at the receiver and the phase measurement will be corrupted. In view of this problem, a series of pulsed signal will be a better choice. The pulse length and time intervals between pulses are chosen so that 1) the target's range increment during the time interval between two pulses will not exceed one wavelength to avoid any phase ambiguity; and 2) the multipath interferences can be separated from the direct path signal based on their different time-of-arrivals.

Four phase detection methods will be investigated in this chapter, starting with the conventional quadrature phase detector. Then the received signal's analytical representation and an envelope extraction method will be introduced. A quadrature sampling method is proposed next. This method has a lower requirement for sampling rate and brings more feasibility for a real-time positioning. The PPHM method needs continuously phase monitoring to recover the target's position in real-time. Any interruptions in the received signal will affect the measurement. With the tethered cable connecting the target and the reference platform, we know when and what kind of signal will be transmitted from the target. With the prerequisite information, the missing data can be predicted using the least square estimation method.

In Chapter 3, a straightforward solution was described to unwrap the estimated phase. This method doesn't work well in a noisy scenario. In this chapter, the phase unwrapping problem will be further investigated so that the phase can be accurately unwrapped at low SNR.

Following topics will be presented in this chapter:

1 Transmitted signal. Advantages and disadvantages of the continuous wave and the pulsed signal will be discussed and compared. The pulsed signal will be used in the PPHM method. The pulse duration and the time intervals between pulses should be chosen carefully to mitigate the phase ambiguity and the multipath interference.

2 Phase detection methods, including the conventional quadrature phase detector, the envelope extraction, and the quadrature sampling method. The least square estimation is proposed for predicting the missed data in the received signal.

3 Phase unwrapping in a noisy environment.

4.1 Transmitted Signal

Within the observation window, the moving target transmits a continuous signal back to the reference platform in acoustic form. On the oscilloscope, the received acoustic signal moves back and forth with respect to the reference signal, reflecting the target's movement. Here the continuous signal (or continuous wave, CW) means a sinusoidal signal with a constant amplitude and frequency. The longer duration a signal has, the narrower bandwidth its spectrum occupies [25]. Theoretically, an ideal CW signal has an infinite duration. Its spectrum has non-zero values at $\pm f_0$ and equals zero elsewhere. In another word, its bandwidth B = 0. When a CW signal arrives at the receiver with noise, a bandpass filter with a very narrow bandwidth will effectively extract the signal and remove the noise. The SNR in front of the phase detector will be increased significantly. The circuit for generating and transmitting a CW signal is considerably simple.

In a practical system, an infinite-long CW signal is not achievable. The transmitted signal has finite duration. In the PPHM method, this duration is the same as, or less than the observation time. For a short-term application such as tracking an ROV in a small area, the transponder on the target will work continuously throughout the entire observation to respond the CW signal generated by the oscillator on the reference signal. For a long-term application which may last for days or even years, the power consumption of transmitting such a long signal will be a big concern. A power link to a main node on seafloor or to an offshore station is necessary. The major concern of CW

transmission is the multipath interferences. The direct path signal will mix up with the multipath signal and the received signal's phase will be contaminated. To discriminate the multipath interferences, a short duration signal will be transmitted periodically with a pre-determined repetition rate. This short-duration signal is called "pulse" in this thesis. All transmitted pulses have identical sinusoidal waveform with the same frequency and duration. The phase shift in each of these pulses is measured. The results are combined and the target's trajectory is recovered accordingly. The challenge of pulsed transmission is to choose the pulse length and the repetition rate. The repetition rate of transmission pulses are chosen such that the target's range increment during the interval between two pulses will not exceed one wavelength, which means that the phase will not change beyond 2π during the interval. By doing so the ambiguity will be avoided when the estimated phases are combined and unwrapped from each pulse.

4.2 Phase Detection

The target's position is estimated through phase detection. In this section the methods for phase detection will be discussed. The zero-phase reference signal and the received noisy signal are re-written as

$$s_0(t) = A_0 \cos(2\pi f_0 t) \tag{4.1}$$

and

$$x(t) = s_1(t) + n(t) = A(t)\cos(2\pi f_0 t - \phi(t)) + n(t) \ . \tag{4.2}$$

Various methods have been proposed for estimating the phase difference between two sinusoidal signals. In the conventional approach, the phase shift between two signals at the same frequency is computed by first converting the two input signals into two square waves and then measuring the time difference between the zero crossings of the two square waves [26]. This method only works well for high SNR. Besides, it requires a sampling rate several times greater than the Nyquist rate to achieve better estimation accuracy, which will limit the possibility for real-time data processing.

4.2.1 Quadrature Phase Detector

Assuming the additive noise is white Gaussian, the maximum likelihood estimator (MLE) of the phase shift $\phi(t)$ in Equation (4.2) is the value that can maximize the likelihood function [27], as shown in (4.3),

$$\hat{\phi}_{MLE}(t) = \max_{\phi} p\{x(t); \phi(t)\} \ , \tag{4.3}$$

where the likelihood function $p\{x(t); \phi(t)\}$ is the PDF of $x(t)$ with ϕ as a parameter. Equation (4.3) reduces to [27]:

$$\hat{\phi}_{MLE}(t) = -\tan^{-1}\left(\frac{LPF\{x_Q(t)\}}{LPF\{x_I(t)\}}\right) = -\tan^{-1}\left(\frac{LPF\{x(t)\cdot\sin(2\pi f_0 t)\}}{LPF\{x(t)\cdot\cos(2\pi f_0 t)\}}\right) . \tag{4.4}$$

In Equation (4.4), $x_I(t)$ and $x_Q(t)$ are the in-phase and in-quadrature components of the received signal, respectively. The operator $LPF\{\}$ denotes the output of a signal passing through a lowpass filter. In practice, the MLE can be accomplished by a conventional quadrature phase detector (QPD) as shown in Figure 4.1.

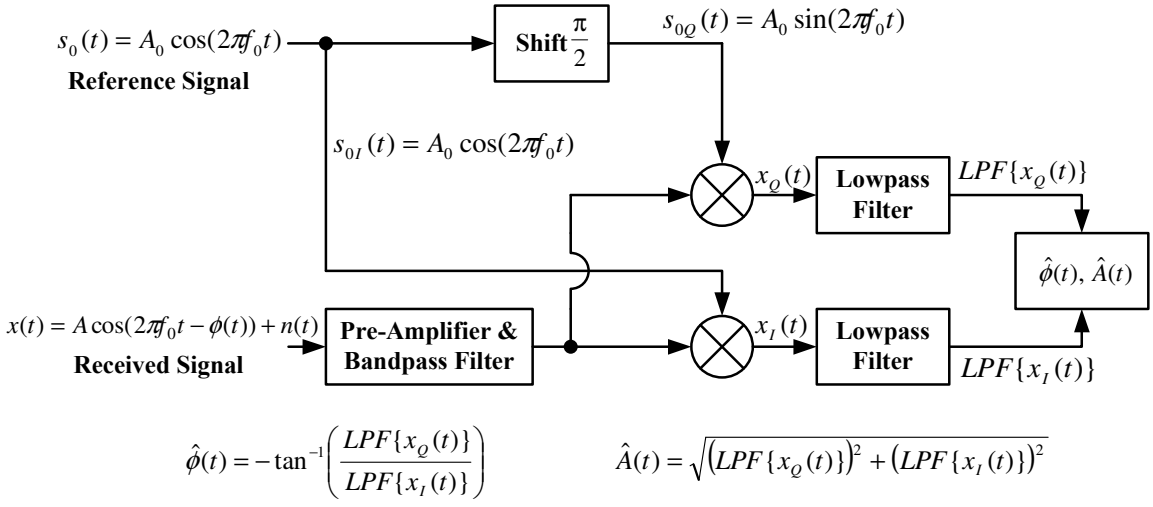

Figure 4.1: Block Diagram of a Conventional Quadrature Phase Detector

In Figure 4.1, the received signal firstly passed through a preamplifier followed by a bandpass filter. The function of the preamplifier is to match the electrical signal from the hydrophone with the dynamics and sensitivity of the processing unit. The bandpass filter

is used here to reduce the noise in the received signal. It's centered at the carrier's frequency f_0. Its bandwidth B_{BPF} should be able to accommodate the frequency shift in the received signal, usually caused by the target's motion (as the result of Doppler's effect) or the environmental fluctuations. For a narrowband system, $B_{BPF} < 10\% f_0$. The received signal's SNR is improved after the bandpass filter. The output of the bandpass filter is fed into a demodulator to bring the signal's useful bandwidth back around zero frequency, or a very low frequency. The demodulator contains a multiplier and a lowpass filter in both the in-phase and in-quadrature paths of the signal. The lowpass filter is used to remove the high frequency components in the in-phase and in-quadrature signals. It can also remove part of the noise. So the signal's SNR will be further improved after the lowpass filter. The simulation results in Section 3.4 were obtained using such a phase detector.

4.2.2 Envelope Extraction

In a realistic case, the received signal is real-valued and its spectrum contains both positive and negative frequency components. The negative frequency components have no physical meaning. They are superfluous and can be discarded with no loss of information. To do so, the real-valued signal's analytic representation is needed. The analytical representation of the sinusoidal signal $s_1(t)$ in Equation (4.2) is written as [25]

$$s_a(t) = s_1(t) + j \cdot \tilde{s}_1(t) = A(t)e^{j(2\pi f_0 t - \phi(t))} = A(t)e^{-j\cdot\phi(t)} \cdot e^{j\cdot 2\pi f_0 t} = \gamma(t) \cdot e^{j\cdot 2\pi f_0 t} \quad , \qquad (4.5)$$

where $\tilde{s}_1(t)$ is the Hilbert transform of $s_1(t)$ and j is the imaginary unit. $\gamma(t) = A(t)e^{-j\cdot\phi(t)}$ is called the complex envelope of the analytic signal. It can be extracted by multiplying $s_a(t)$ with $e^{-j\cdot 2\pi f_0 t}$. This process is called the envelope extraction. The output of the multiplier is $\gamma(t)$. The phase of $s_1(t)$ will then be retrieved as

$$\hat{\phi}(t) = -\arg\{\gamma(t)\} \ . \qquad (4.6)$$

If $s_1(t)$ is corrupted by the noise and the received signal at the receiver is $x(t)$ given in Equation (4.2), the analytical signal is re-written as

$$\begin{aligned} x_a(t) &= x(t) + j \cdot \tilde{x}(t) = A(t)e^{j(2\pi f_0 t - \phi(t))} + n_a(t) \\ &= A(t)e^{-j\cdot\phi(t)} \cdot e^{j\cdot 2\pi f_0 t} + n_a(t) = \gamma(t) \cdot e^{j\cdot 2\pi f_0 t} + n_a(t)\,, \end{aligned} \tag{4.7}$$

where $x(t)$ is the received real-valued noisy signal. $\tilde{x}(t)$ is the Hilbert transform of $x(t)$. $n_a(t)$ is the analytic representation of the noise $n(t)$. As depicted in Figure 4.2, $x(t)$ is converted to an analytic signal by means of a Hilbert transformer. The Hilbert transformer is implemented by an all-pass linear filter which shifts the phase of its input signal by 90 degrees. Then the analytic signal is multiplied by a local oscillator generated signal $e^{-j\cdot 2\pi f_0 t}$ for demodulation purpose. The phase will be retrieved using Equation (4.6). Meanwhile, the amplitude of $s(t)$ is obtained as

$$\hat{A}(t) = \left|\gamma(t)\right|. \tag{4.8}$$

The analytic signal facilitated mathematical calculations and makes the demodulation process easier than that in the conventional quadrature phase detector. In the spectral domain, the analytic signal only contains positive frequencies and therefore can avoid aliasing. For a narrowband signal, this approach is essentially identical with the quadrature phase detector.

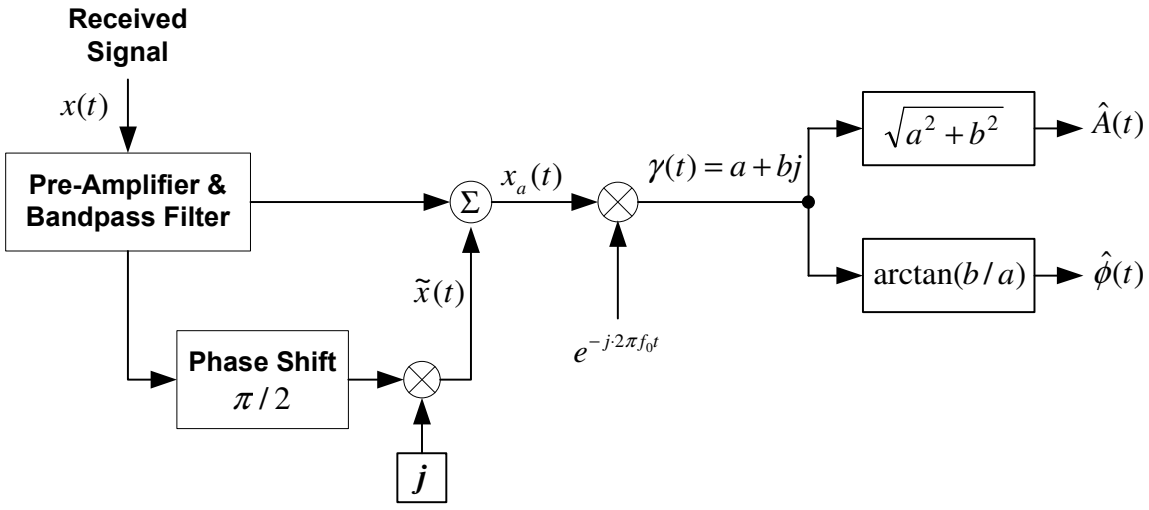

Figure 4.2: Phase Detection using Envelope Extraction

4.2.3 Quadrature Sampling

The proposed positioning method uses a sinusoidal transmission, which has some unique properties. We take advantage of them and propose to use a phase detection method based on quadrature sampling. The purpose is to reduce the system complexity and increase the processing speed.

As shown in Figure 4.3, the received signal $s_1(t)$ is sampled, within its m^{th} cycle, at two time instants t_m and $t_m + \frac{T}{4}$. These two instants of time are separated by one quarter of the signal period T, where $T = 1/f_0$. The values of this pair of samples (called a doublet) are

$$A_{m1} = A_m \cos(2\pi f_0 t_m - \phi_m) \tag{4.9a}$$

and

$$\begin{aligned} A_{m2} &= A_m \cos(2\pi f_0 (t_m + \frac{T}{4}) - \phi_m) = A_m \cos(2\pi f_0 t_m + \frac{\pi}{2} - \phi_m) \\ &= -A_m \sin(2\pi f_0 t_m - \phi_m) \end{aligned} . \tag{4.9b}$$

This sampling pattern is named the quadrature sampling. Here an assumption was made that the amplitude and the phase remain constant within the m^{th} cycle, i.e.

$$A(t) = A_m = A(t_m),\ \phi(t) = \phi_m = \phi(t_m) \text{ for } (m-1)T \le t < mT . \tag{4.10}$$

This assumption is reasonable because T is at milliseconds level in the PPHM method and the target is not moving that fast. Based on Equation (4.9) there are

$$\hat{A}_m = \sqrt{A_{m1}^2 + A_{m2}^2} \text{ , and} \tag{4.11a}$$

$$\hat{\phi}_m = -\tan^{-1}\left(\frac{A_{m2}}{A_{m1}}\right) - 2\pi f_0 t_m . \tag{4.11b}$$

The second term in Equation (4.11b), $-2\pi f_0 t_m$, is a constant and can be calculated when f_0 and t_m are known. $\{\hat{A}_m, \hat{\phi}_m\}$ are the estimates of the amplitude and the phase in the m^{th}

cycle. The same procedure is repeated in the $(m+1)^{th}$ cycle to get another estimates of the amplitude and the phase $\{\hat{A}_{m+1}, \hat{\phi}_{m+1}\}$.

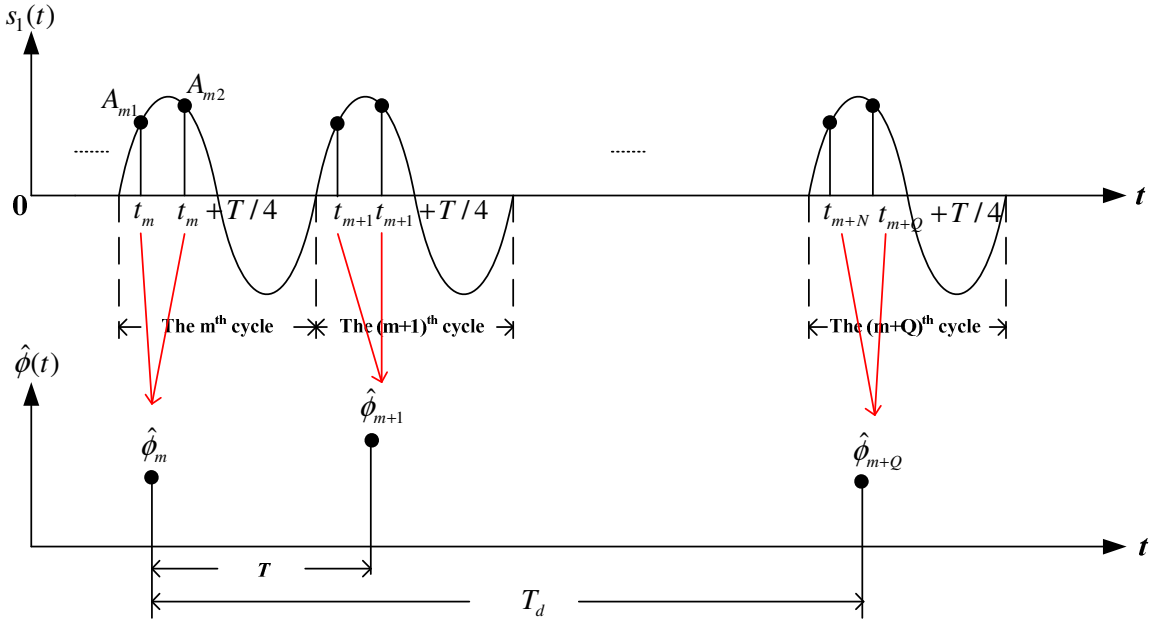

Figure 4.3: Illustration of Quadrature Sampling

The minimum quadrature sampling interval is the signal's period T; therefore, the maximum doublet sampling frequency is $f_d = 1/T = f_0$. In practice, the sampling doesn't need to be performed in each cycle of the received signal. This is because the environment fluctuations and the target speed variations are negligible, as compared to the received signal's frequency f_0, which could be up to several tens of kilohertz. A(t) and ϕ(t) will remain approximately the same over quite some cycles. The rate at which the quadrature sampling will be performed for amplitude and phase estimation is determined by the frequency shift due to the target's speed and the drifting of the oscillator which generates the sinusoidal signal at the reference platform, as shown in Equation (4.12).

$$f_d \geq 2\left(\frac{v_{\max}}{c} f_0 + f_{drift}\right). \tag{4.12}$$

In Equation (4.12), $v_{\max}$ is the target's maximum speed. f_{drift} is frequency caused by the oscillator drifting and environmental fluctuations. In another word, there will be sufficient information to correctly retrieve the amplitude and the phase when the received

data is sampled every T_d seconds ($T_d = 1/f_d$), or every Q cycles, where Q is the smallest integer that satisfies

$$Q > T_d / T \ . \tag{4.13}$$

When quadrature sampling is performed in these cycles, the positions of the doublet in the cycles should be the same, i.e. the time instant at which the received signal will be sampled in the $(m+Q)^{th}$ cycle has to satisfy Equation (4.14) as given below

$$t_{m+Q} = t_m + QT \ . \tag{4.14}$$

The system flowchart is depicted in Figure 4.4.

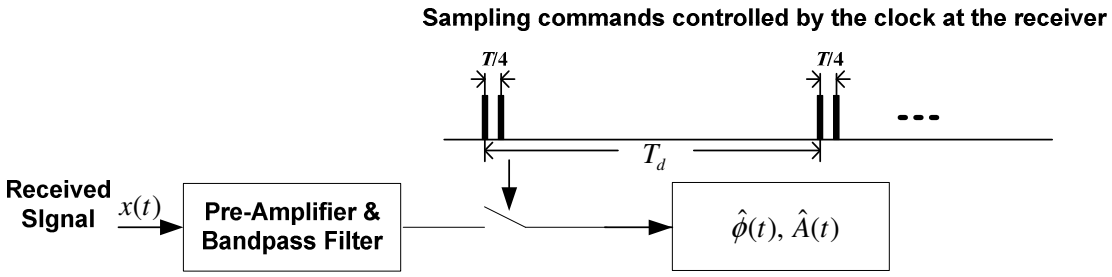

Figure 4.4: Block Diagram of Quadrature Sampling

To reduce the estimation error resulting from the measurement of the sampled data A_{m1} and A_{m2}, samples could be taken within a number of consecutive cycles. A pair of estimates is obtained in each of the cycles, then followed by an averaging. Specifically, starting from $t = t_m$, K consecutive cycles are selected (K<<Q). In each of the K cycles we get the estimated amplitude and the phase $\{A_m^k, \phi_m^k\}, 1 \le k \le K$ using Equation (4.11). Then an average is performed as following

$$A_m = \frac{1}{K}\sum_{k=1}^{K} A_m^k \ , \tag{4.15a}$$

$$\phi_m = \frac{1}{K}\sum_{k=1}^{K} \phi_m^k \ . \tag{4.15b}$$

The same average procedure will take place in the $(m+Q)^{th}$ cycle. In order to reduce the quantization noise during the analog-to-digital (A/D) conversion, a generalized quadrature sampling has been developed, in which four samples (a quadruplet), instead of two samples (a doublet) per period T are taken within one cycle and suitable averaging is performed consequently [28].

Figure 4.5(a) and (b) depict the simulation results of the quadrature sampling method. The simulation parameters were given in Table 3.1. The solid line indicates the result from a conventional quadrature phase detector and the "*" indicate the values obtained by using quadrature sampling.

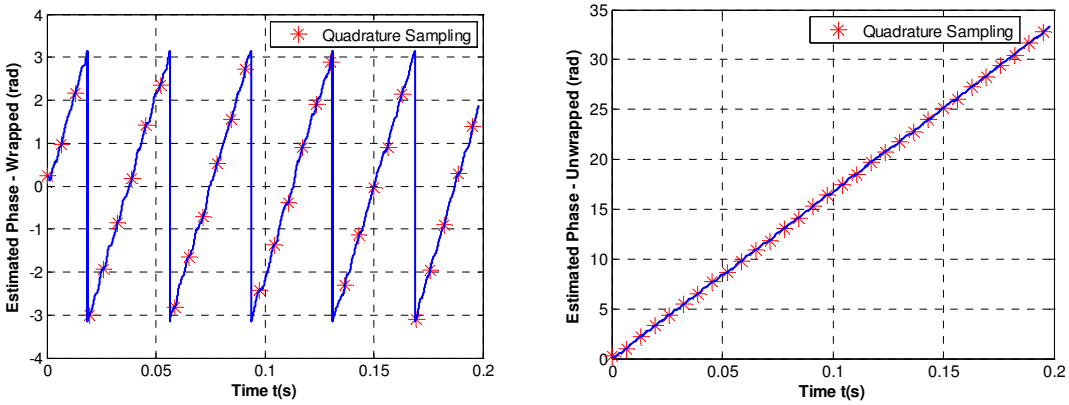

(a) (b)

Figure 4.5: Phase Estimation using Quadrature Sampling (a) Wrapped Phase (b) Unwrapped Phase

4.2.4 Phase Estimation Using Least Squares Technique

Many reasons cause signal loss at the receiver in a realistic scenario. For example, a big fish could block the light-of-sight from the target to the reference platform for a few seconds. Also, the target signal arrives at the receiver along more than one path. When the target is at a certain position, signals from different paths could cancel with each other and result in discontinuities in the received signal.

A simple solution is to use a receiver array. With the spacing between hydrophones, the signal destructive cancellation (because of opposite phases of two returns) happens at one hydrophone whereas the signal reinforcement will be obtained by another hydrophone in the array. The condition is that the array must be aligned with the received signal's direction of arrival.

The phase information carried in the missing data can also be restored based on a predicted signal model and previously received data, by means of appropriate signal processing techniques. With the tethered cable, we know the frequency and the amplitude of the transmitted sinusoidal signal. Assuming the environment is slow changing, and the target's speed is moderate, the transmitted signal's frequency and amplitude will not change too much when the signal arrives the receiver. It is reasonable to assume that the received signal can be expressed as

$$x_p(t) = \hat{A}(t)\cos(2\pi f_0 t - \hat{\phi}(t)) \ , \tag{4.16}$$

where $\hat{A}(t)$ and $\hat{\phi}(t)$ are the predicted amplitude and phase, respectively. Good estimates of $\hat{A}(t)$ and $\hat{\phi}(t)$ are those minimizing the difference between the received signal in (4.2) and the predicted model in Equation (4.16) based on some certain criteria. Here the least square error (LSE) criterion is used, which minimizes the square error between the predicted model and the received signal, i.e.

$$\{\hat{A}_{LSE}, \hat{\phi}_{LSE}\} = \min_{\hat{A},\hat{\phi}} E = \min_{\hat{A},\hat{\phi}} \int_0^{T_t} [x(t) - x_p(t)]^2 dt \ . \tag{4.17}$$

Here T_t is the observing window duration. Ideally it equals to the received signal length. For a continuous transmission, the received signal needs to be split into many segments. In each segment, we get an estimated phase using a phase detector described in previous sections. These segments could be overlapped with each other in order to get a smoothed phase monitoring. This method is essentially a sliding-window approach. By using trigonometric identities, Equation (4.16) can be re-written as

$$\begin{aligned} x_p(t) &= \hat{A}\cos(2\pi f_0 t - \hat{\phi}) = \hat{A}\cos(2\pi f_0 t)\cos\hat{\phi} + \hat{A}\sin(2\pi f_0 t)\sin\hat{\phi} \\ &= a\cos(2\pi f_0 t) + b\sin(2\pi f_0 t) \end{aligned} \ , \tag{4.18}$$

where $a = \hat{A}\cos\hat{\phi}$ and $b = \hat{A}\sin\hat{\phi}$. Here it is assumed that $\hat{A}(t) = \hat{A}, \hat{\phi}(t) = \hat{\phi}$ within one segment. The square error is

$$E(a,b) = \int_0^{T_t} [x(t) - x_p(t)]^2 dt = \int_0^{T_t} [x(t) - a\cos(2\pi f_0 t) - b\sin(2\pi f_0 t)]^2 dt \ . \tag{4.19}$$

According to the least square error criterion, $E(a,b)$ should be minimized with respect to a and b, so that the predicted sinusoidal model $x_p(t)$ can be fit into the received data $x(t)$. Therefore,

$$\frac{\partial E(a,b)}{\partial a} = 0 \ , \tag{4.20a}$$

$$\frac{\partial E(a,b)}{\partial b} = 0 \ . \tag{4.20b}$$

Expending Equation (4.20),

$$\frac{\partial E(a,b)}{\partial a} = 2\int_0^{T_t} [a\cos(2\pi f_0 t) + b\sin(2\pi f_0 t) - x(t)]dt \cdot \cos(2\pi f_0 t) = 0 \ , \tag{4.21a}$$

$$\frac{\partial E(a,b)}{\partial b} = 2\int_0^{T_t} [a\cos(2\pi f_0 t) + b\sin(2\pi f_0 t) - x(t)]dt \cdot \sin(2\pi f_0 t) = 0 \ . \tag{4.21b}$$

Consequently,

$$\int_0^{T_t} a\cos(2\pi f_0 t)\cos(2\pi f_0 t)dt + \int_0^{T_t} b\sin(2\pi f_0 t)\cos(2\pi f_0 t)dt = \int_0^{T_t} x(t)\cos(2\pi f_0 t)dt \ , \tag{4.22a}$$

$$\int_0^{T_t} a\cos(2\pi f_0 t)\sin(2\pi f_0 t)dt + \int_0^{T_t} b\sin(2\pi f_0 t)\sin(2\pi f_0 t)dt = \int_0^{T_t} x(t)\sin(2\pi f_0 t)dt \ . \tag{4.22b}$$

Since the incoming data will be digitized in most cases for follow-up processing, we assume that there are N data samples $x[n], n = 0, 1, \cdots, N-1$ within the observation window $0 \le t \le T_t$. These samples are denoted as a vector $\mathbf{x} = \mathbf{x}[\mathbf{n}]$. Furthermore, let

$$\mathbf{c} = \cos(2\pi f_0 \mathbf{n}) = [\cos(0)\ \cos(2\pi f_0 \cdot 1)\ \cos(2\pi f_0 \cdot 2) \cdots \cos(2\pi f_0 \cdot (N-1))]^{\mathbf{T}}_{1\times(N-1)} \ , \tag{4.23a}$$

$$\mathbf{d} = \sin(2\pi f_0 \mathbf{n}) = [\sin(0)\ \sin(2\pi f_0 \cdot 1)\ \sin(2\pi f_0 \cdot 2) \cdots \sin(2\pi f_0 \cdot (N-1))]^{\mathbf{T}}_{1\times(N-1)} \ . \tag{4.23b}$$

Here **T** represents the transposition of a vector (or a matrix). Equation (4.22) can be re-written in a matrix-form as

$$a \cdot \mathbf{c} \cdot \mathbf{c}^{\mathbf{T}} + b \cdot \mathbf{d} \cdot \mathbf{c}^{\mathbf{T}} = \mathbf{x} \cdot \mathbf{c}^{\mathbf{T}} \ , \tag{4.24a}$$

$$a \cdot \mathbf{c} \cdot \mathbf{d}^{\mathbf{T}} + b \cdot \mathbf{d} \cdot \mathbf{d}^{\mathbf{T}} = \mathbf{x} \cdot \mathbf{d}^{\mathbf{T}} \ , \tag{4.24b}$$

and consequently

$$\begin{bmatrix} \mathbf{c}\cdot\mathbf{c}^{\mathbf{T}} & \mathbf{d}\cdot\mathbf{c}^{\mathbf{T}} \\ \mathbf{c}\cdot\mathbf{d}^{\mathbf{T}} & \mathbf{d}\cdot\mathbf{d}^{\mathbf{T}} \end{bmatrix} \begin{bmatrix} a \\ b \end{bmatrix} = \begin{bmatrix} \mathbf{x}\cdot\mathbf{c}^{\mathbf{T}} \\ \mathbf{x}\cdot\mathbf{d}^{\mathbf{T}} \end{bmatrix} . \tag{4.25}$$

Solve for a and b in Equation (4.25),

$$\begin{bmatrix} a \\ b \end{bmatrix} = \begin{bmatrix} \mathbf{c}\cdot\mathbf{c}^{\mathbf{T}} & \mathbf{d}\cdot\mathbf{c}^{\mathbf{T}} \\ \mathbf{c}\cdot\mathbf{d}^{\mathbf{T}} & \mathbf{d}\cdot\mathbf{d}^{\mathbf{T}} \end{bmatrix}^{-1} \begin{bmatrix} \mathbf{x}\cdot\mathbf{c}^{\mathbf{T}} \\ \mathbf{x}\cdot\mathbf{d}^{\mathbf{T}} \end{bmatrix} . \tag{4.26}$$

With the values of a and b, the amplitude and phase of the received signal in the observing segment are obtained using following formulas:

$$\hat{A} = \sqrt{a^2 + b^2} \quad , \tag{4.27a}$$

$$\hat{\phi} = \angle(a + jb) \ . \tag{4.27b}$$

4.3 Phase Unwrapping

As the target moves, Δr increases. From Equation (3.5), $\Delta\phi$ will accumulate and will go far beyond (-π, π). However, the estimated phase from a phase detector has a "sawtooth" shape ranging between –π and π, as shown in Figure 3.7. This is because the phase detector uses the inverse tangent function to obtain the phase but the inverse tangent function is a many-to-one function. Any value beyond the interval (-π, π) will be mapped back into this interval [29]. The phase with ambiguity cannot correctly reflect the range increment. It needs to be unwrapped before being converted into the range increment. The process of "stretching" the wrapped phase is called phase unwrapping.

The unwrapping method used is based on searching and compensating. We observe the wrapped phase continuously to identify any difference between two adjacent data that is greater than 2π. These jumps are then corrected by adding a factor of 2π to all subsequent terms in the data sequence. This unwrapping method works well when the received signal is clean, as shown in Figure 4.6(a) and (b). However, for a weak signal embedded in strong noise like Figure 4.6(c), there will be many oscillating false phase jumps between $+\pi$ and - π, as demonstrated in Figure 4.6 (d). If these false jumps all get

the 2π compensation, the unwrapped phase will be seriously diverged from the true value, as depicted in Figure 4.6(e).

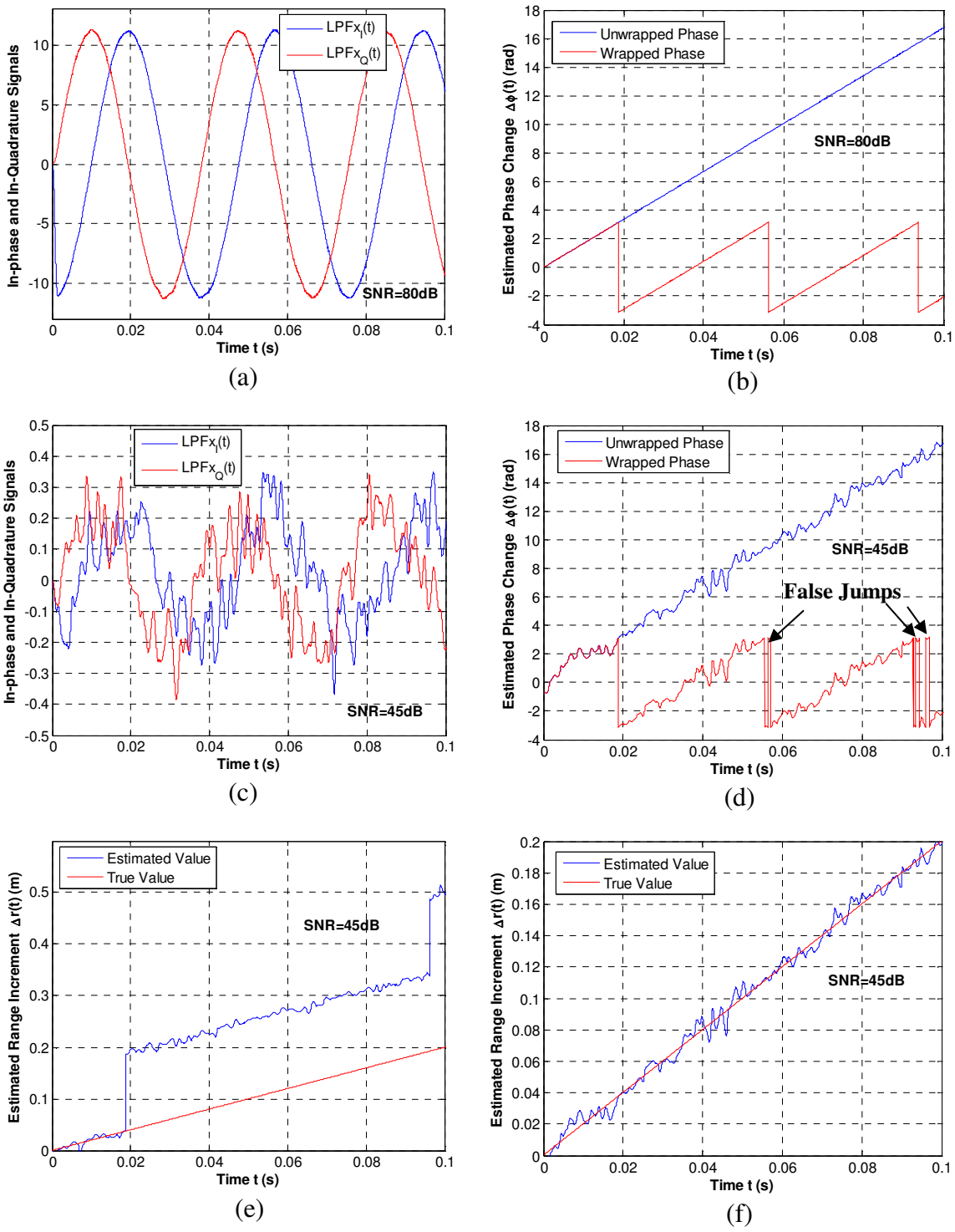

Figure 4.6: Phase Unwrapping of a Noisy Signal

The solution for the false phase jumps is to search the wrapped phase sequence and mark all phase jumps. For those downward jumps, 2π is added to all subsequent samples. For the upward jumps, 2π will be subtracted from all subsequent samples. The simulation result is given in Figure 4.6(f). In this way the divergence due to false phase jumps will be corrected.

Chapter 5 Error Sources from Propagation Medium

Discussions in Chapter 3 were based on the assumption of an ideal underwater environment, where the propagation medium is homogeneous and the acoustic wave travels from the target directly to the receiver along a straight line with constant velocity. The PPHM method requires a continuous phase monitoring. It is very sensitive to changes in the propagation medium.

In this chapter, we will discuss the error sources from a realistic underwater environment and will analyze their influences on the proposed system, with emphasis on sound speed variations, ocean currents, and multipath interferences from the seafloor. Solutions will be proposed to overcome the measurement errors due to these effects. Topics that will be covered in this chapter are:

- Sound speed variations
- Ocean currents
- Multipath interferences from the seafloor
- Other influence factors, including noise, acoustic scintillation, and water turbulences.

5.1 Sound Speed Variations

When the measured phase is converted into range increment using Equation (3.6), the sound speed c in water needs known. Since the propagation medium is varying in both space and time, c does not remain constant at all time. Generally, sound speed is related to the medium's density and compressibility. Particularly in the ocean, the sound speed is an increasing function of temperature, salinity, and pressure, the latter being a function of depth. It is customary to express c as an empirical function of these three independent variables: temperature (T) in degrees centigrade, salinity (S) in parts per thousand, and depth (z) in meters. An expression for this dependence is given as [30]

$$c = 1449.2 + 4.6\,T - 0.055\,T^2 + 0.00029\,T^3 + (1.34 - 0.010\,T)(S - 35) + 0.016\,z\,, \quad (5.1)$$

and a simplified formula is given as [31]

$$c = c_0 + 4.6T + 0.016z + 1.3(S\text{-}35), \tag{5.2}$$

where c_0 is the sound speed at the sea surface. T and S are the temperature and salinity at depth z, respectively. In shallow water, where the impact of z on c is small, the primary contributor to sound speed variations is the temperature.

Assuming the sound speed has variation Δc, then c is replaced by $c+\Delta c$ in Equation (3.6) as

$$\Delta\phi\frac{c+\Delta c}{2\pi f_0} = \Delta\phi\frac{c}{2\pi f_0} + \Delta\phi\frac{\Delta c}{2\pi f_0} = \Delta r + e_{\Delta c}\ , \tag{5.3}$$

where $e_{\Delta c} = \Delta\phi\frac{\Delta c}{2\pi f_0}$ is the range increment error caused by the sound speed variations. Since Δc is very small as compared to f_0, $e_{\Delta c}$ is negligible.

To get a real-time measurement of c, a sound velocimeter is installed on the reference platform and the claimed accuracy is up to a few centimeters per second [32, 33]. Or we can measure the sound speed's constitutive parameters - temperature, salinity and pressure – in real-time at the reference platform and calculate the sound velocity using Equation (5.1) or (5.2). For a short-term small area application, it can be further assumed that the sound velocity remains the same along the transmission path throughout the positioning task. The sound speed variation is more prominent in a shallow water environment because of the instability of the medium. If this method is applied in deep water, where the water depth is a few thousands of meters, water temperature and salinity usually are quite stable and sound speed is primarily determined by the water depth.

5.2 Ocean Currents

A prominent error source of the PPHM method comes from ocean currents. Ocean currents are continuous horizontal movements of bulk seawater along certain directions at or beneath the ocean's surface for a considerably period of time. Surface ocean currents flow horizontally within the upper 400 meters measured down from the sea surface and are generally driven by the wind. Deep ocean currents move between the ocean bottom and 400 meter below the surface. They are usually driven by seawater density and temperature gradients (or called thermohaline) [34]. There are a number of currents

flowing in the oceans around the world. Their speeds are different, varying from a few centimeters per second, to a few meters per second [34, 35]. Even within the same current, its speed changes in different seasons. The three currents flowing around British Columbia area are Alaska current, North Pacific current and California current [36]. These currents encounter the coast of North America and their velocities vary considerably, up to 1m/s [37].

In our positioning system, a current with speed v_c will introduce an additional phase shift in the received signal. To facilitate the discussion, it is assumed that there is no relative movement between the target and the reference platform. Not considering the noise, the received signal under the ocean current's influence is given as [38]

$$s(t) = \cos(2\pi f_0 (t - \tau_{AB})) = \cos\left(2\pi f_0 (t - \frac{r_0}{c + v_{AB}(t)})\right) = \cos(2\pi f_0 t - \phi(t)) \ , \qquad (5.4)$$

where $v_{AB}(t)$ is the current's speed.

$$\phi(t) = \frac{2\pi f_0 r_0}{c + v_{AB}(t)} \qquad (5.5)$$

is the phase shift of the received signal. Multiplying the numerator and denominator of Equation (5.5) by $\left[c - v_{AB}(t)\right]$ and assuming $c^2 >> v_{AB}^2$ [38], there is

$$\phi(t) \approx \frac{2\pi f_0 r_0}{c} - \frac{2\pi f_0 r_0}{c^2} v_{AB}(t) = \phi_0 - \frac{2\pi f_0 r_0}{c^2} v_{AB}(t) = \phi_0 - \Delta\phi_c(t) \, . \qquad (5.6)$$

In Equation (5.6), ϕ_0 is a constant value as along as r_0 and c are pre-determined.

$$\Delta\phi_c(t) = \frac{2\pi f_0 r_0}{c^2} v_{AB}(t) \qquad (5.7)$$

is the phase shift caused by the ocean current. It takes a positive sign if the signal is travelling in the same direction as that of the current and vice versa. Unlike the phase fluctuations due to random environmental variations, which are in all directions and transient, the phase shift caused by a current is accumulating over time. This is because the current is flowing steady along one direction, although its speed may vary. Observing from the receiver's end, the received signal's phase is changing as compared to the

reference signal when the ocean current presents. If this happens when tracking a moving target, the phase shift due to the target's movement will mix up with the phase shift due to the current. As a result the target's position cannot be tracked precisely.

A reciprocal transmission scheme is proposed here to eliminate the phase shift due to an ocean current [39]. This method has been used to measure ocean currents over a long term and distance in [40]. To remove the phase measurement error caused by currents, both a transmitter and a receiver (array) are needed at the reference platform (A) as well as at the target (B). The current flows from A to B. At $t = 0$, $s_0(t) = A\cos(\omega_0 t)$ is transmitted from A to B in the acoustic form through the water, and in the electrical form via the cable. It causes a positive phase shift in the acoustic signal received at B. Upon this acoustic signal's arrival, at $t = T$, the transducer at B sends the same signal $s_0(t)$ to A in both electrical and acoustic forms. The current causes a negative phase shift in the acoustic signal received at A. The received acoustic signal at B is

$$s_B(t) = A\cos[2\pi f_0 t - \phi_0 + \Delta\phi_c^B(t)] = A\cos[2\pi f_0 t - \phi_1(t)]. \tag{5.8}$$

The received acoustic signal at A is

$$s_A(t) = A\cos[2\pi f_0 t - \phi_0 - \Delta\phi_c^A(t)] = A\cos[2\pi f_0 t - \phi_2(t)]. \tag{5.9}$$

Assuming the current remains stable in the above process such that

$$\Delta\phi_c^B(t) = \Delta\phi_c^A(t). \tag{5.10}$$

$\phi_1(t)$ and $\phi_2(t)$ will be collected and transferred via the tethered cable to a processing center. By adding $\phi_1(t)$ and $\phi_2(t)$, the phase shift due to the ocean current will be removed as

$$\phi_1(t) + \phi_2(t) = 2\phi_0. \tag{5.11}$$

The block diagram of the reciprocal transmission is given in Figure 5.1. Performance of the reciprocal transmission scheme is evaluated using a simulated noisy signal at f_0 = 20 kHz. Figure 5.2 depicts the standard deviation of the estimated range increment $\Delta\hat{r}(t)$ versus SNR for 100 trials using the reciprocal transmission. The current speed is $v_c = 0.1$m/s. At SNR = 0 dB, the range increment estimation accuracy is within 1 mm. So

the reciprocal transmission method can effectively eliminate the phase shift due to a current.

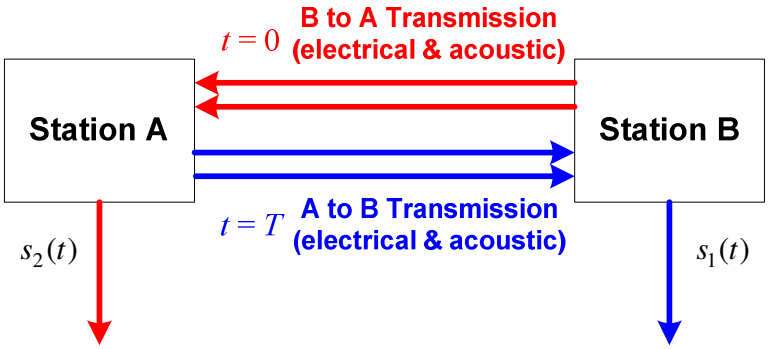

Figure 5.1: Block Diagram of the Reciprocal Transmission Method

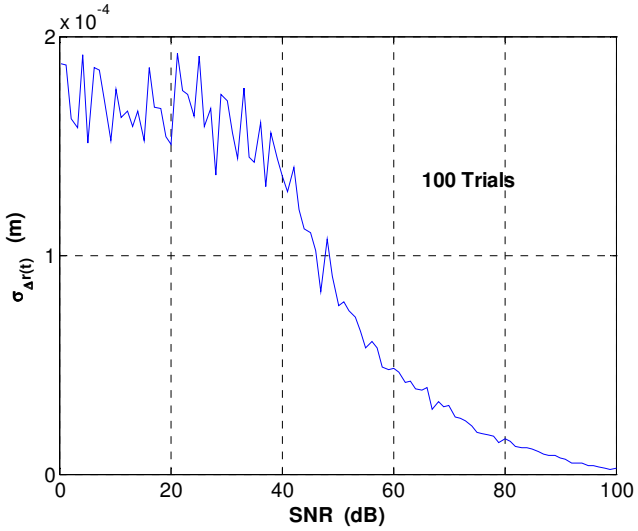

Figure 5.2: Standard Deviation of the Estimated Range Increment vs. SNR

5.3 Multipath Interference

In previous discussions, it was assumed that the acoustic signal is transmitted from the target to the reference platform only along the direct path. A clear line-of-sight between the transmitter and the receiver is assured with no discontinuities. In reality, the ocean is an acoustic waveguide limited above by the sea surface and below by the seafloor (called medium boundaries). As illustrated in Figure 5.3, the transmitted signal will undergo successive reflections at both boundaries and will travel toward the receiver along distinct paths, corresponding to distinct directions and durations. The received signals include the desired signal from the direct path, and a series of delayed parasite interference. The

positioning performance of the system will be highly degraded by these parasite signals. They are called the multipath interferences.

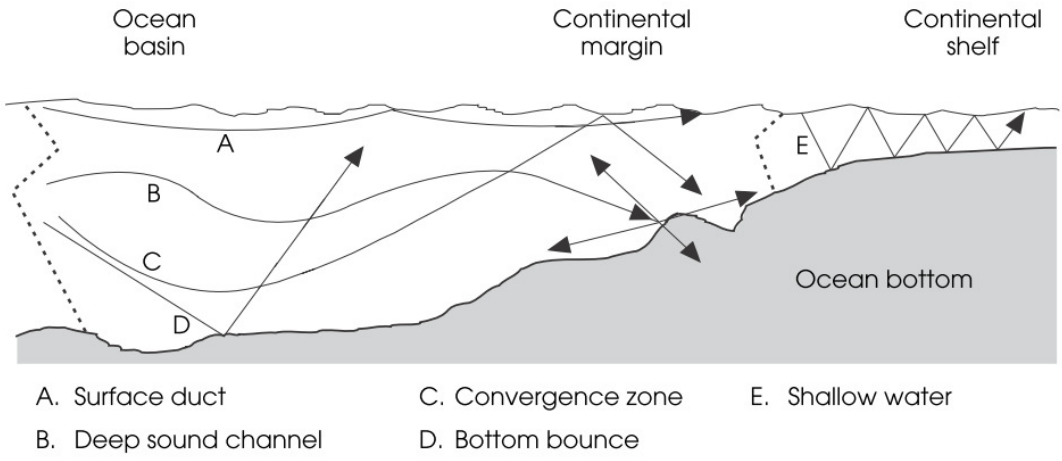

Figure 5.3: Schematic of Sound Propagation and the Multipaths Interferences in the Ocean [30]

Here is an example showing the phase measurement error caused by the multipath interferences. The receiver at the reference platform and the transmitter on the target are at the same height H as measured from the seafloor. r_0 is the initial range between the transmitter and the receiver. At $t=0$, the target starts moving horizontally. At $t=t_1$, the range from reference platform to the target is r. For simplicity, there is only one multipath, which is a reflected path from the seafloor. As shown in Figure 5.4, the length of the direct path is

$$r_d = r = r_0 + \Delta r \ . \tag{5.12}$$

The length of the path reflect from the seafloor is

$$r_f = 2H\sqrt{1+\frac{r^2}{4H^2}} \ . \tag{5.13}$$

Both the direct path signal and the seafloor reflected signal arrive at the receiver. They add and interfere with each other. Not considering the noise, the received signal is given in a complex form (to facilitate the discussion) as

$$s(t) = s_d(t) + s_f(t) = Ae^{j2\pi f_0(t-\frac{r_d}{c})} + MAe^{j2\pi f_0(t-\frac{r_f}{c})}$$
$$= \left[e^{-j2\pi f_0 \frac{r_d}{c}} + Me^{-j2\pi f_0 \frac{r_f}{c}} \right] Ae^{j2\pi f_0 t} = s_r(r) \cdot Ae^{j2\pi f_0 t} \quad . \tag{5.14}$$

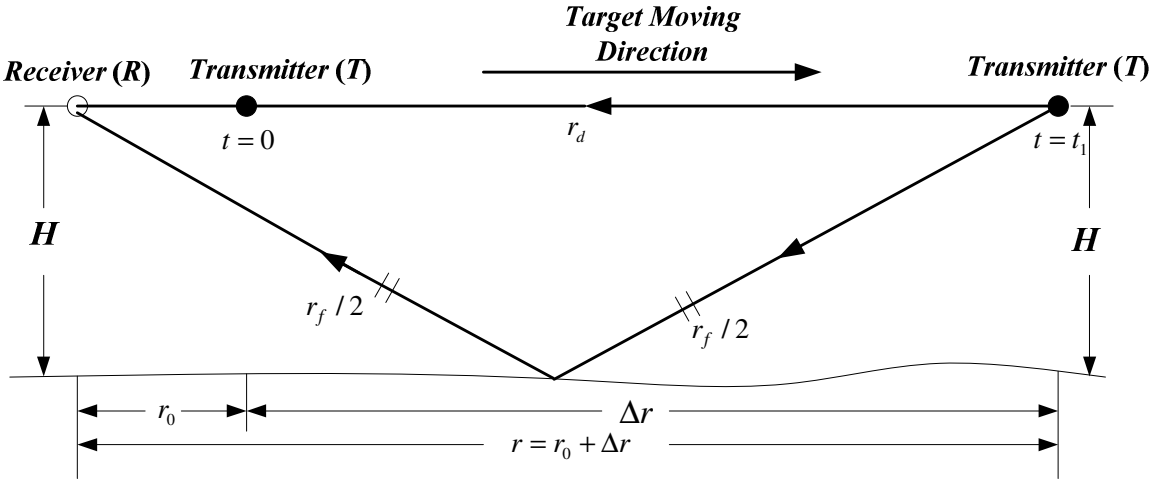

Figure 5.4: Direct Path and Reflected Path from the Seafloor

In Equation (5.14), $s_r(r)$ is the received signal's envelope. M is the relative strength of the multipath signal, which is a function of the transducer radiation pattern, distance, and incident angle as well as bottom properties. The signal is assumed to have a complete reflection from the sea bottom and no phase-shift is induced by the reflection. Phase measurement error $e_{\Delta\hat{\phi}}$ caused by the multipath is be obtained as

$$e_{\Delta\hat{\phi}} = \arg\left[\frac{s(t)}{s_d(t)}\right] = \arg\left[1 + Me^{j2\pi f_0 \frac{r_d - r_f}{c}}\right] = \arg\left[1 + M\cos(2\pi f_0 \frac{r_d - r_f}{c}) + jM\sin(2\pi f_0 \frac{r_d - r_f}{c})\right]$$
$$= \tan^{-1} \frac{M\sin(2\pi f_0 \frac{r_d - r_f}{c})}{1 + M\cos(2\pi f_0 \frac{r_d - r_f}{c})} = \tan^{-1} \frac{M\sin\left\{\frac{2\pi}{\lambda}\left[r - \sqrt{4H^2 + r^2}\right]\right\}}{1 + M\cos\left\{\frac{2\pi}{\lambda}\left[r - \sqrt{4H^2 + r^2}\right]\right\}} \tag{5.15}$$

The range measurement error $e_{\Delta\hat{r}}$ is proportional to $e_{\Delta\hat{\phi}}$ with a fraction of the wavelength, as given in Equation (3.8).

Figure 5.5 plots $e_{\Delta\hat{r}}$ as the function of Δr. M is assumed to be a constant. $e_{\Delta\hat{r}}$ presents a series of maxima and minima with a decreased frequency as Δr increases, but has a constant maximum amplitude $e_{\Delta\hat{r}\_\max}$ that depends only on M. The oscillating nature of $e_{\Delta\hat{r}}$ is called the Lloyd mirror effect [31]. Figure 5.6 (a) ~ (c) depict $e_{\Delta\hat{r}}$ as the function of Δr for different values of H. As H goes higher, the difference between the direct path and the reflected path gets bigger. $e_{\Delta\hat{r}}$ exhibits more oscillations when the direct path signal and the reflected path signal cancel or reinforce with each other. On the other hand, the oscillating $e_{\Delta\hat{r}}$ means that the range estimation error will not accumulating, as long as the distance between the transmitter and the receiver is appropriate. Figure 5.7 depicts the unwrapped phase shift as range increases. As M goes up, the phase error increases. But as long as M is fixed, the phase error will fluctuate within a certain range, which means that $e_{\Delta\hat{\phi}}$ could be either positive or negative, but cannot exceed a limit. The limit of $e_{\Delta\hat{\phi}}$ could be obtained by solving the following optimization problem:

$$\max_{0\le y\le 2\pi} f(y) = \max_{0\le y\le 2\pi} \left\{ \tan^{-1}\left[(M\sin y)/(1+M\cos y) \right] \right\}. \tag{5.16}$$

Solving Equation (5.16) yields the maximum phase error

$$e_{\Delta\hat{\phi}\_\max} = f_{\max}(y) = \tan^{-1}(M/\sqrt{1-M^2}) \qquad at \quad y = \cos^{-1}(-M)\ . \tag{5.17}$$

The maximum measurement error for Δr is

$$e_{\Delta\hat{r}\_\max} = \lambda e_{\Delta\hat{\phi}\_\max}/2\pi\ . \tag{5.18}$$

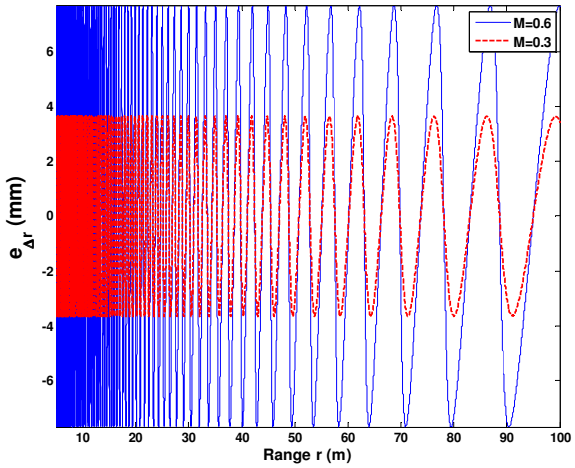

Figure 5.5: Range Measurement Error from Multipath Interferences

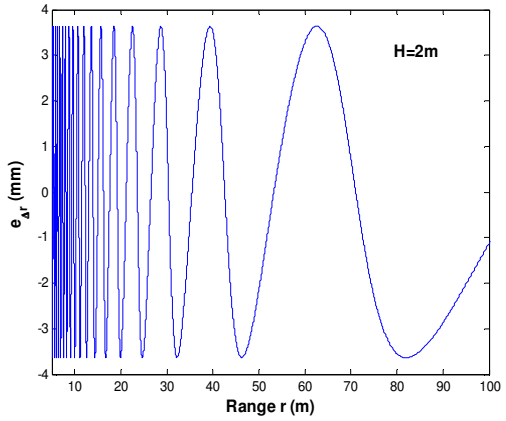

(a)

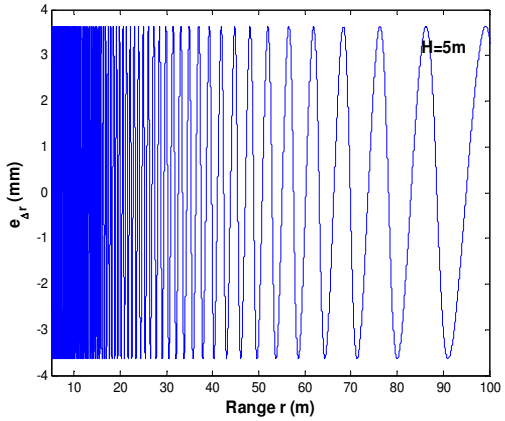

(b)

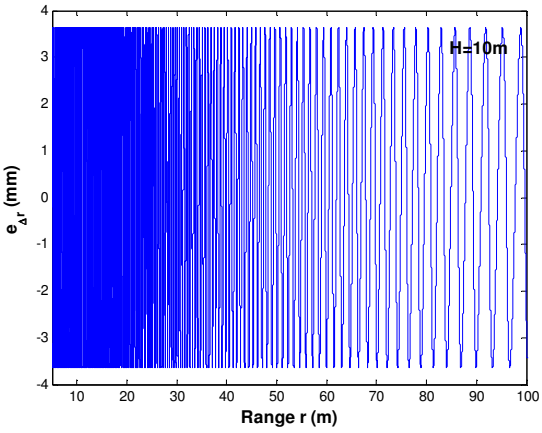

(c)

Figure 5.6: Range Measurement Error from Multipath Interferences as H changes (a) H=2m; (b) H=5m; (c) H=10m.

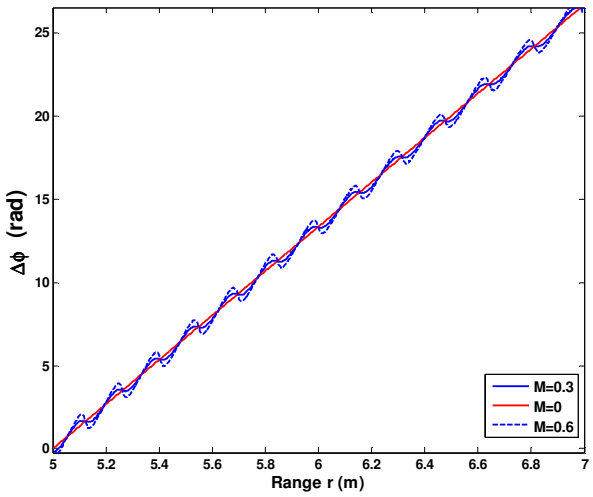

Figure 5.7: Unwrapped Phase w/o Multipath Interferences

The phase error due to multipath interferences has to be minimized to maintain the positioning accuracy. If the positions of the transmitter and the receiver are known, and the target is stationary or moving very slowly, it is reasonable to assume that the reflected-path signals are coming from specific directions. Propagation modes of acoustic wave in ocean, such as the ray theory or the normal modes theory, could then be used to calculate the possible propagating paths linking the transmitter and receiver [41~43]. Since multipath signals generally arrive from directions different from that of the direct path signal, they could be suppressed by utilizing suitable radiation patterns at the transmitter and the receiver. Such patterns will consist of a narrow mainlobe and small side lobes. The transmitting or receiving beams should be kept aligned along the direct path. Calculations of propagating paths assumes iso-speed acoustic channel. Taking account of the sound speed variations and the turbulence in the water, adaptive beamforming method will be a better choice. By using an adaptive beamformer, we are able to achieve maximum reception in the direct-path direction while reject interference signals from other directions. The weights of each of the hydrophones in the array are varied and iteratively computed based upon different criteria [44].

In the application of tracking a moving target with considerably fast speed, the multipath is not easy to be rejected by means of beamforming. This is because the directions of multipath interferences are varying all the time. Direct path signal could be

isolated from multipath signals by their different time of arrival if short pulse transmission is used. This requires a broadband receiver and transmitter. The primary disadvantage of using a short transmission pulse is that the overall amount of energy that the system is capable of putting into water is reduced. Hence the overall SNR is reduced and the system performance will be degraded.

Here is a numerical example to show the overlap of direct path signal with the reflected path signal. The transmitted signal is a continuous sinusoidal wave. Figure 5.8 shows the spectrograms of the transmitted signal and the received signal ($f_0 = 20kHz$, observing time $T_t = 11ms$). The transmitter and the receiver are assumed to be at the same heights measured from the seafloor. $H = 5m$. The maximum range from the transmitter to the receiver is $r = 50m$. If there is only one reflected path from the seafloor, according to Equation (5.13), the signal from the reflected path will arrive the receiver 0.66 ms later than the direct path signal. In Figure 5.8(b), these two returns overlap with each other.

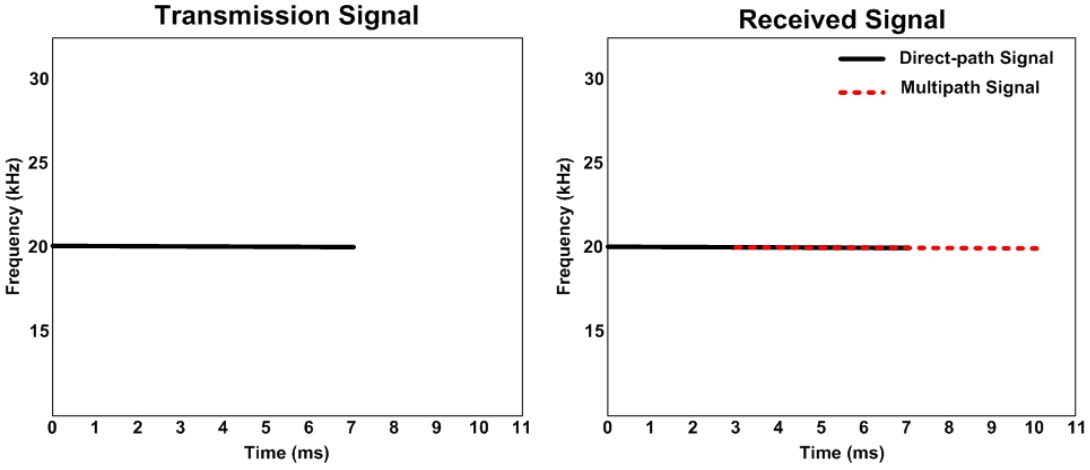

Figure 5.8: Spectrogram of a Single Frequency Signal (a) Transmitted Signal; (b) Received Signal

To separate the multipath signal from the direct path signal, the transmission should contain more information, and this information will undergo different changes when travelling along direct path or reflected paths. One example has been presented in [45], where a 67 kHz acoustic signal with a 127 bit phase modulated pseudo-random-noise (PRN) code is used as the transmission to monitor the acoustic scintillations in Saanich

Inlet. The bit width of the code was chosen such that multipaths separated in arrival time by 266μs (18 cycles) could be distinguished.

The phase modulation is not applicable in our method because the information in the phase should be preserved for range recovery. We choose to modulate the frequency. The transmitted signal is proposed as a sequence of tones with different frequencies. These frequencies are located closely to reduce the system bandwidth and maintain the narrowband property. Figure 5.9 shows how this method works. In Figure 5.9(a), the transmitted signal starts with a pulse (P1) which has its frequency at $f_1 = 15$ kHz and duration $\tau_1 = 0.2$ ms. The pulse (P2) following P1 has its frequency at $f_2 = 20$ kHz and duration $\tau_2 = 0.5$ ms. The third pulse (P3) in this sequence has $f_3 = 25$kHz and $\tau_3 = 0.5$ ms. After that, the same pattern P1→P2→P3 repeats throughout the entire transmission.

In Figure 5.9(b), the direct path signal (the solid line) arrives at the receiver at $t = 0$. The reflected-path signal (the dash line) arrives $t_1 = 0.66$ ms later. The direct path signal overlaps with the multipath signal along the time index. But their differences along the frequency axis can be identified. Under most circumstances, the direct path signal arrives earlier at the receiver and experiences less propagation loss. So the multipath signal can be isolated by observing its TOA in the time axis and its spectrum in the frequency axis. Then a time-varying filter is applied to the received data. This filter $h(t, f)$ has a comb-like spectrum. It rejects data with $f = f_1$ at $t_1 \le t \le t_1 + \tau_1$, rejects data with $f = f_2$ at $t_1 + \tau_1 \le t \le t_1 + \tau_1 + \tau_2$, and rejects data with $f = f_3$ at $t_1 + \tau_1 + \tau_2 \le t \le t_1 + \tau_1 + \tau_2 + \tau_3$, as indicated in Figure 5.9(c) by the blue dash-dotted lines. Finally in Figure 5.9(d), the output of the time-varying filter contains all the information of the direct path signal whereas rejects the reflected path signal. A phase detector will be used next for target position recovering. Here the solution works only if there is one multipath signal. A general conclusion could be drawn in a similar but more complicated manner when more multipath path signals are presented in the received data.

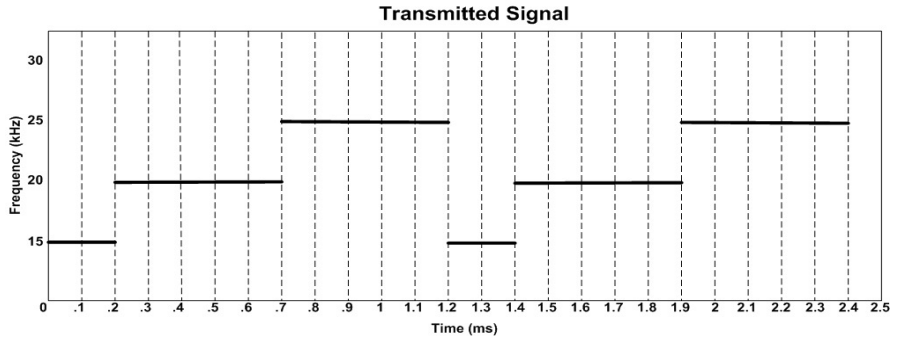

(a)

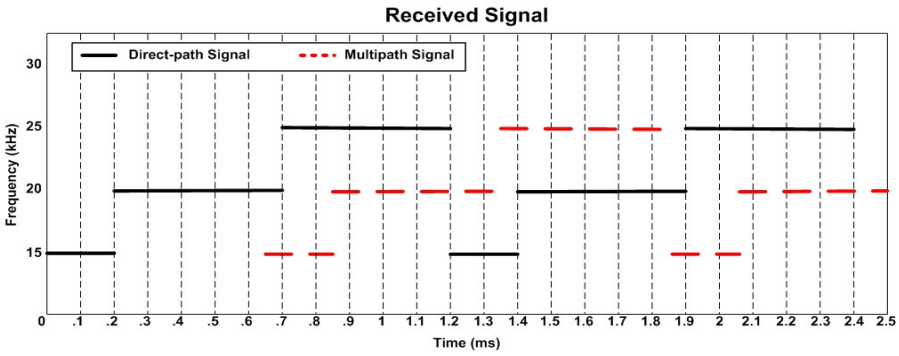

(b)

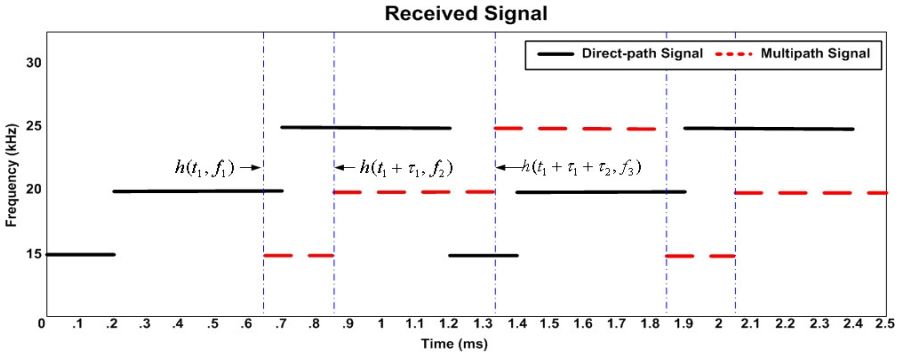

(c)

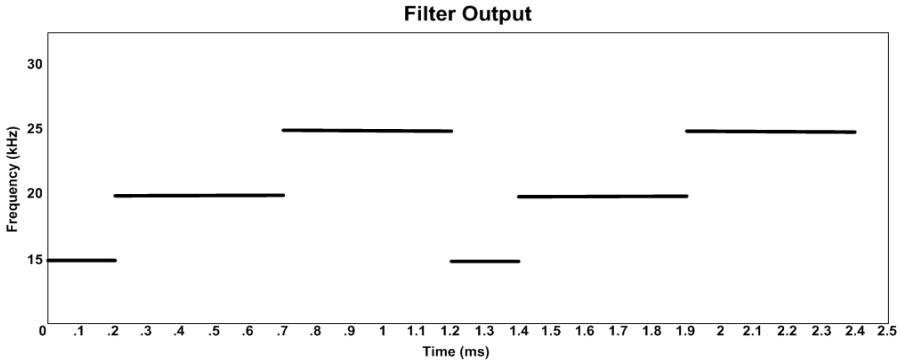

(d)

Figure 5.9: Transmission Pulses on Different Frequencies

There is only one reflected path considered in above discussions. In reality, the number of reflected paths is variable depending on the configuration. It could be several tens or hundreds in a long-distance propagation and will show up in the received signal as a continuous signal trail. A commonly used model in an underwater acoustic channel is Rician fading model [46]. In this model, the received signal arriving from a large number of reflected paths can be expressed as

$$x(t) = A_1 \cos(2\pi f_0 t - \phi) + \sum_{k=1}^{K} a_k(t) \cos[2\pi f_0 (t - \tau_k(t))] \tag{5.19}$$

if the transmitted signal is given in Equation (3.1). In Equation (5.19), there is one dominant direct path signal in the received signal. This model will be the basis for future investigation of multipath interference cancellation.

In most cases, the direct path signal undergoes less transmission loss and will exhibits larger amplitude at the receiver, as compared to the multipath signal. Therefore the received signal's amplitude can be used as auxiliary information for multipath interference separation. It is obtained at the same time the phase estimation is performed, as shown in Figure 4.1, 4.2, and Equation (4.11), (4.27).

5.4 Other Environmental Factors

In the ocean, refractive index irregularities associated with variability in temperature, density and salinity distort the spherically spreading acoustical wave fronts as they travel away from the transmitter towards the receiver. As a result, the amplitude and the phase of the signal at the receiver show variations that evolving with time. These fluctuations are referred to as acoustical scintillations and are analogous to the "twinkling" of stars as a result of the turbulent atmosphere. Acoustical scintillation, by analogy with similar atmospheric and astronomical studies using electromagnetic radiation, analyses the received fluctuation of an acoustic signal to infer properties of the propagation medium. The experiment results provided by Di Iorio and Farmer [37, 45, 47, 48] show that the acoustic scintillations caused by the inhomogeneous medium are rapidly fluctuations in both the received signal's amplitude and the phase. In their experiments, an acoustic signal is transmitted from one end of the designated channel to the other end. The received signal's amplitude and phase are measured using the cross-correlation method. The recorded amplitude and phase are analyzed in both the time domain and the

frequency domain. The fluctuations due to the acoustic scintillations appear as many small high frequency components in the frequency domain as shown in [37]. These fluctuations can be removed by a lowpass filter.

Transmitted signal propagates in the ocean and arrives at the receiver along with noise. There are three sources of noise to be considered in underwater positioning systems: thermal noise, ambient noise, and shipping noise. In common with any electrical receiving system, a receiver in a positioning system adds its own noise to the signals it receives. The thermal motion of electrons in wires, resistors, and etc, is the source of a thermal noise. Usually the thermal noise is negligible compared to other noises coming from the ocean. Ambient noise, or called background noise, is the noise from the ocean. Examples of sources contributing to ambient noise in the ocean include waves, marine creatures, wind, rain, earthquakes, and volcanoes. Ships are also important noise sources. Shipping noise mainly comes from the propulsion machinery, the auxiliary machinery and the propellers. If the system is deployed deep under the water, there is no need to consider the ship noise. Generally, all these noise tend to mask the useful part of the signal. As demonstrated by simulation results in Chapter 4, the phase unwrapping does not work well in an environment with strong noise. To improve the phase measurement quality, the SNR can be improved through: 1) using directional narrow-beam transmitter and receiver (or receiver array); 2) using higher order bandpass and lowpass filters before the phase estimation.

In addition to ocean currents, turbulences also cause measurement error in the PPHM method. For a long-term, large-scale turbulence induced by the rotation of the Earth, a reciprocal transmission will eliminate the errors [49]. However, the effects of a short-term, small-scale turbulence due to local temperature and salinity variations on the PPHM method is still unclear and needs more explorations in the future.

Chapter 6 Applications

In this chapter three potential applications for the PPHM method will be investigated. They are: 1) monitoring of submerged tectonic plate movements; 2) measurement of ocean current speed and perturbations along a path; and 3) tracking an ROV within an underwater acoustic sensor network.

The long-term monitoring of submerged tectonic plate movement is important in the verification of theoretical models in ocean seismology and in the prediction of earthquakes and associated tsunamis. The PPHM method can be employed to monitor the relative movements or deformations between two adjacent tectonic plates. To do this, two observing stations are installed on each of two adjacent plates within a short distance to the plate boundary. A tether cable links them for data transmission and power supply. Transceivers are mounted on both stations. An acoustic signal is transmitted from one station to the other. The phase of this signal will be monitored at the receiver's end. Any displacement between plates along their boundary will cause a phase shift in the received acoustic signal. We analysis the phase shift and conclude the plates movement.

Phase error caused by ocean currents was discussed in Chapter 5 and the reciprocal transmission scheme was proposed to maintain positioning accuracy. From another point of view, we can capture the phase shift caused by the current and convert it to the current speed. Unlike the conventional current meter which measures the current speed at one location, this method will help us observe the slow changes and rapid perturbations in the current speed along the propagation path. This method requires two or more stations on the seafloor, synchronized through a connecting underwater electrical cable, that can transmit and receive an acoustic signal.

Underwater acoustic networks have gained more and more attention in the past few years [23, 50]. ROVs play an important role in the underwater acoustic network for several tasks including scientific data collection. Chapter 3 investigated the positioning of a moving ROV in a horizontal plane. A proper receiver array's configuration and associated coordinate calculations are still needed for locating a ROV in the 3D space in real-time. Another technical challenge of tracking the moving ROV is how to separate multipath interferences from the direct path signal, considering the uncertain arriving

times and directions of multipath interferences. The solution could be good coding of the duration and frequency of the transmission signal.

6.1 Monitoring of Submerged Tectonic Plate Movements using Acoustic Signals

6.1.1 Tectonic Plates

Natural hazards, especially earthquakes, tsunamis, and volcanic eruptions have occurred frequently in the past few years. Examples include the earthquakes that struck Haiti and Chile earlier this year, and the tsunami that occurred in the Indian Ocean as the consequence of an ocean earthquake in 2004. These violent changes of the Earth's crust have taken place primarily at the boundaries of tectonic plates. Tectonic plates are defined as the seven major and many minor plates that compose the Earth's outermost layer (called the crust) and a portion of the mantle layer beneath it [51], as shown in Figure 6.1. Tectonic plates are rigid, but in constant motion because they float atop the planet's liquid interior. Their movements result in three types of plate boundaries [51]: convergent boundaries, divergent boundaries, and transform boundaries (shown in Figure 6.2).

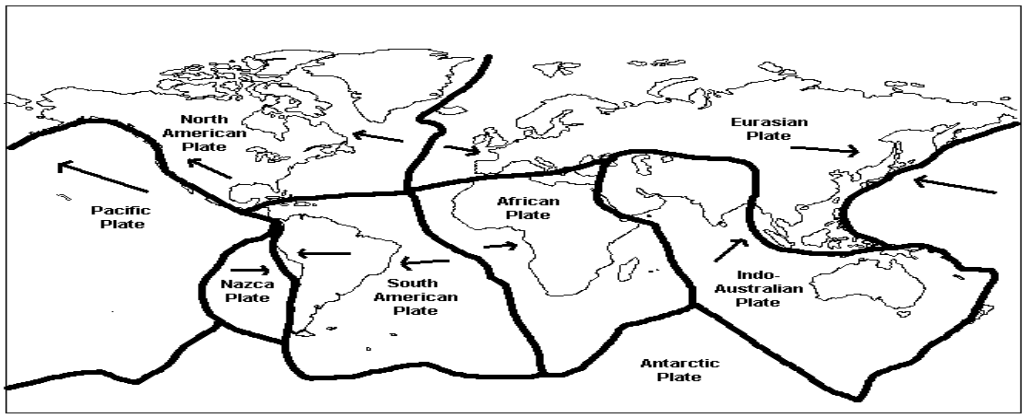

Figure 6.1: Tectonic Plates on Earth [52]

It is essential to understand how plates move and to monitor their motions in a long term to make reliable and timely forecasts of these hazards. Measurement of plate tectonic movement is of particular concern in the northeast Pacific off the coasts of British Columbia, Washington, and Oregon, due to the presence of the Juan de Fuca tectonic plate. This plate is one of the smallest of Earth's several dozen plates, bounded

by the coast of Oregon, Washington, and British Columbia to the east and the gigantic Pacific tectonic plate a few hundred kilometers to the west.

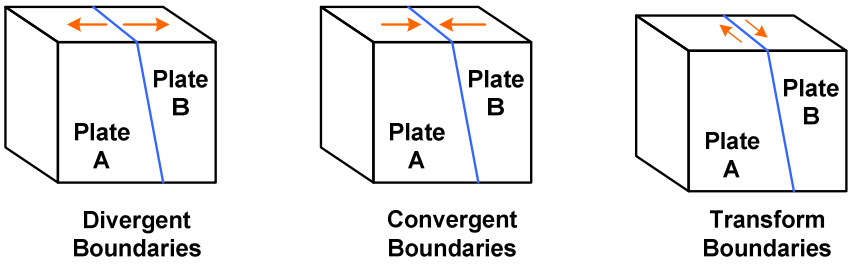

Figure 6.2: Tectonic Plate Movements: Three Types of Plate Boundaries

The motion of tectonic plates can either be estimated using mathematical models based on geodetic data collected from the seafloor, or be directly measured with proper positioning strategies and instruments. In the former, plate motions are formulated as a set of equations encompassing angular velocities of the motion of each of the major tectonic plates covering the Earth's surface. Mathematical models, such as the NUVEL-1 model, the NUVEL-1A model, and the MORVEL model [53] have been developed to estimate the relative motions between plates. Among these models, the recently proposed MORVEL (Mid-Ocean Ridge Velocities) model achieves considerable accuracy with the help of multibeam sonar, side-scan sonar, dense magnetic surveys, and GPS stations [53].

Plate movement can also be monitored directly by means of ground-based or space-based geodetic measurements. Ground-based measurements are made with conventional, but very precise ground-surveying techniques, using laser-electronic instruments. However, because plate motions are global in scale, they are best measured by space-based or satellite-based methods, which take precise, repeated measurements of carefully chosen points on the Earth's surface separated by hundreds to thousands of kilometers. The three most commonly used space-based geodetic techniques - very long baseline interferometry (VLBI), satellite laser ranging (SLR), and the GPS - are based on technologies developed for military and aerospace research, notably radio astronomy and satellite tracking. Among the three techniques, to date the GPS has been the most useful for studying the Earth's crustal movements.

Plate tectonic boundaries are among the most dynamic geologic environments on the planet and the majority of them are located underwater. The three above common measurement techniques are not applicable to the measurement of undersea plate

movement since all of them involve the use of electromagnetic energy that does not penetrate significantly into sea water. Traditional solutions for seafloor plate tectonic motion measurements are to estimate the strain accumulation and stress release on the seafloor using seismic slip records or onshore geodetic techniques. A system that combines GPS and acoustic technique (GPS/A) has been developed by the seafloor geodesy group at Scripps Institution of Oceanography to determine the absolute position of seafloor reference points [16, 32, 54]. This GPS/A system involves synchronizing data collection to locate geodetically a research vessel in the terrestrial reference frame by means of the GPS system, while simultaneously locating a seafloor transponder array with respect to the research vessel using a LBL localization approach. The relative locations of the seafloor transponders can be determined with centimeter accuracy. The technical challenges within this GPS/A method include synchronous GPS and acoustic data collection, determination of onshore geodetic reference motions, knowledge of the sound speed profile through the water column, tidal variations, and orientation of the seafloor units [16].

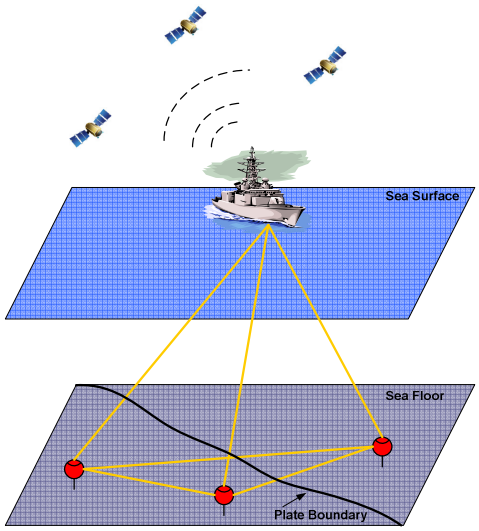

Figure 6.3: GPS/Acoustic Measuring System

The measurement accuracy of GPS/A method is approximately 1-2 cm at an operating range of 4-5 km. Localization beneath the sea surface is performed by means of the LBL method because GPS radio frequencies do not propagate well in water. To achieve maximum accuracy in an LBL configuration, the locations of the hydrophones must be precisely determined, which requires time-consuming and expensive location tests.

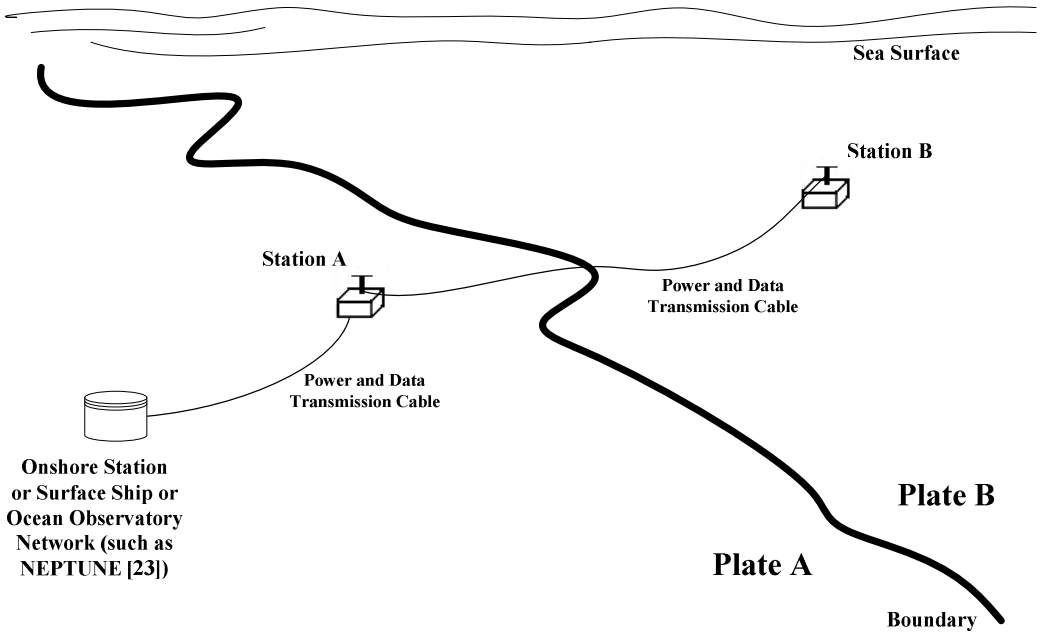

Figure 6.4: Monitoring of Submerged Tectonic Plate Movements using Phase Measurement

6.1.2 Monitoring of Submerged Tectonic Plate Movements

The PPHM method measures the displacement between the points of interest, instead of their individual positions. Therefore it can be used to measure the relative motions of two adjacent tectonic plates. The configuration of the PPHM system is depicted in Figure 6.4. Plate A and B are two adjacent oceanic plates. Any displacement along their boundary will be notified and their relative movement will be deduced accordingly. For this purpose, one station is installed on each of the two plates within a pre-determined distance to the plate boundary. The two stations are connected by a tethered cable, which is a data transmission link between stations. Power is supplied by a cable connected to an onshore station or a seafloor observatory node. The seafloor is assumed smooth and flat to ensure a clear line of sight between Station A and Station B. The oscillator on A generates the sinusoidal signal $s_0(t) = A\cos(2\pi f_0 t)$ and sends it to B through the tethered cable. This electrical signal will serve as a reference for phase estimation at B. At the same time, $s_0(t)$ is passed to a hydrophone and sent out to B through water in the acoustic form. If there is no movement between the two plates, the received signal at B only contains a phase shift ϕ_0 caused by the distance between A and B, r_0. If Plate B moves, an

additional phase shift occurs in the received signal. Putting it simply, Plate B is assumed moving away in the radial direction with respect to Plate A and the displacement between A and B is Δr . The received signal at B is

$$s(t) = A\cos(2\pi f_0(t-\Delta t)) = A\cos(2\pi f_0 t - \phi_0 - \Delta\phi), \tag{6.1}$$

where

$$\Delta\phi = \frac{2\pi}{\lambda}\Delta r \tag{6.2}$$

is the phase shift introduced by the displacement Δr . The relative movement between the two plates is obtained by continuously monitoring $\Delta\phi$.

The observing stations will be deployed on the tectonic plates at a depth of up to a few thousands of meters. In such deep water, the temperature and salinity are quite stable and sound speed is primarily determined by the water depth [31]. If the transmitter and the receiver are at the same heights, the sound speed is approximately constant and can be calculated from measurements of the local temperature, pressure, and salinity, or can be measured directly with the claimed accuracy of a few centimeters per second [16, 33]. Ocean current and turbulence exist in deep water. They can be eliminated by using the reciprocal transmission method investigated in Chapter 5.

6.1.3 Acoustic Ray Refraction

The plate boundary and the area around it have very complicated topographical features. The overlap of two tectonic plates usually stretches up to a few kilometers. When the observing stations are installed on the seafloor, the distance between the two stations should be comparable to the width of the overlap region. However, an acoustic wave will travel along a bent path instead of a straight line in deep water. This phenomenon is called the acoustic ray refraction and it put an upper limit on the distance between the observatory stations.

The direction of sound propagation path is determined by the sound speed profile. As the water depth increases, so will be the pressure and therefore the sound speed. According to Snell's law, the sound ray will bend toward the direction with lower sound speed [31]. As a result, the propagation path of the acoustic signal in the deep sea is a

curve bending upward, as shown in Figure 6.5(a). This refraction causes shadow zones in the propagation path. It also brings errors in determination of the distance between the transmitter and the receiver.

To avoid shadow zone, the installation sites and heights of the transmitter and the receiver should be chosen carefully. Here is a numerical example to illustrate the refraction problem. Let the sound speed profile given by the simplified formula [31]

$$c = c_0 + 4.6\mathrm{T} + 0.016z + 1.3(\mathrm{S}-35). \tag{6.3}$$

Assuming the sound speed at the sea surface c_0 = 1450 m/s, the temperature T = 0°C, and the constant salinity S = 35 ppt, the sound speed will be

$$c = 1450 + 0.016z. \tag{6.4}$$

If a transmitter is installed on a tower with its height h = 5m measuring from the seafloor and the water depth is z_2 = 2000 m, the depth of the transmitter will be $z_1 = z_2 - 5 = 1995$ m. From Equation (6.4), the sound speed at the transmitter is $c_1 = 1450 + 0.016z_1 = 1481.92$ m/s. The transmitter sends out an acoustic signal to the receiver at $\theta_1 = 90°$. The sound ray will be refracted upwards. The radius of its arc is [31]

$$R = (ab)^{-1}, \tag{6.5}$$

where $a = \sin\theta_1/c_1$. In this example, $R = c_1/b = 1481.92/0.016 = 92620$ m. If a receiver is installed at the same height as that of the transmitter, in order to avoid the shadow zone the distance between the transmitter and the receiver should be smaller than

$$r_d = 2\sqrt{R^2 - (R-h)^2}\ , \tag{6.6}$$

where h is the height of the transmitter/receiver with respect to the seafloor. In this example, $r_d \approx 1925$ m. It is the maximum distance between the transmitter and the receiver that will avoid the shadow zone. This distance can be extended if the heights of the transmitter and the receiver are increased. In practice, the tower on which the transmitter or the receiver be installed has a maximum height of a few meters. To further increase the height, the transmitter and the receiver can be installed on slopes or hills with the valley in between, as depicted in Figure 6.5(b). This demands an intensive survey on the seafloor's topographic map.

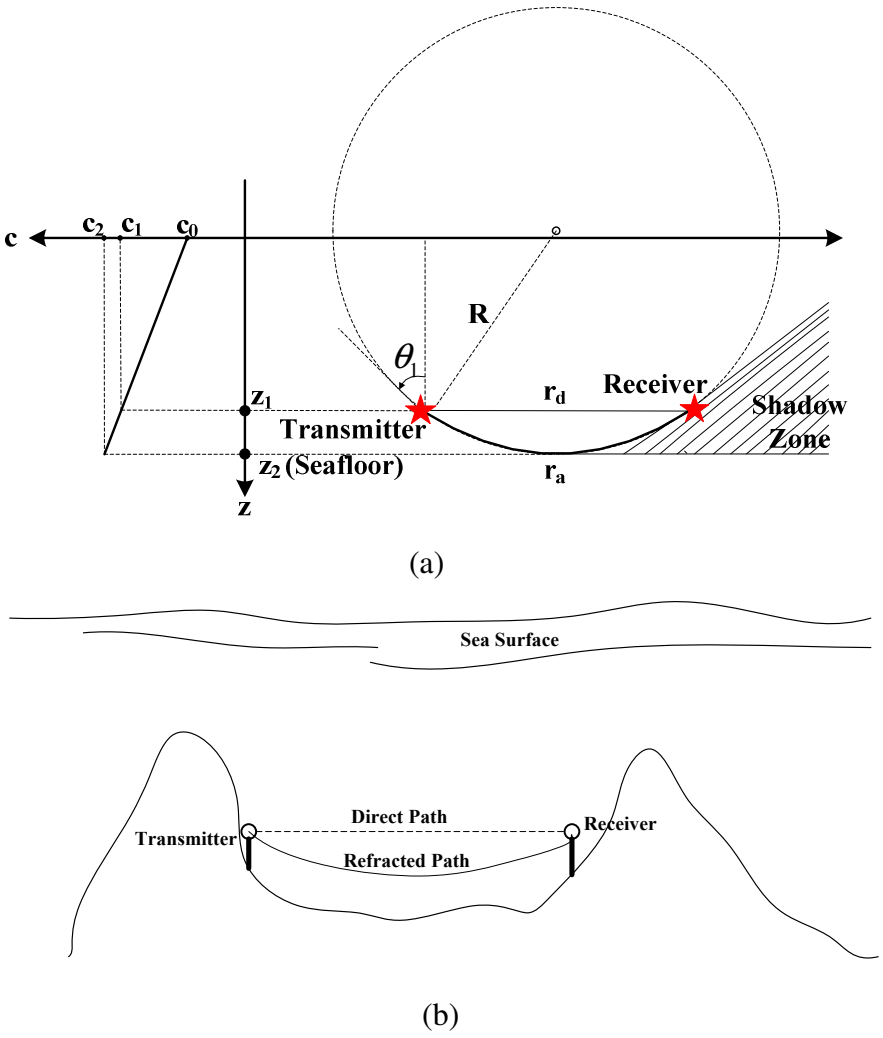

Figure 6.5: (a) Acoustic Ray Refraction (b) Installation of the Observing Stations

A second problem associated with acoustic refraction is the calculation of the direct distance between the transmitter and the receiver. Since the sound does not propagate along a straight line, the estimated distance obtained via the phase measurement is actually the arc length r_a. The relation between r_a and the direct distance r_d is

$$r_a = 2R\cos^{-1}\left(\frac{z_1}{R}\right) = 2\sqrt{{z_1}^2 + \left(\frac{r_d}{2}\right)^2}\ \cos^{-1}\left(\frac{z_1}{\sqrt{{z_1}^2 + \left(\frac{r_d}{2}\right)^2}}\right) \quad . \tag{6.7}$$

r_a and r_d have a linear relationship, as depicted in Figure 6.6. Assuming the receiver is moving away from its initial position due to plate movement, both r_a and r_d will change. r_a is obtained using phase measurement. Then by Equation (6.7) we will find r_d.

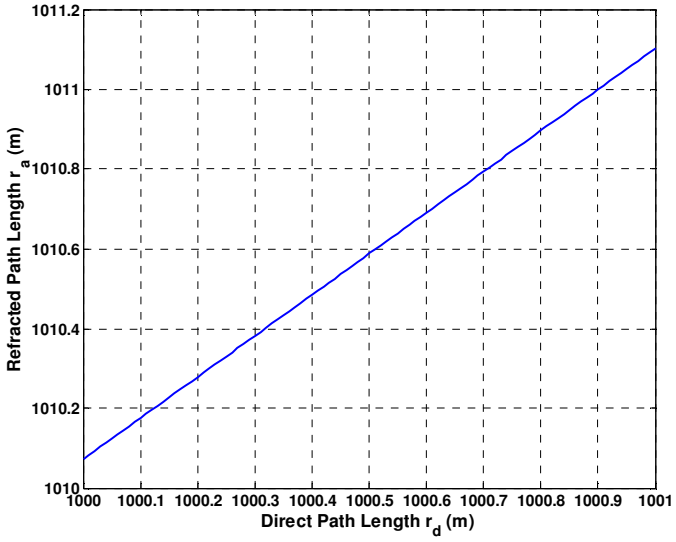

Figure 6.6: Refraction Path vs. Direct Path

6.1.4 Other Considerations

In this application, the distance between the transmitter and receiver r_d is much greater than their heights h. As a result, the bottom-reflected path length r_f is approximately equal to the direct path length r_d. If h = 5m, r_d = 1925m, then $r_f - r_d$ = 0.03 m. This is about the half wavelength if the acoustic signal is at f_0=20 kHz. The direct path signal and the reflected path signal will cancel with each other at the receiver. As shown in Figure 5.5, at some distances the range measurement error attains zero, which means at these locations the effect of multipath is minimum. Therefore the transmitter and the receiver can be installed accordingly. Also, we use a receiver array and choose the maximum outputs among hydrophones for the phase detection. Since the locations of transmitter and receiver are stationary in most of the time (unless earthquake occurs), the error caused by the multipath interferences is fixed and can be calibrated.

Monitoring of tectonic plate movements is a long-term project which could last for years. The observing stations A and B will be installed permanently on the seafloor. Acoustic pulses are transmitted between the two stations periodically with a

predetermined repetition rate. Phase information will be processed and recorded in a processing center. This processing center could be located at a surface vessel, a shore station, or a braching unit within a cabled seafloor observatory network [23]. They are connected to Station A and B by tether cables for data transmission and power supply. In addition, the processing center archives the processed data. These data is stored in a buffer for a short period of time, for example, a few days. If the averaged displacement between plates is below a threshold, we claim that there are no obvious plate motions and the data stored in buffer will be discarded and the space of data storage is saved. If however the averaged displacement between plates exceeds the threshold, the repetition rate of the pulse transmission should be increased for intense observation. Generally speaking, by using sensitive, bottom-mounted instruments and the PPHM method, we can greatly increase our understanding of local tectonic plates subduction processes and improve estimates of seismic risks, distortions of oil pipeline and other vulnerable installations, thereby reducing the costs produced by these hazards.

6.2 Measurement of Ocean Current Speed and Perturbations

6.2.1 Conventional Methods for Current Measurement

Knowledge of ocean currents is important for shipping industry, oil production industry, ocean meteorology, and so on. The methods of ocean current measurement fall into four main categories: mechanical, electromagnetic, acoustic time-of-flight, and acoustic Doppler [38, 55]. The first generation current meter relies on a mechanical rotor for sensing current motion. Since a mechanical rotor always has a threshold speed and will easily be inhibited or fouled by drifting seaweed, this type of current meter is not presently used widely.

An electromagnetic principle is commonly used for current measurement. Since seawater is conductive, a magnetic field applied perpendicularly to a flow induces an electric potential. In this type of system, an electromagnet generates an alternating magnetic field around the sensor. By measuring the alternating voltage induced between two electrodes in water, the current perpendicular to the magnetic field can be calculated.

Another method often used for measuring ocean current speed is based on estimating the time of travel of an acoustic pulse over a fixed distance. The travel time will decrease

if the water is moving in the same direction as the acoustic wave, and will increase when the direction of movement of the water is opposite that of the ping. In this type of system, one transducer transmits a ping; when a second transducer receives this ping, it will send back a similar pulse to the first transducer and so on. The difference between the travel times along the two directions will then be a measure of the current speed [56].

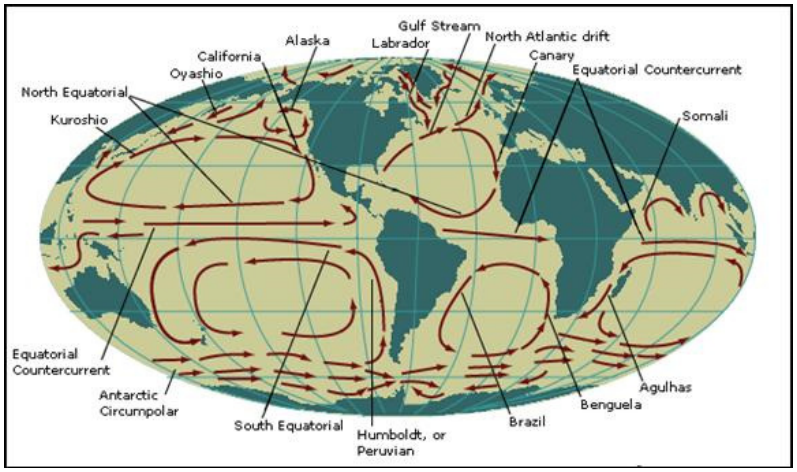

(a)

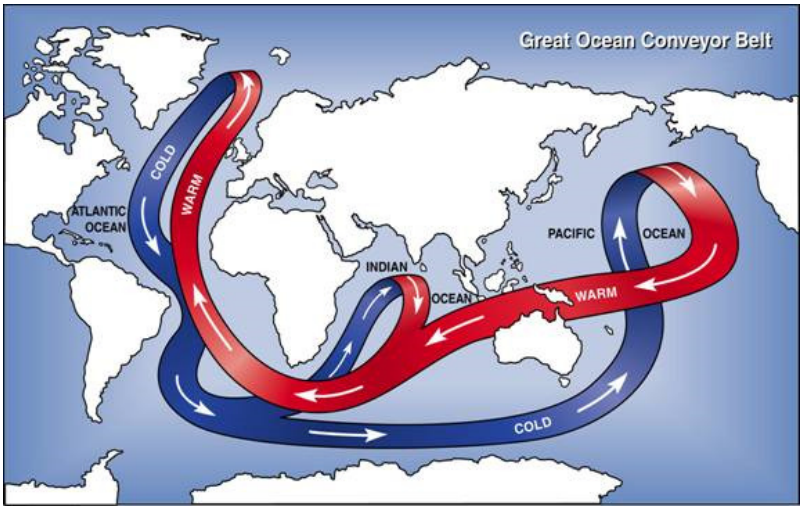

(b)

Figure 6.7: (a) Major Surface Ocean Currents [36]; (b) Deep Ocean Currents. Blue indicates cold, deep currents. Red indicates warmer currents closer to surface [36]

Current measurements based on the Doppler effect have been extensively investigated in recent years and many systems have been developed successfully. These systems include the Acoustic Doppler Velocimeter and the Acoustic Doppler Current Profiler

(ADCP). A Doppler measurement starts by sending out a ping. Due to particles and bubbles in the water, a fraction of the transmitted sound is reflected backwards. A receiver, normally the same transducer used for transmitting the ping, then receives this echo. If the reflecting particles are moving, the frequency of the reflected signal will change in accord with the Doppler principle. Assuming that the reflectors have the same speed as the water, the frequency difference between the transmitted sound and reflected sound will be a measure of the current speed. The accuracy of the Doppler measurements depends on the transmitted frequency, the length of the pulse, and the beam geometry.

Current meters are usually mounted on a wire of a mooring, which is deployed from a ship, and ADCPs can be mounted on a mooring, the bottom, or the underside of a vessel. Both will provide a time series of the velocity of the ocean's water at a single geographic location. To measure the velocity of ocean currents along a path, a convenient method is to track a drifting object, such as a buoy, in water with a ship. The principal disadvantage is that this method is applicable only to surface or near-surface current measurements and the measured current velocity is relevant to the ship's speed. Except for the direct measurement of ocean currents, oceanographers often employ an indirect method in which hydrodynamical equations of motion are used. The dynamic computation of currents depends upon the accurate measurement of temperature, salinity, and depth, and techniques are used which enables these measurements to be made [56~58].

6.2.2 Measurement of Ocean Current Speed over a Path

Measurement of the ocean current speed is a simple application of the PPHM method. To measure a deep ocean current, the system configuration is similar to that was used for tectonic plate motion surveillance given in Figure 6.4. Two stations, A and B, are installed on the seafloor on the opposite sides of the channel to be measured. The distance r_0 is pre-determined. Station A and B are connected by an underwater electric cable, which allows the synchronization between them. There is no relative movement between observing stations. The current flows from A to B with the speed $v_{AB}(t)$.

Without considering the noise, the phase shift of the acoustic signal transmitted from A to B was given in Equation (5.6) and is re-written here as below

$$\phi_{AB}(t) \approx \frac{2\pi f_0 r_0}{c} - \frac{2\pi f_0 r_0}{c^2} v_{AB}(t) = \phi_0 - \frac{2\pi f_0 r_0}{c^2} v_{AB}(t) = \phi_0 - \Delta\phi_c(t) \ , \tag{6.8}$$

where ϕ_0 is a constant and $\Delta\phi_c(t)$ is phase shift caused by the ocean current. Dropping ϕ_0 in Equation (6.8) without affecting our discussion, the current speed will be recovered as

$$v_{AB}(t) \approx -\frac{c^2}{2\pi f_0 r_0} \phi_{AB}(t) \ . \tag{6.9}$$

From Equation (6.9), any small current perturbation δv_{AB} is reflected by the phase variations $\delta\phi_{AB}$ as

$$\delta v_{AB} \approx -\frac{c^2}{2\pi f_0 r_0} \delta\phi_{AB} \ . \tag{6.10}$$

Over time, the observed phase may flip by 2π and needs to be unwrapped. The unwrapped phase will reflect both the slowly varying trend and the quickly fluctuating perturbations in the ocean current speed.

6.2.3 Simulation Results and Discussions

Computer simulations were conducted to support above discussions. The current speed $v_{AB}(t)$ consists of both slowly and quickly varying components. The slowly varying component represents the current's forwarding speed. It is modeled by a low frequency signal $v_{dc}(t)$. The quickly varying component represents the small fluctuations superimposed on the current by acoustic scintillation or small-scale turbulences [59]. It was modeled as a signal with higher frequency, $v_{ac}(t)$. So $v_{AB}(t)$ is given as [38]

$$v_{AB}(t) = v_{dc}(t) + v_{ac}(t) \tag{6.11}$$

and is depicted in Figure 6.8. The recovered phase is shown in Figure 6.9a (wrapped) and 6.9b (unwrapped).

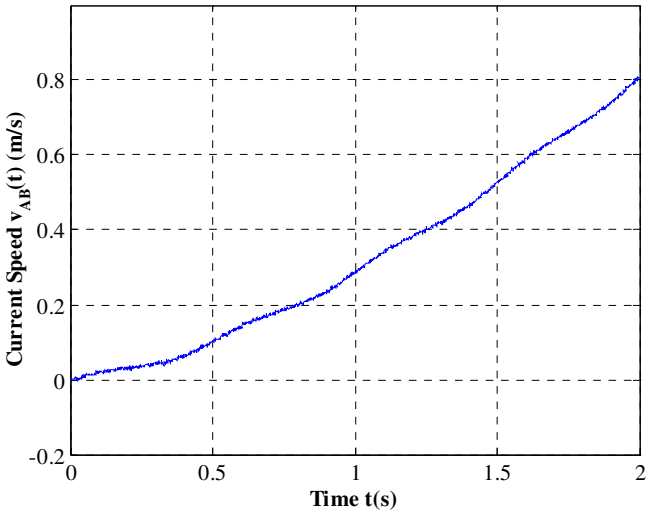

Figure 6.8: Ocean Current Speed with Slowly and Quickly Varying Components

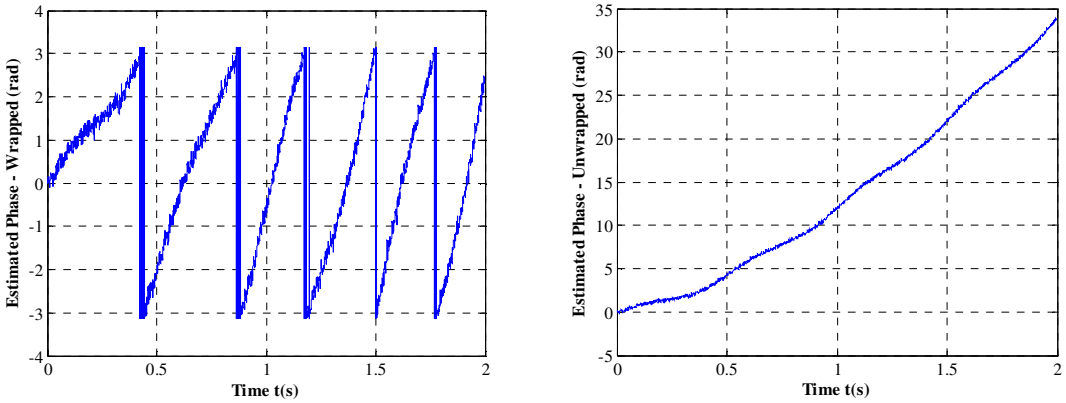

(a) (b)

Figure 6.9: (a) Recovered Phase and (b) Unwrapped Phase proportional to the Current Speed

To separate $v_{dc}(t)$ and $v_{ac}(t)$, one approach is to use wavelet tools [38, 60]. In [38], the discrete Meyer wavelet was employed to de-noise the estimated phase. Computer simulations showed its effectiveness. However, the drawback of the wavelet de-noising is the difficulty of choosing a proper wavelet. We need to have the data ready, and study its trend to select a good wavelet that suits for it. If the trend is changed, a different wavelet is needed for good de-noising performance.

The classical moving averaging (MA) filter is another solution to separate $v_{dc}(t)$ and $v_{ac}(t)$. Specifically, we take the average of the first 2000 points in the data series $\hat{v}_{AB}(t)$, and then we move forward by one point and take the average of the 2000 points backwards from this point. This process is repeated over the entire data series. The plot line connecting all the averages is the moving average of the raw data series. By doing so the short-term fluctuations are smoothed out and the longer-term trends are highlighted. The MA filter is an FIR filter and it introduces a group delay, which needs to be compensated. The de-noising results by using a MA filter are shown in Figure 6.10 (a) and (b). Figure 6.10(a) is $\hat{v}_{dc}(t)$, the estimated slowly varying component of the ocean current speed. Then $\hat{v}_{dc}(t)$ is subtracted from $\hat{v}_{AB}(t)$ and $\hat{v}_{dc}(t)$ is obtained. The result is shown in Figure 6.10(b). In this way, both the slowly varying current speed and its perturbations can be observed along a path. The characteristics of acoustical scintillations or turbulences will then be obtained by analyzing the current perturbations.

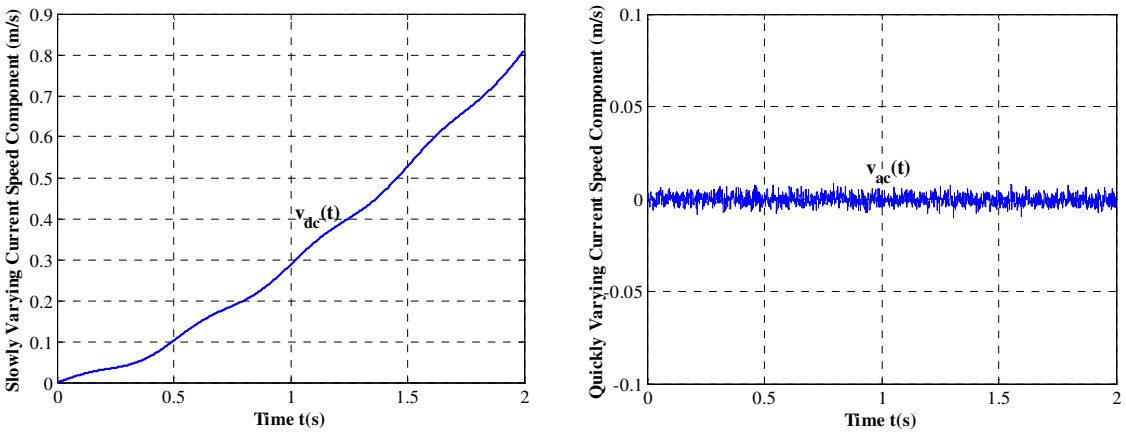

(a) (b)

Figure 6.10: (a) Slowly Varying Ocean Current Speed (b) Quickly Varying Ocean Current Perturbations

In a realistic scenario, for various reasons a signal loss may occur at the receiver. For example, the line-of-sight from the transmitter to the receiver could be blocked for a few seconds. Therefore, a conventional current meter is still needed at station A to provide readings when signal loss occurs. During the measurement, the sound speed along the path needs to be known, as shown in Equation (6.11). An important assumption of the PPHM method is that the sound speed along the path is constant. For this purpose, a

sound velocimeter is installed at the receiver. Its averaged reading over the observation time is used for current speed calculation.

The measurement error of the PPHM method is related to the multipath signal. In Chapter 5, an example was given which shows the phase error caused by bottom-reflected signals. This phase error has a boundary determined by the energy of the reflected signal. To minimize the error introduced by multipath signals, one solution is to choose the transmitted signal length so that the direct path signal and the boundary-reflected signals have no overlap in time. This method becomes complicated when more than one multipath signal is presented. Moreover, as the range between the transmitter and the receiver increases, the travel time along the direct path becomes close to that along the reflected path. To separate the direct path signal, the transmission should have a short duration, which means a decreased observation window for phase measurement. The consequence is that the phase measurement error will increase. The direct path signal can be separated in the spatial domain. Given a prior knowledge of the depth of the stations and the range between them, it is reasonable to assume that the multipath signals come from a small number of specific directions. This advantage provides feasible solutions for multipath cancellation, which include suitable beamforming and array design methods.

In above discussions, v_{AB} is the projection of the current speed along the A→B direction. A third station, C, installed in the same horizontal plane as A and B, and will provide the projection of the current speed along the A→C direction. The station positions are controlled by a GPS on a surface vessel employed to anchor these stations. The angle between the AB-axis and AC-axis is obtained using proper beamforming techniques. Ideally, the AB-axis is perpendicular to the AC-axis for easy calculation. Since these stations are fixed a few meters above the seafloor, it is reasonable to assume that no current moves vertically. The current under observation is moving horizontally in the A-B-C plane as shown in Figure 6.11. A complete representation of the current speed in a vector form is given as follows:

$$\mathbf{v} = v_{AB}\mathbf{i} + v_{AC}\mathbf{j}, \tag{6.12}$$

where **i** and **j** are unit vectors that point in the increasing directions of the AB and AC axes, respectively.

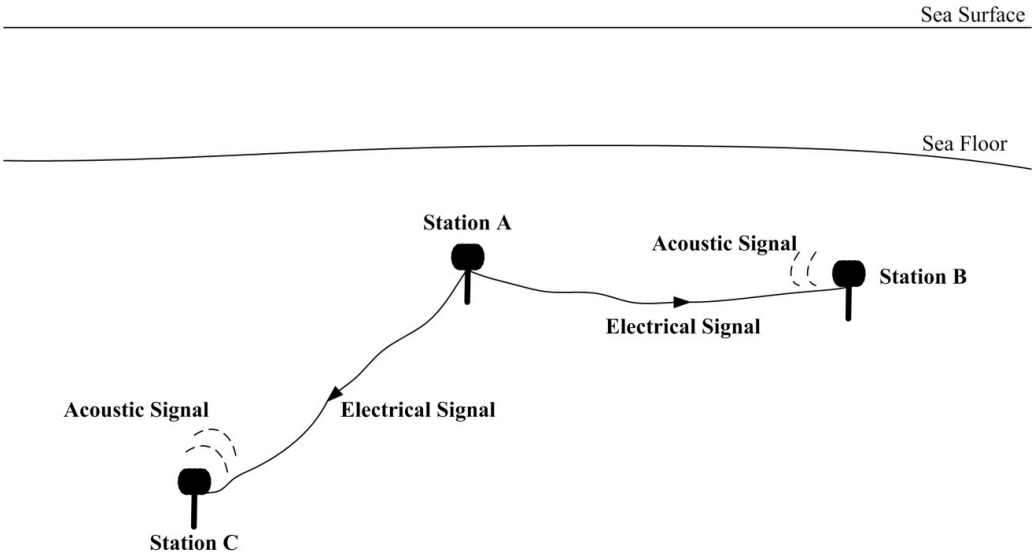

Figure 6.11: System Configuration for Current Speed Monitoring with Three Stations

The proposed configuration could be used for monitoring the deep ocean current speed and the movement of tectonic plates simultaneously. To observe the surface current speed, the transmitter and the receiver can be suspended from sea surface buoys, or ships, with solid rods. GPS receives are installed on the buoys or ships to position them on the sea surface in real-time. The propagation medium has more fluctuations near surface so there will be more measurement errors as compared to the deep water current speed monitoring.

6.3 ROV Positioning within an Underwater Acoustic Sensor Network

There are significant environmental, commercial, security, and military reasons to monitor aquatic environments. A highly precise, real-time, fine grained spatial-temporal sampling of the ocean environment is required for these purposes. Examples include the on-going NEPTUNE (North-East Pacific Time-Series Undersea Networked Experiments) project and ORION (Ocean Research Interactive Observatory Networks) project [23, 50]. In these observing systems, multiple nodes composing an underwater acoustic sensor network (UWSN) are placed on the seafloor. Each node is connected by an underwater cable to a shore control station. To collect and tag data, or place and retrieve devices on

the bottom, a networked ocean observatory system might incorporate intelligent unmanned underwater vehicles such as ROV connected to a bottom node and capable of navigating to exact bottom locations or along a precise path. Positioning of ROV therefore becomes a major issue and a challenging task.

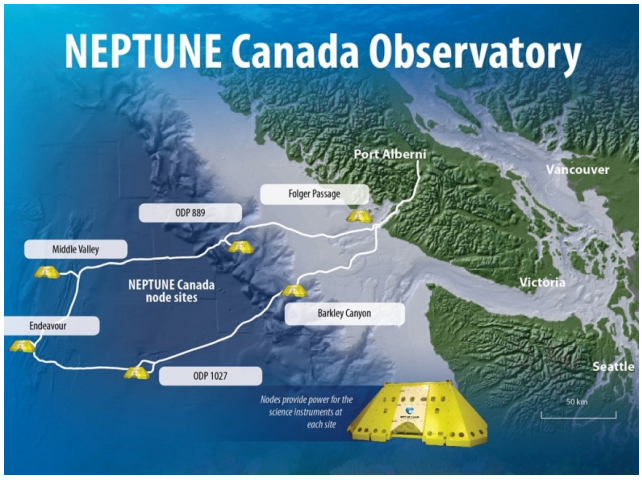

Figure 6.12: NEPTUNE Canada Observatory Layout [23]

The structure of the UWSN provides us a few advantages which makes the PPHM method very useful. In this scenario, an ROV controlled by the node is tethered with a cable to the bottom node. Its task is to collect data in the vicinity of the node. The operating frequency is around a few hundred kilohertz because the ROV's probing area is generally around the observatory node within a circle with radius at maximum 100 m. The position of the ROV with respect to the node, in terms of slant range and bearing, is monitored real-time, by measuring phase shift in the acoustic pulses transmitted from the ROV to the node. Although the ROV cannot be controlled with high precision, its trajectory can be precisely monitored.

The signal processing is more complicated in ROV positioning, as compared to the ocean currents measurement and tectonic plate monitoring. To get a continuous trajectory of the ROV, a continuous signal or a very long pulsed CW signal is preferred. However, continuous or long pulse transmission is power consuming. Within the UWSN, the power is provided by the bottom nodes and cables, which will not be a critical issue. But the continuous or long pulse transmission is more vulnerable to environmental changes, especially the multipath interferences. In the application of ocean current measurement,

both the transmitter and the receiver are fixed. Their positions are also known so the direction of arrival of the multipath signals can be calculated. When tracking a mobile ROV, the direction of arrival of the multipath signals will be uncertain. The ROV could be positioned with a predictable error, as discussed in Chapter 5. The PPHM method of transmitting a sequence of tones in Figure 5.8 could be a solution and is worthy of more exploration in future research.

There is another problem when reciprocal transmission is used to eliminate the current effect in ROV positioning. If a continuous signal or very long pulse is transmitted from the reference platform and the ROV to each other, there could be serious signal destruction between the transmitted signal and the received signal at the receivers. When it occurs, resuming of the phase will be a big issue. To solve this problem, the transmitted signals from the reference platform and the ROV should have different but known frequencies. To simplify the system, these frequencies are proportional and can be easily scaled down at the receivers output before the phase estimation.

Chapter 7 Experiments with an Air Prototype

To evaluate the proposed positioning method, a scale-down air prototype has been designed and implemented using ultrasonic transmission. Two experiments were conducted: 1) trajectory tracking of a moving target; and 2) monitoring of air flow speed. Experimental data was collected and digitized using an A/D device. The digital data are processed on computer. In this chapter, the experiment setup will be presented first, including the consideration for instrument selection. The data acquisition device and software will be introduced. Then the experimental results are compared with the true values and their performance will be evaluated. Practical problems encountered during the experiment will be addressed at last.

7.1 Experiment Description

The experiment is constructed to operate at 40 kHz ultrasonic transmission. This frequency is selected because it provides the same wavelength in the air as which a 200 kHz frequency offers in the water for a near field ROV tracking task. The transmitter is Kobitone 400ST16 ultrasonic transmitter. The receiver is Kobitone 400SR12 ultrasonic receiver. Their images are illustrated in Figure 7.1. The datasheets can be found in Appendix B.

(a) (b)

Figure 7.1: Ultrasonic Transmitter and Kobitone 400SR12 Ultrasonic Receiver

(a) Top View (b) Front View

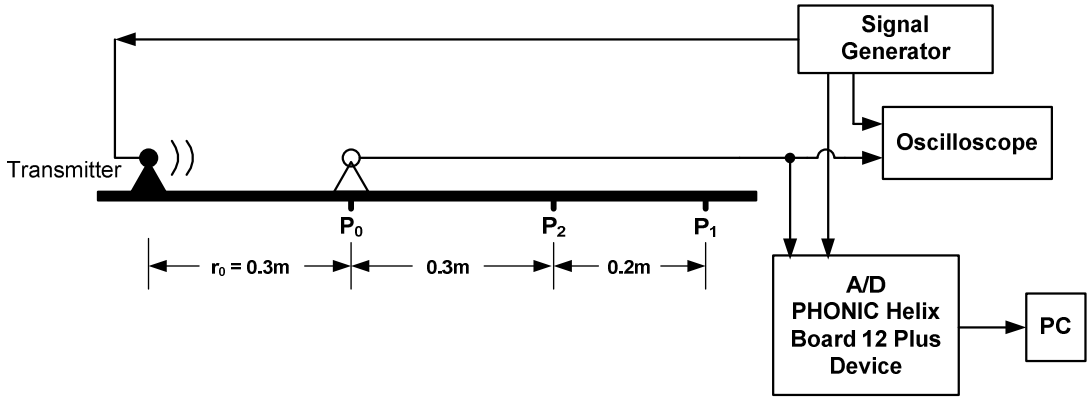

Figure 7.2: Experiment 1: Trajectory Tracking Experiment Setup

7.2 Experiment 1: Trajectory Tracking of a Moving Target

The configuration for tracking a moving target is shown in Figure 7.2. The transmitter is fixed at one end of an aluminum track. The track is used here to assure that all movements are forward or backward along a straight line. The receiver sits on a moveable carriage on the track and is moved back or forth by the operator. An indicator along the track points to a ruler and indicates the carriage's range increment. The carriage moves slowly with a uniform speed. The initial distance between the transmitter and the receiver is r_0 = 0.3 m. A function generator produced the 40 kHz sinusoidal signal to drive the transmitter and, at the same time, to serve as the reference signal for phase measurement. The transmitter sends out this ultrasonic signal continuously to the receiver.

The reference signal from the function generator and the receiver's output are analog. An A/D device collects and digitizes the analog signal. The digital data are fed into a computer for phase estimation. The A/D device used here is the PHONIC Helix Board 12 Plus. Its specifications are attached in Appendix C. The analog signals were sampled at 96 kHz sampling frequency and digitized with 24-bit resolution. The data recording software on the computer is the Plogue Bidule.

Data recording starts at t_0 = 0 s. At t = 10 s, the carriage is moved by the operator from P_0 to P_1. While moving, the phase between the reference signal and the receiver's output changed, as shown in Figure 7.3. Throughout the experiment, an oscilloscope is used for observing the received waveform. The carriage's moving distance is Δr = 0.5 m.

The digitized data is processed on computer. The estimated phase (wrapped) is shown in Figure 7.4. Then it is unwrapped and converted into the carriage's range increment, as shown in Figure 7.5. The measured trajectory agrees with the carriage's movement very well.

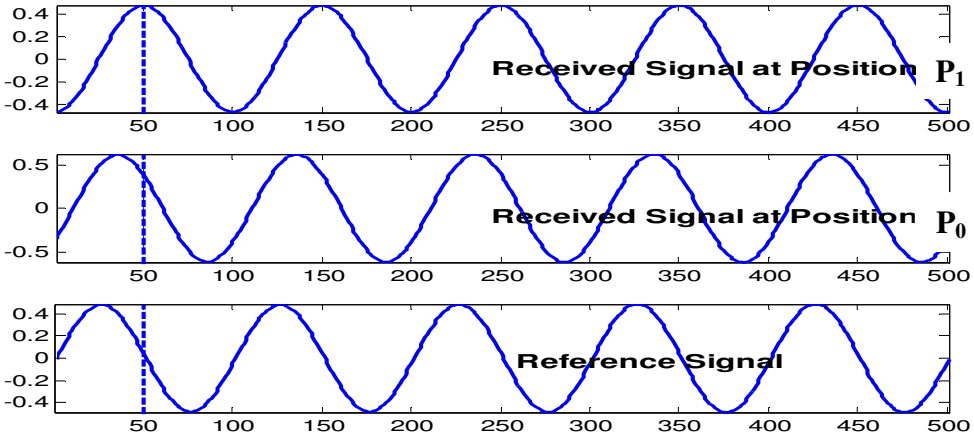

Figure 7.3: Digitized Signals from PHONIC Helix Board 12 Plus

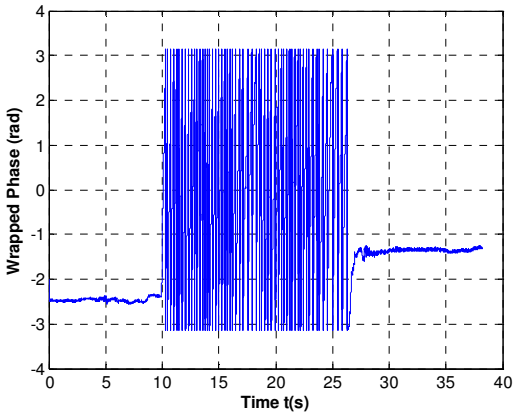

Figure 7.4: Wrapped Phase from a Phase Detector

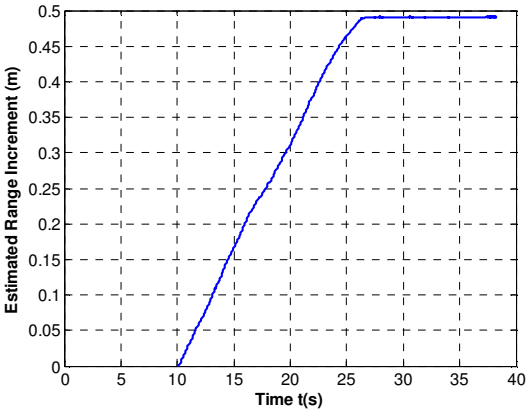

Figure 7.5: Test 1: Recovered Trajectory

In the second test, the carriage starts moving at t = 4 s. It moves from P_0 to P_2, stops at P_2 for about 2 s, then continues moving to P_1. In the third test, the carriage starts moving at t = 4 s. It moves from P_0 to P_2, back to P_0, then to P_1. The recovered trajectories for Test 2 and Test 3 are shown in Figure 7.6 and 7.7, respectively. The experimental results verified the effectiveness of target tracking using phase measurement.

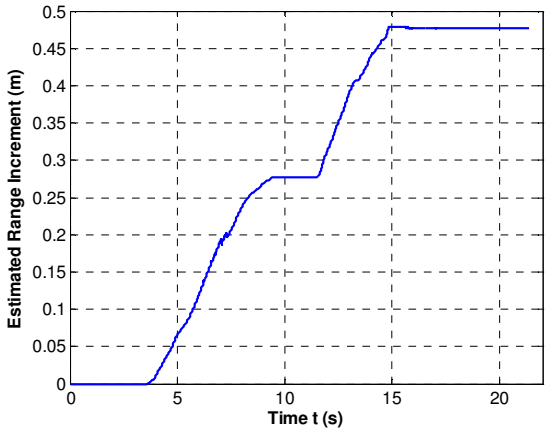

Figure 7.6: Test 2: Recovered Trajectory

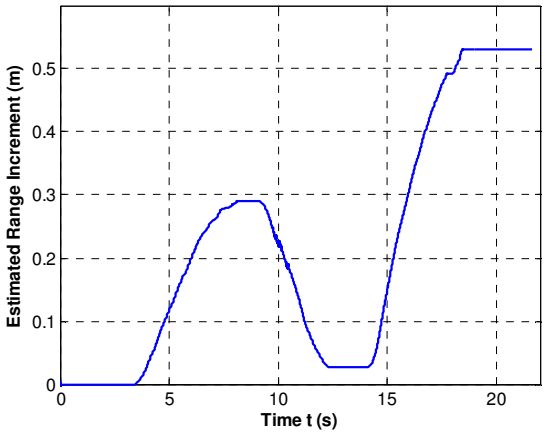

Figure 7.7: Test 3: Recovered Trajectory

7.3 Experiment 2: Air Flow Speed Monitoring

The second experiment is to demonstrate the speed and perturbation monitoring of air flow (in analogy to an ocean current) by phase measurement. The experiment setup is shown in Figure 7.8. The receiver is placed in line with the transmitter and faces toward it. The receiver and the transmitter are placed inside a plastic tube and separated by a distance r_0. The plastic tube is used here to confine the air flow inside the tube. The multipath signals from the tube boundary will be cancelled out because the transmitter and the receiver are placed along the tube' axis. An electrical fan blows air through the tube and an anemometer positioned at the end of the tube to measure the speed of the air flow. A function generator produces a 40 kHz sinusoidal wave to drive the transmitter and the phase difference between it and the receiver's output is measured by a phase detector.

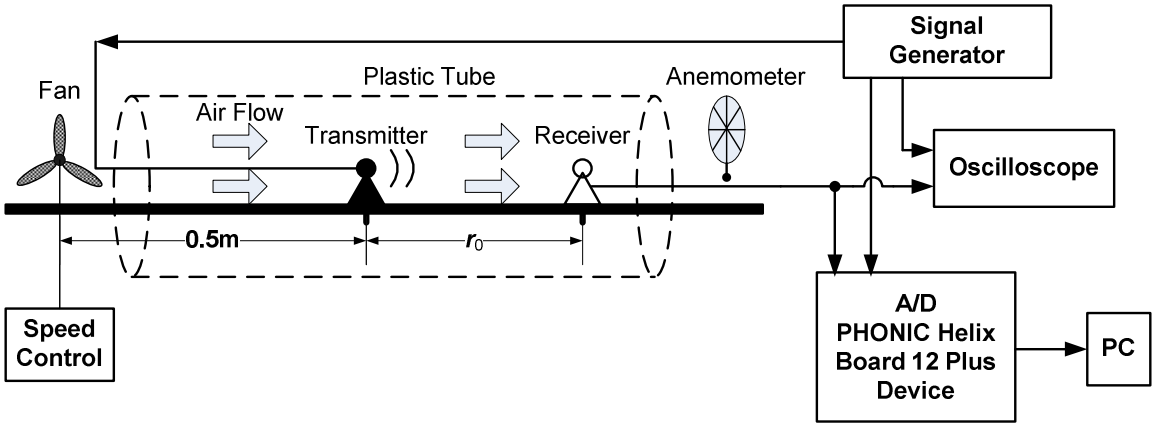

Figure 7.8: Experiment 2: Air Flow Speed Monitoring Experiment Setup

Before the fan is turned on, there is an initial phase ϕ_0 in the received signal as compared to the reference signal. It is the result of the distance from the receiver to the transmitter. Then the fan is turned on to generate an air flow. Its speed is measured by the anemometer. The phase in the received signal was measured as ϕ_1. The phase difference, $\Delta\phi = \phi_1 - \phi_0$, corresponds to the change in airflow speed. The procedure is repeated for three different airflow speeds and three different r_0.

In Test 1.1, the air flow speed is v = 1.2 m/s and r_0 = 0.06 m. The expected phase change was calculated using Equation (6.8) as

$$\Delta\phi = \frac{2\pi f r_0}{c^2} v = \frac{2\pi \cdot 40000 \cdot 0.06 \cdot 1.2}{345^2} = 0.1520 \text{ rad} \ . \tag{7.1}$$

Here the sound velocity in the air is c = 345 m/s. The measured phase shift was $\Delta\hat{\phi} = 0.1501\,\text{rad}$. The acoustically measured speed change was, therefore, $\hat{v} = 1.1707\,\text{m/s}$ as given by Equation (6.9). The error is within the ±0.1 m/s resolution of the anemometer used as the reference. Experimental results for different air speeds and r_0, are shown in Table 7.1.

Table 7.1: Experimental Results for Air Flow Speed Monitoring

Test	r_0 **(m)**	$\Delta\hat{\phi}$ **(rad)**	**Estimated Speed Using Phase Measurement** $\hat{v}$ **(m/s)**	**Anemometer Reading** v **(m/s)**	**Error** $\lvert\hat{v}-v\rvert$ **(m/s)**	**Relative Error** $\frac{\lvert\hat{v}-v\rvert}{v}\times 100\%$ **(%)**
1.1	0.06	0.1501	1.1707	1.2	0.0293	2.44
1.2	0.06	0.0750	0.5854	0.6	0.0146	2.44
1.3	0.06	0.0501	0.3902	0.4	0.0098	2.44
2.1	0.12	0.3222	1.2567	1.3	0.0433	3.33
2.2	0.12	0.2416	0.9425	1.0	0.0575	5.75
2.3	0.12	0.1342	0.5236	0.5	0.0236	4.72
3.1	0.18	0.4642	1.3072	1.3	0.0072	0.50
3.2	0.18	0.2646	0.6880	0.7	0.0120	1.71
3.3	0.18	0.1587	0.4128	0.4	0.0128	3.20

A similar experiment was conducted in [38] to verify the air flow speed measurement. In that experiment, the phase was estimated by comparing the signals from two Kobitone 400SR12 receivers. In our experiment, the reference signal for phase estimation is directly imported from the function generator. This signal is more stable as a reference for phase measurement.

During the experiment, the working frequency was set to be 40 kHz but the function generator was drifting around 39.99 ~ 40.01 kHz. This drifting had negligible impact on the results. What caused dramatic changes in the results is the accuracy of the distance between the transmitter and the receiver, as well as the sound speed (related to the room temperature). During the experiment, the room temperature was around 23 °C and the sound speed in the calculation is 345 m/s.

Chapter 8 Summary and Future Work

This chapter summarizes the work done in the thesis. Then directions for future research will be recommended.

8.1 Summary

In this thesis, a detailed review was given for three major groups of underwater positioning systems and the recently developed GPS-involved positioning systems. Based on a good understanding of the conventional systems, a novel positioning method was proposed for underwater applications. The proposed PPHM method overcomes the disadvantages of conventional underwater acoustic positioning systems. Compared with existing solutions, the proposed system offers the following key benefits:

1. It provides outstanding positioning accuracy, as proven by simulations results and laboratory experiments.
2. It has less complexity and can be easily operated.
3. It saves the cost and time for surface vessel deployment.
4. It monitors the target's movement continuously in real-time.
5. It can be installed permanently for a long-term application.

Signal processing techniques were employed extensively in the proposed positioning system. Classical quadrature phase detector and its equivalent – the envelope extraction – were studied. The latter one is more easily to be implemented. A quadrature sampling method was proposed for phase estimation, which took advantage of the sinusoidal transmission signal. This method allows more feasibility of a real-time positioning. The phase unwrapping method was also discussed and revised for a noisy signal.

The PPHM method is vulnerable to environmental changes. The effects of environmental factors on the PPHM method were investigated, with emphasis on sound speed variation, ocean currents, multipath interferences, and acoustic ray refractions. Solutions have been proposed to alleviate their effects on positioning accuracy.

The initial motivation of the proposed positioning system is for trajectory tracking of an underwater target. This system can also be used to monitor the movements of tectonic plates, or to measure the speed and perturbations of an ocean current over a path. In this thesis, the configuration for each of these applications was presented, and their technical difficulties were addressed.

In this thesis, some problems from the engineering aspect have been notified. One of these concerns is to determine the transmitted signal's duration to reduce power consumption whereas at the same time to avoid the multipath interferences. We also discussed the data storage problem and the solutions if discontinuities occur in the received data.

An air-prototype was designed and implemented using ultrasonic transmission. Experiments were conducted to verify the effectiveness of the PPHM method in tracking the trajectory of a moving target, and in monitoring of the air flow's speed. The experiment results supported the theoretical analysis.

8.2 Future Work

Following directions are recommended for future research:

1. The laboratory experiment has been set up for the slant range measurement. This setup can be used for the bearing angle measurement. The A/D device has enough input ports for data digitizing and recording.
2. In this thesis, the target positioning within a horizontal plane has been investigated. Proper array configuration is still needed such that the target can be positioned in a 3D space in real-time. Another solution is to use a depth meter working with the array for azimuth angle measurement. The target's 3D position is calculated based on the estimated slant range and the azimuth angle plus its depth with respected to the receiver array.
3. We need a better understanding of the ocean turbulences, including its physics and mathematical model. The effect of a small-area short-term turbulence on the PPHM positioning accuracy should be figured out and eliminated. With a good understanding of the turbulence, we can create artificial air turbulence in the laboratory and evaluate its effect on the phase measurement.

4. The strategy of ocean current speed monitoring can be used for water temperature or salinity surveillance over a long path.
5. The multipath interferences cancellation is still a problem, especially in the application of tracking a fast moving target. The working direction to solve this problem is proper array processing, and transmission signal coding.
6. If we have good time synchronization between the reference platform and the target, the tethered cable can be removed. This will give more freedom to the moving target.

Bibliography

[1] Xu, Guochang, *GPS Theory, Algorithms and Applications*, 2nd ed., Springer Berlin Heidelberg, 2007.

[2] Leonard, J. John, Andrew A. Bennett, Christopher M. Smith, Hans Jacob S. Feder, "Autonomous underwater vehicle navigation," *MIT Marine Robotics Laboratory Technical Memorandum 98-1*, pp. 1-17, 1998.

[3] Vickery, K., "Acoustic positioning systems - a practical overview of current systems," *Proceedings of the Workshop on Autonomous Underwater Vehicles,* pp. 5-17, Aug. 20-21, 1998.

[4] Philip, D. R. C., "An evaluation of USBL and SBL acoustic systems and the optimization of methods of calibration," *The Hydrographic Journal,* no. 108, pp. 18-25, Apr. 2003.

[5] Zielinski, A. and L. Zhou, "Precision acoustic navigation for remotely operated vehicles (ROV)," *Journal of Hydroacoustics*, vol. 8, pp. 255-264, 2005.

[6] Zielinski, A., and L. Zhou, "Precise acoustic navigation for ocean observing systems," *Symposium PACON 2005*, Taipei, Taiwan, pp. 211-220, Nov. 6-9, 2005.

[7] Milne, P. H., *Underwater Acoustic Positioning Systems*, Gulf Publishing, Houston, 1983.

[8] Vickry, K., **"**Acoustic positioning systems. New concepts-the future," *Proceedings of the 1998 Workshop on Autonomous Underwater Vehicles*, pp.103-110, Aug. 1998.

[9] Jonsson, P., I. Sillitoe, B. Dushaw, J. Nystuen, and J. Heltne, "Observing using sound and light – a short review of underwater acoustic and video-based methods," *Ocean Science Discussions*, no. 6, pp.819-870, 2009.

[10] Davis, Jonathan P., "Flexible acoustic positioning system architecture," *Presented in the Dynamic Positioning Conference* 2002**.**

[11] Hsu, L., Ramon R. Costa, Fernando Lizarralde, Jose Paulo Vilela Soares Da Cunha, "Dynamic positioning of remotely operated underwater vehicles," *IEEE Robotics & Automation Magazine*, pp. 21-31, Spetember 2000.

[12] Alcocer, A., P. Oliveira, A. Pascoal, "Underwater acoustic positioning systems based on buoys with GPS," *Proceedings of the Eighth European Conference on Underwater Acoustics*, 8th ECUA, Carvoeiro, Portugal, pp. 1-8, June 2006.

[13] http://www.underwater-gps.com/uk/technology-GIB-concept.php, *visited on July 19, 2010*.

[14] http://www.naval-technology.com/contractors/satellite/ixsea/ixsea4.html, *visited on July 19, 2010*.

[15] Kussat, N. H., C. D. Chadwell and R. Zimmerman, "Absolute positioning of an autonomous underwater vehicle using GPS and acoustic measurements," *IEEE Journal of Oceanic Engineering*, vol. 30, no. 1, pp. 153-164, Jan. 2005.

[16] Spiess, Fred N., C. David Chadwell, John A. Hildebrand, Larry E. Young, George H. Purcell Jr. and Herb Dragert, "Precise GPS/acoustic positioning of seafloor reference points for tectonic studies," *Physics of the Earth and Planetary Interiors*, vol. 108, pp. 101-112, 1998.

[17] Ferrel J., M. Barth, *The Global Positioning System and Inertial Navigation*, S. Chapman, Ed. McGraw-Hill, 1998.

[18] Gamroth, E. D. H., "Design, implementation and testing of an underwater global positioning system," *Master Thesis*, University of Victoria, 2000.

[19] Case Studies in Navigation & Positioning, *Underwater Magazine*, January/February 2002.

[20] http://www.km.kongsberg.com/, *visited on July 19, 2010*.

[21] http://www.sonardyne.co.uk/Products/PositioningNavigation/index.html, *visited on July 19, 2010*.

[22] Bingham, B., David Mindell, Thomas Wilcox and Andy Bowen, "Integrating precision relative positioning into JASON/MEDEA ROV operations," *Marine Technology Society Journal*, vol. 40, No. 1, pp. 80-89, 2006.

[23] Fairly, P., "Neptune rising," *Spectrum IEEE*, vol. 42, Issue 11, pp.38-45, Nov. 2005.

[24] Van Trees, Harry L., *Optimum Array Processing - Part IV, Detection, Estimation, and Modulation Theory*, 2002 John Wiley & Sons.

[25] Franks, L., *Signal Theory*, Prentice Hall, 1969.

[26] Howard, J. and H. Landgraf, "Quadrature sampling phase detection", *Rev. Sci. Instrum*., vol.65, No. 6, Jun. pp.2130-2133, 1994.

[27] Kay, S. M., *Fundamentals of Statistical Signal Processing, Volume I: Estimation Theory*, Prentice Hall, 1998.

[28] Xiong, X. and A. Zielinski, "An adaptive algorithm for amplitude and phase measurements based on multiple samples," *Proceedings of MTS/IEEE Oceans'07*, Oct. 2007.

[29] Hansen, J., "Selected approaches to estimation of signal phase", *technical report*, University of Rhode Island, 2003.

[30] Havelock, David; Kuwano, Sonoko; Vorländer, Michael (Eds.) *Handbook of Signal Processing in Acoustics; Part XVI Underwater and Oceanographic Acoustics*, Springer New York, 2008.

[31] Urick, R. J., *Principles of Underwater Sound*, New York: McGraw-Hill, 1983.

[32] Sweeney, A. D., C. D. Chadwell, J. A. Hildebrand, and F. N. Spiess, "Centimeter-level positioning of seafloor acoustic transponders from a deeply-towed interrogator," *Marine Geodesy* 28, 39-70, 2005.

[33] http://www.amloceanographic.com/Xchange™_Sensors/SV.Xchange™.aspx, *visited on May 31, 2010*.

[34] Neumann, G., *Ocean Currents*, New York: Elsevier, 1968.

[35] http://hypertextbook.com/facts/2002/EugeneStatnikov.shtml - Speed of Ocean Currents, *visited on July 19, 2010*.

[36] http://www.crd.bc.ca/watersheds/protection/geology-processes/globaloceancurrents.htm - Global Ocean Currents, *visited on July 19, 2010*.

[37] Di Iorio, D., “Measurements of turbulence parameters and observations of multipath arrivals in two contrasting costal environments using acoustical scintillation analysis,” *PhD Thesis*, University of Victoria, 1988.

[38] Zielinski, A., and M. Butowski, "Monitoring of ocean current perturbations using acoustic phase,” *XXV Symposium on Acoustics*, Leba, Poland, May 26-29, 2009.

[39] Zhou, L.; Zielinski, A.; Kraeutner, P.; “A precise acoustic distance measuring system for tectonic plate motion,” *Proceedings of MTS/IEEE Oceans’07*, Oct. 2007.

[40] Zheng, H., Gohda, N., Noguchi, H., Ito, T., Yamaoka, H., Tamura, T., Takasugi, Y., Kaneko, A., “Reciprocal sound transmission experiment for current measurement in the Seto inland sea, Japan.” *Journal of Oceanography,* vol. 53, pp. 117-127, 1997.

[41] Deffenbaugh, M.; Schmidt, H.; Bellingham, J.G.; “Acoustic positioning in a fading multipath environment,” *Conference Proceedings of MTS/IEEE OCEANS '96*, vol. 2, pp. 596 – 600, Sep. 1996.

[42] Li, S.; Tuteur, F.B.; “Estimation of underwater source parameters by use of multipath information,” *Proceedings of Fourth Annual ASSP Workshop on Spectrum Estimation and Modeling*, pp.258 – 263, Aug. 1988.

[43] Wu, L.; Zielinski, A.; “Multipath rejection using narrow beam acoustic link,” *Proceedings of OCEANS '88*, vol.2, pp. 287 – 290, 1988.

[44] Haykin, S., *Adaptive Filter Theory*, 4th ed., Prentice Hall, 1996.

[45] Di Iorio, D. and D. Farmer, “Path-averaged turbulent dissipation measurements using high-frequency acoustical scintillation analysis,” *Journal of Acoustical Society of America*, vol. 96, No. 2, pp.1056-1069, Aug. 1994.

[46] Lurton, X.; *An Introduction to Underwater Acoustics: Principles and Applications*, Springer-Verlag, 2004.

[47] Di Iorio, D. and D. Farmer, “Separation of current and sound speed in the effective refractive index for a turbulent environment using reciprocal acoustic transmission,” *Journal of Acoustical Society of America*, vol. 103, No. 1, pp.321-329, Jan. 1998.

[48] Di Iorio, D. and D. Farmer, "Observations of acoustical scintillations in Saanich Inlet," *Proceedings of Oceans'93*, vol.1, pp.1416-1420, Oct. 1993.

[49] Lueck, R., Rockland Scientific International Inc., private communication with Li Zhou, May 18, 2010.

[50] Edgington, D.R.; Davis, D.; O'Reilly, T.C.; "Ocean observing system instrument network infrastructure," *Oceans 2006*, pp.1-4, Sep. 2006.

[51] Naomi Oreskes, editor, with Homer Le Grand, *Plate tectonics: an insider's history of the modern theory of the Earth*, Westview Press, 2001

[52] http://www.bennett.karoo.net/images/nathaz/worldsplatesarrows.gif , *visited on May 09, 2010.*

[53] DeMets, C., R. G. Gordon, and D. F. Argus, "Geologically current plate motions," *Geophys. J. Int.*, 1-80, 2010.

[54] Gagnon, K., D. Chadwell and F. N. Spiess, "Evolving method to measure seafloor plate tectonic motions," *Sea Technology July 2005*, 49-52 (2005)

[55] Thurman, H., *Introductory Oceanography*, 8th ed., Prentice-Hall Canada, 1997.

[56] Bugnon, F.J., Whitehouse, I.A., "Acoustic Doppler current meter," *IEEE Journal of Oceanic Engineering*, vol. 16, no. 4, pp. 420-426, Oct. 1991.

[57] Plueddernann, A.J.; Lentz, S.J.; Terray, E.A.; "Comparison of five current meters in a tidally dominated flow," *Proceedings of the IEEE/OES Seventh Working Conference on Current Measurement Technology*, pp.176 – 181, Mar. 2003.

[58] Rowsell, R.D.; Skafel, M.G.; "Comparison of current meters in a coastal environment," *Proceedings of Oceans '02 MTS/IEEE*, vol. 2, pp.724 – 729, Oct. 2002.

[59] Lu, Youyu, Rolf G. Lueck, "Using a broadband ADCP in a tidal channel. Part I: mean flow and shear," *Journal of Atmospheric and Oceanic Technology*, 16, pp. 1556-1567, 1999.

[60] Alexandrov, T., Bianconcini, S., Dagum, E.B., Maass, P., McElroy, T., "A review of some modern approaches to the problem of trend extraction." *Statistical Research Division U.S. Census Bureau*, March 2008.

[61] El-Sharkawi, M.A.; Upadhye, A.; Shuai Lu; Kirkham, H.; Howe, B.M.; McGinnis, T.; Lancaster, P., "North east pacific time-integrated undersea networked experiments (NEPTUNE): cable switching and protection," *Oceanic Engineering, IEEE Journal of*, Vol. 30, Issue 1, pp.232-240, Jan. 2005.

[62] Barnes, C. R.; Best, M. M. R.; Bornhold, B. D.; Juniper, S. K.; Pirenne, B.; Phibbs, P., "The NEPTUNE Project - a cabled ocean observatory in the NE Pacific: Overview, challenges and scientific objectives for the installation and operation of Stage I in Canadian waters," *Underwater Technology and Workshop on Scientific Use of Submarine Cables and Related Technologies,* pp.308-313, Apr. 17-20, 2007.

[63] Phonic HELIX Board 12 Plus User's Manual

Appendix A A Study on Band-limited Noise

A.1 Sources of Noise

There are three sources of noise to be considered in underwater positioning systems: thermal noise, ambient noise, and shipping noise. In common with any electrical receiving system, a sonar receiver adds its own noise to the signals it receives. The thermal motion of electrons in wires, resistors, and etc, is the source of a thermal noise. Usually the thermal noise is negligible compared to other noises coming from the ocean. Ambient noise, or called background noise, is the noise from the ocean. Examples of sources contributing to ambient noise in the ocean include waves, marine creatures, wind, rain, earthquakes, and volcanoes. Ships are also important noise sources. Shipping noise mainly comes from the propulsion machinery, the auxiliary machinery and the propellers.

A.2 Gaussian Noise

Each noise type outlined above is the result of a large number of statistically independent and random contributions. According to the central limit theorem, the distribution of such random noise follows a Gaussian distribution (or normal distribution). Its probability density function is given in Equation (A.1) and plotted in Figure A.1,

$$p(v_n) = \frac{1}{\sigma\sqrt{2\pi}} e^{\left(-\frac{(v_n-\mu)^2}{2\sigma^2}\right)}. \tag{A.1}$$

In Equation (A.1), v_n is the noise voltage. μ is the mean of v_n. σ^2 is the variance of v_n. If $\mu = 0$, its power equals the mean square voltage, i.e.

$$P_n = v_n^2 = \sigma^2 \ . \tag{A.2}$$

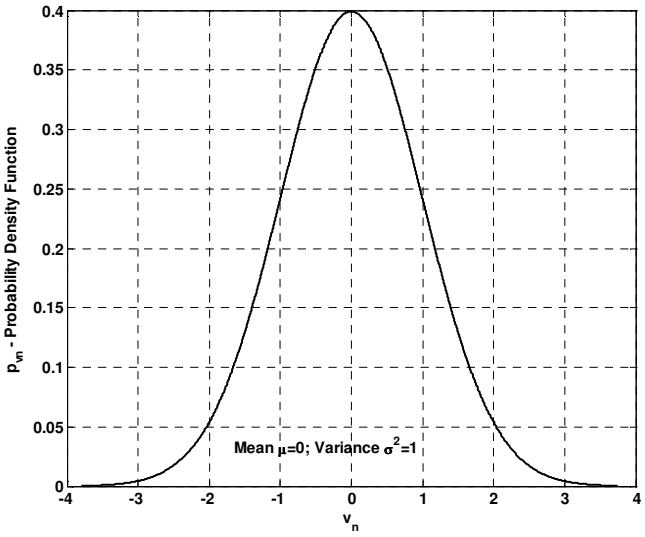

Figure A.1: Probability Density Function of a Standard Gaussian Distribution

A.3 White Noise

The time-average autocorrelation function of the noise voltage is

$$R_n(\tau) = \lim_{T\to\infty} \frac{1}{T} \int_0^T v_n(t) v_n(t+\tau) dt \,. \tag{A.3}$$

For a zero-mean v_n, if its autocorrelation function is given by Equation (A.3),

$$R_n(\tau) = \frac{N_0}{2} \delta(\tau) \,, \tag{A.4}$$

where $\delta(\tau)$ is the delta function, then we say that the noise is a white noise. This is because the power spectral density (PSD), which is the Fourier transform of the autocorrelation function, is a constant $\frac{N_0}{2}$ over all frequencies. We call it white as an analogy to the frequency spectrum of white light. Since $R_v(\tau) = 0$ as $\tau \neq 0$, any two different samples of a Gaussian white noise are uncorrelated and hence statistically independent.

Figure A.2 and A.3 show the autocorrelation function $R_n(\tau)$ and the PSD $S_n(f)$ of a white noise. The total power of a white noise equals to the area under its PSD. Since its PSD has an infinite bandwidth, the power goes to infinity and therefore impossible to be generated in practice. Usually we generate a noise with flat PSD over a much larger bandwidth than that of the system and regard it as a white noise.

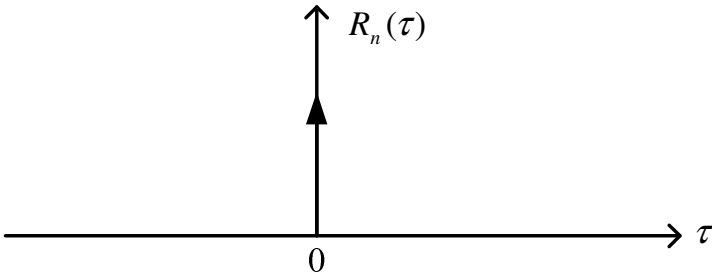

Figure A.2: Autocorrelation Function of a White Gaussian Noise

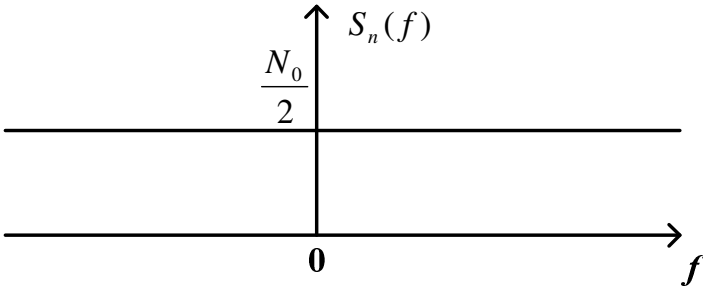

Figure A.3: Power Spectrum Density of a White Gaussian Noise

A.4 Band-limited Noise

When a white noise is fed into a linear, time-invariant filter with transfer function *H*(*f*), its PSD will be modified by *H*(*f*), as illustrated in Figure A.4.

$$S_{out}(f) = S_{in}(f)\left|H(f)\right|^2$$

Figure A.4: White Noise Fed into an LTI Filter

The PSD of the output noise is calculated as

$$S_{out}(f) = S_{in}(f)\left|H(f)\right|^2, \tag{A.5}$$

where $S_{in}(f)$ and $S_{out}(f)$ are the PSD functions of the input white noise and output noise, respectively. Since $S_{in}(f)$ is flat over a wide range of frequencies, $S_{out}(f)$ will take the shape of $\left|H(f)\right|^2$, as shown in Figure A.5. We therefore say that filtering white noise produces colored noise with frequency content primarily in the range passed by the filter.
0

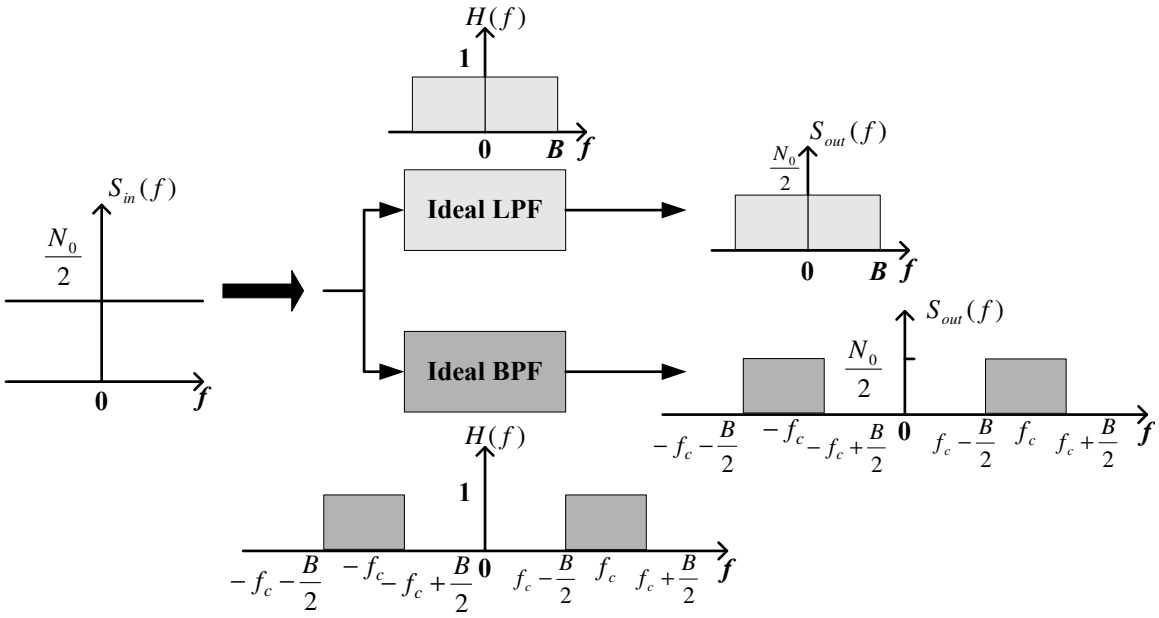

Figure A.5: PSD of a White Noise Shaped by the Lowpass/Bandpass Filter

Specifically, if $H(f) = \Pi\left(\frac{f}{2B}\right)$ is the transfer function of an ideal lowpass function, then we have

$$S_{out}(f) = \frac{N_0}{2} \cdot \left|H(f)\right|^2 = \frac{N_0}{2} \cdot \Pi\left(\frac{f}{2B}\right) \tag{A.6}$$

and

$$R_{out}(\tau) = N_0 B \,\mathrm{sinc}(2\mathrm{B}\tau). \tag{A.7}$$

Here, $\Pi\left(\frac{f}{2B}\right)$ is a function that takes a constant value 1 over [-B, B] and equals zero elsewhere. For a lowpass filter, its total bandwidth is 2B. But we usually only consider the positive half. To get a bandpass filter centered at f_c with bandwidth B, usually we construct a lowpass filter first then shift it by f_c. This lowpass filter has unit gain from –B/2 to B/2. After we shift it to f_c, the bandwidth of the bandpass filter is B.

In Equation (A.7), as $B \to \infty$, the sinc function shrinks to a delta function as shown in (A.4). The power of the output noise is

$$P_{out} = \overline{y^2} = \int_{=\infty}^{\infty} S_{out}(f)df = N_0 B \text{ (the area under } S_{out}(f)) . \tag{A.8}$$

So the output power is directly proportional to the filter's bandwidth B. Furthermore, the output noise is correlated over time intervals of about 1/2B.

A.5 Noise Equivalent Bandwidth

The total power is the integration of PSD over all frequencies, as given by

$$P_n = \int_{-\infty}^{\infty} S_n(f)df . \tag{A.9}$$

Theoretically the white noise has infinite power. Filtered white noise usually has finite power. From Equation (A.6) and (A.8) we have

$$P_{out} = \overline{y^2} = \int_{=\infty}^{\infty} S_{out}(f)df = \int_{-\infty}^{\infty} S_{in}(f)\left|H(f)\right|^2 df = \frac{N_0}{2}\int_{-\infty}^{\infty}\left|H(f)\right|^2 df = N_0\int_0^{\infty}\left|H(f)\right|^2 df = N_0 B_N \tag{A.10}$$

where

$$B_N \overset{\Delta}{=} \int_0^{\infty}\left|H(f)\right|^2 df \tag{A.11}$$

is defined as the noise equivalent bandwidth (NEB). As illustrated in Figure A.6 for a lowpass or bandpass filter, B_N equals the bandwidth of an ideal rectangular filter that would pass as much a white noise power as the filter in question. Here we made an

assumption that $|H(f)|_{\max} = 1$. By definition, the NEB of an ideal lowpass or bandpass filter is its actual bandwidth. For practical filters, B_N is somewhat greater than the -3dB bandwidth B. However, as the filter becomes more selective (i.e. the filter has higher order and sharper cutoff characteristics), its NEB approaches the -3dB bandwidth, and hence we can take them to be equal for most applications.

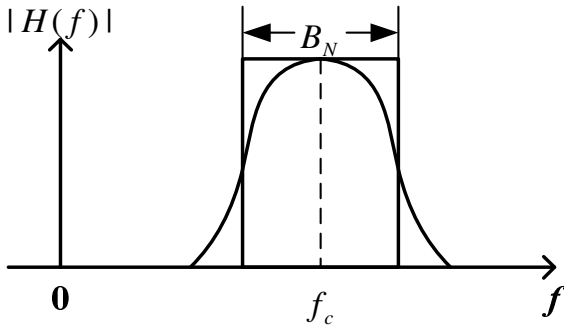

Figure A.6: Noise Equivalent Bandwidth of a Bandpass Filter

A.6 Examples

Example 1 Generate a white Gaussian noise and evaluate its power spectrum density.

In MATLAB, a white Gaussian noise is represented by a set of random numbers, which are generated using the function `randn`. Suppose we need N=10000 random numbers, we write

```
N = 10000;
n = randn(1, N);
```

Then `n` returns a pseudorandom, scalar value drawn from a Gaussian distribution with mean 0 and standard deviation 1. The algorithm used in the function `randn` is based on [3] by Moler.

To verify the distribution of the generated signal, we observe its histogram as

```
x = -5:0.1:5;
hist(n, x)
```

which gives us the histogram from the generated data between (-5:5).

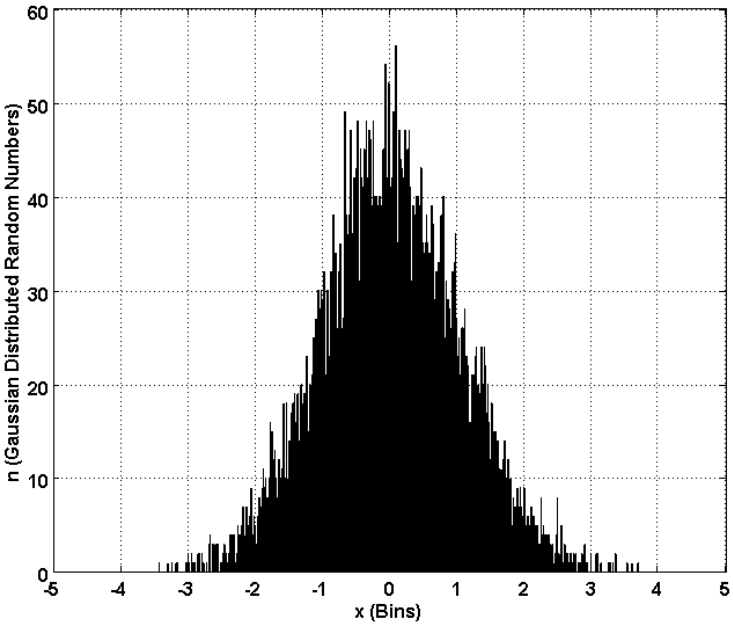

Figure A.7: Histogram of Generated White Gaussian Noise

To generate a random distribution with a specific mean and variance, we can multiply the output of `randn` by the desired standard deviation, and then add the desired mean. For example, to generate a 1-by-5 vector of random numbers with a mean of .6 that are distributed with a variance of 0.1, the MATLAB command is as follows.

```
x = .6 + sqrt(0.1) * randn(1,5)
```

To evaluate the power spectrum density, we use the Fast Fourier Transform (FFT) method. Suppose the noise data are obtained by sampling the input noise every $t_s = 0.1\,\text{ms}$, i.e. the sampling frequency $f_s = 1/t_s = 10\text{k}\,\text{Hz}$. The power spectrum density is calculated and plotted as

```
function P_yy = Power_Spec(y, fs)
N = 2^(ceil(log2(fs)));
y = fft(y,N);
P_yy = y.* conj(y) /N/2/pi;
f = fs*(0:N/2)/N;
figure;
plot(f,P_yy(1:N/2+1))
xlabel('Frequency (Hz)')
ylabel('Power Spectrum Density S_n(f)')
```

The result is shown in Figure 8.8. The width of the observation window (0 ~ 5 kHz) is determined by the sampling frequency.

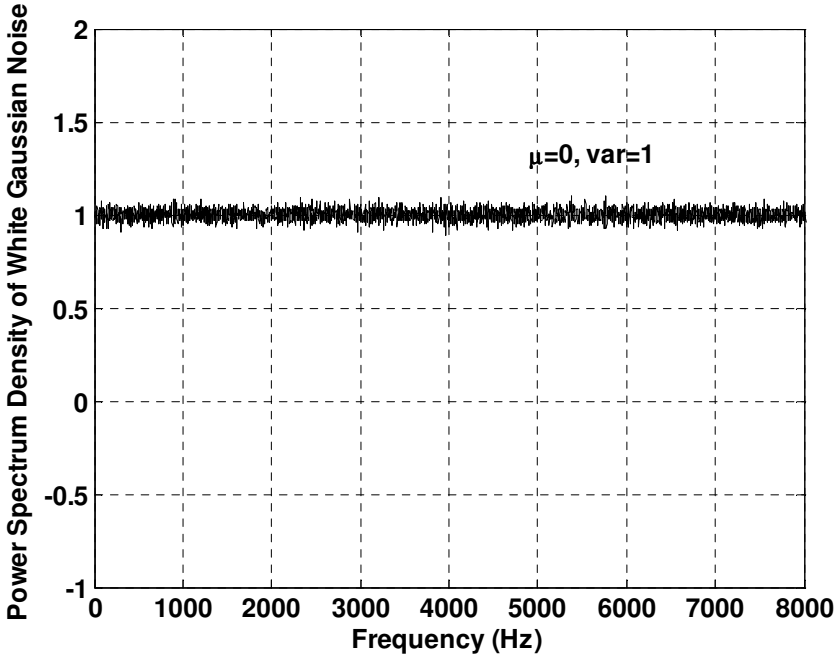

Figure A.8: PSD of Generated White Gaussian Noise (μ=0, σ^2=1)

Example 2 Evaluate the noise equivalent bandwidth for a first-order RC lowpass filter.

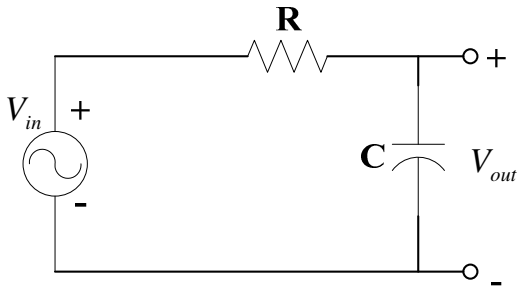

Figure A.9: Circuit Layout of a First-order RC Lowpass Filter

The circuit layout of a first–order RC lowpass filter is shown in Figure 18. Its transfer function is given as

$$H(f) = \frac{1}{\sqrt{1+\left(\frac{f}{B}\right)^2}} \tag{A.12}$$

where

$$B = \frac{1}{2\pi RC} \tag{A.13}$$

is the -3dB bandwidth [4]. The NEB is calculated with Equation (A.11) as

$$B_N = \int_0^\infty \frac{df}{1+(f/B)^2} = \frac{\pi}{2} B = \frac{1}{4RC} \tag{A.14}$$

Assuming the -3dB bandwidth B = 1k Hz, then from Equation (A.13) we have $B_N = \frac{1}{4} \cdot B \cdot 2\pi = \frac{\pi}{2} B \approx 1571\,\text{Hz}$. So for the first-order lowpass filter, B_N is about 50% greater than B. Now we will verify the result in Equation (A.14) with MATLAB and Simulink experiment.

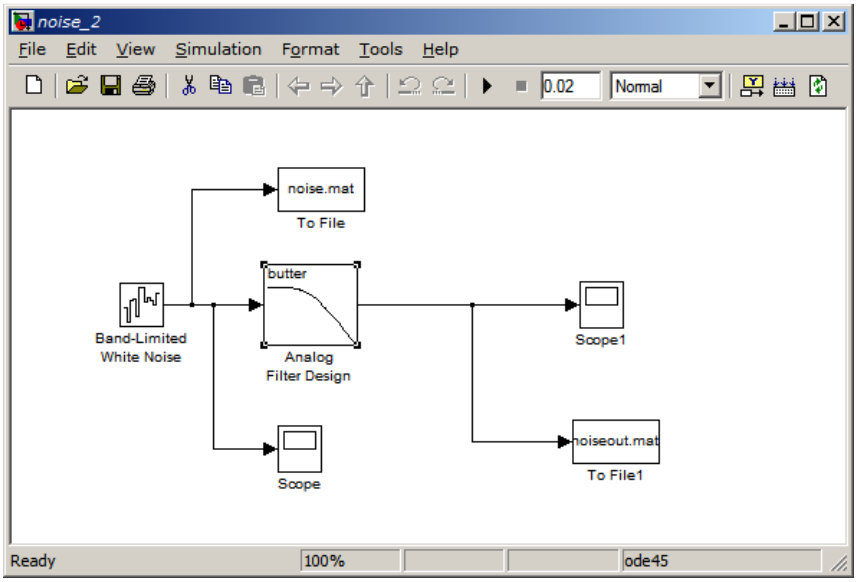

Figure A.10: White Gaussian Noise Passing through a 1st Order LPF – Simulink Layout

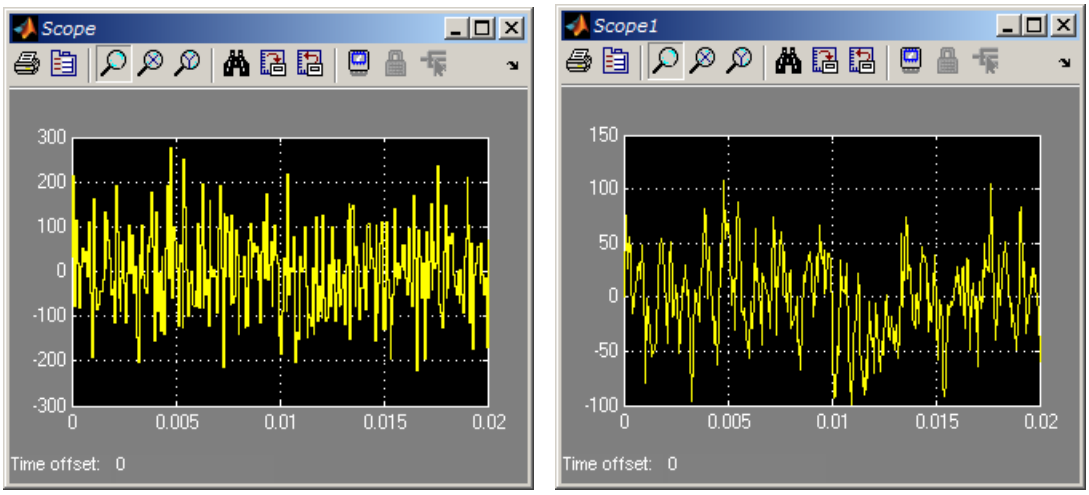

(a) (b)

Figure A.11: (a) Input Noise (b) Output Noise

The Simulink layout in Figure A.10 shows a white Gaussian noise passing through a first-order RC lowpass Butterworth filter. The input noise is connected to an oscilloscope for observation, as well as to a data sink for further computation in MATLAB. So is the output noise. The NEB of the lowpass filter will be calculated based on the powers of the input noise and output noise.

We use Simulink `Band-limited White Noise` block to generate the input noise. It is essentially a pseudo "white" noise because its bandwidth is not infinite. The data in the generated noise is obtained every t_c seconds, where

$$t_c \approx \frac{1}{100}\frac{2\pi}{f_{\max}} \tag{A.15}$$

In Equation (A.15), f_{max} is the maximum frequency of the system. For a lowpass system, f_{max} equals the -3dB bandwidth B. In our simulation, B = 1k Hz. We set t_c = 1/16000 seconds, which means the sampling frequency of the noise is 16k Hz and its bandwidth is B_{in}=8 kHz. We see that this noise has a bandwidth much wider than that of the lowpass system under investigation.

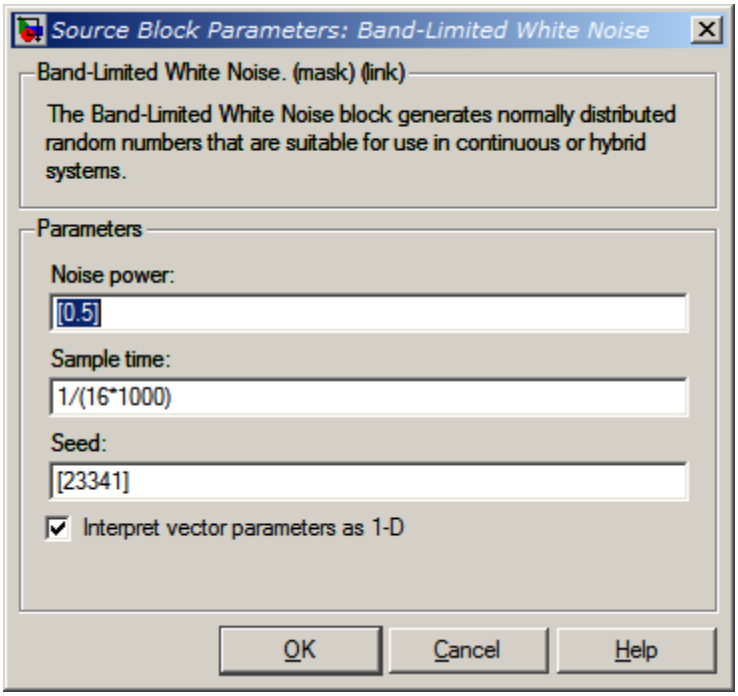

Figure A.12: Parameters Dialog Box

Due to the algorithm used in the block implementation, the Noise Power specified in the Parameters Dialog Box in Figure A.12 is actually the half height of the PSD of the generated noise within its bandwidth. To verify this, we feed the noise into an average-power meter (or a mean square voltage meter). The reading, which is the noise power P_{in}, equals 7.9989×10^{3}. Here B = 8k Hz. So $S_{in}(f) = \frac{P_{in}}{B} \approx 1$ within B.

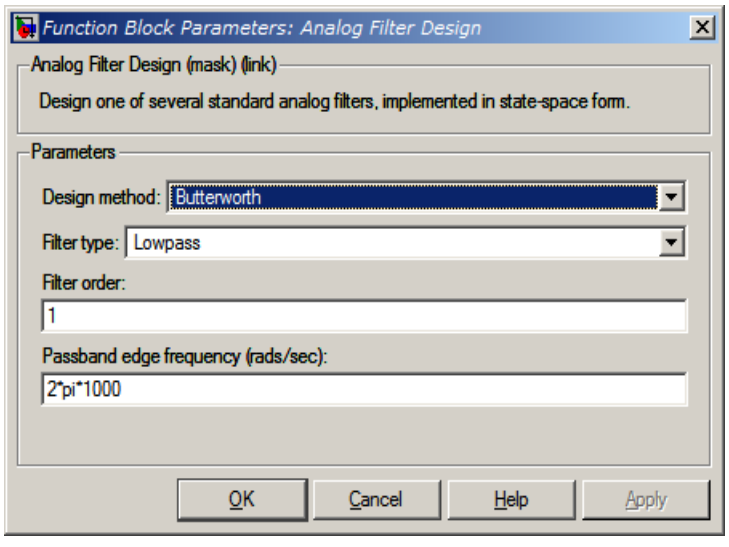

Figure A.13: Parameters Dialog Box

The lowpass filter is generated using the Simulink Analog Filter Design block. It is a first-order Butterworth filter with cutoff frequency f_{-3dB} =1k Hz. The amplitude response of its transfer function is shown in Figure A.14.

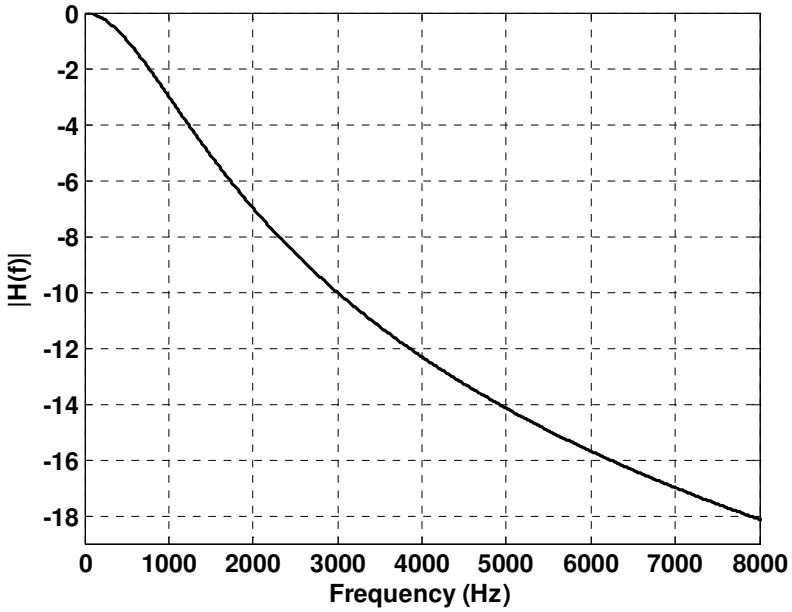

Figure A.14: First-order Lowpass Butterworth Filter Transfer Function – Amplitude Response

The white noise is passing through this filter and the PSD of the output noise is shown in Figure 24. Its shape follows the transfer function of the filter.

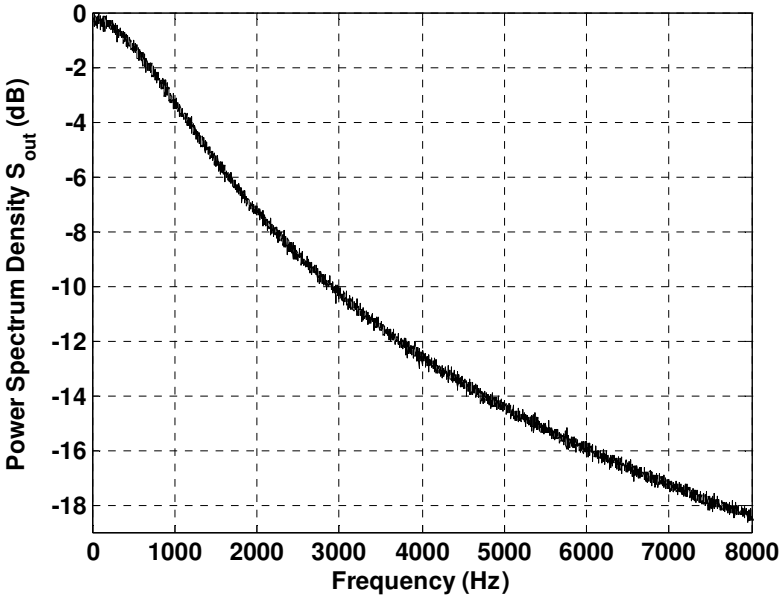

Figure A.15: PSD of Output Band-limited Noise (M=1, 1650 Snapshots)

The power of the output Band-limited noise is obtained by feeding the noise data to the mean square voltage meter. The meter reads P_{out} = 1.5369×10^3 W. From Equation (3.9), we obtain the NEB of the lowpass filter as $B_N = \frac{P_{out}}{S_{in}(f)} = 1.5369\times10^3$ Hz, which is close to the theoretical prediction 1571 Hz.

As the filter's order M becomes higher, B_N is getting closer to B. For example, as M = 5, B_N = 1008.4 Hz and as M = 7, B_N = 1001 Hz. Figure 25 and 26 show the transfer function (amplitude response) and the PSD of output noise when the lowpass filter order M = 5.

The inaccuracy of the measured NEB can be explained by the input "pseudo" white noise. Its bandwidth is 8 kHz instead of infinity. As seen from Figure 27, the PSD of the output Band-limited noise from the first-order lowpass filter has values greater than zero at the cutoff frequency 8 kHz and dies out slowly. If we truncate data beyond 8 kHz, we will lose data of the PSD and therefore the measured NEB is smaller than the predicted value. For the PSD from the 5th-order filter, its PSD is almost zero at 8 kHz. Truncating data beyond this frequency has very little impact on it. That's why a higher-order filter gives a more accurate NEB.

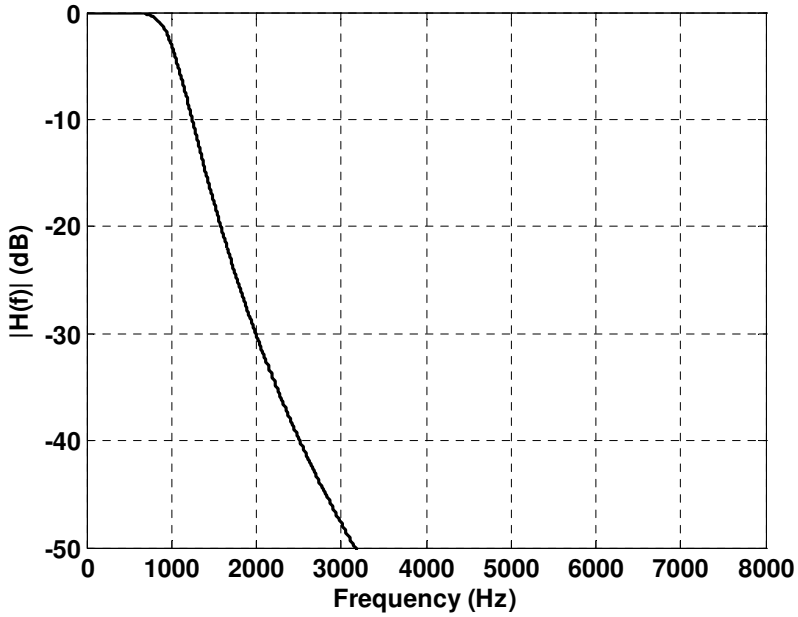

Figure A.16: Fifth-order Lowpass Butterworth Filter Transfer Function – Amplitude Response

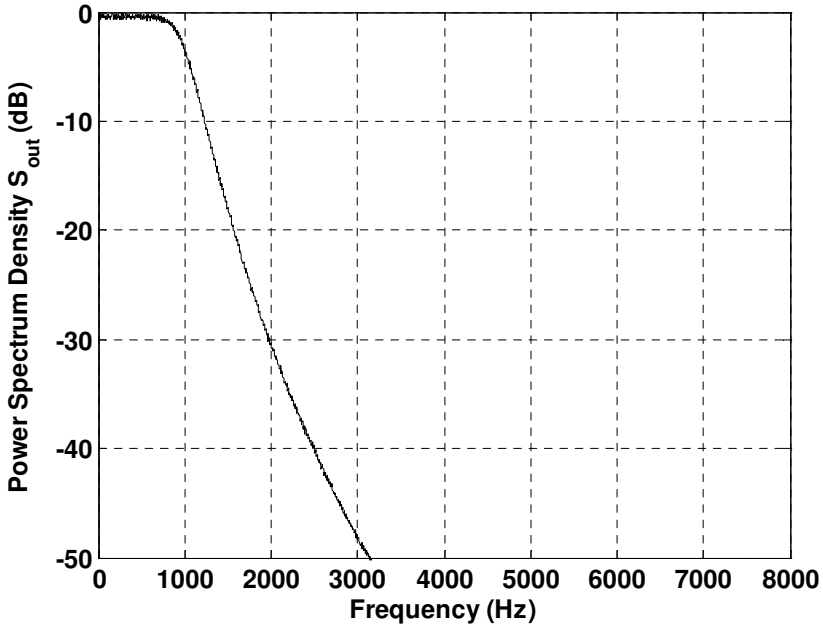

Figure A.17: PSD of Output Band-limited Noise (M=5, 1650 Snapshots)

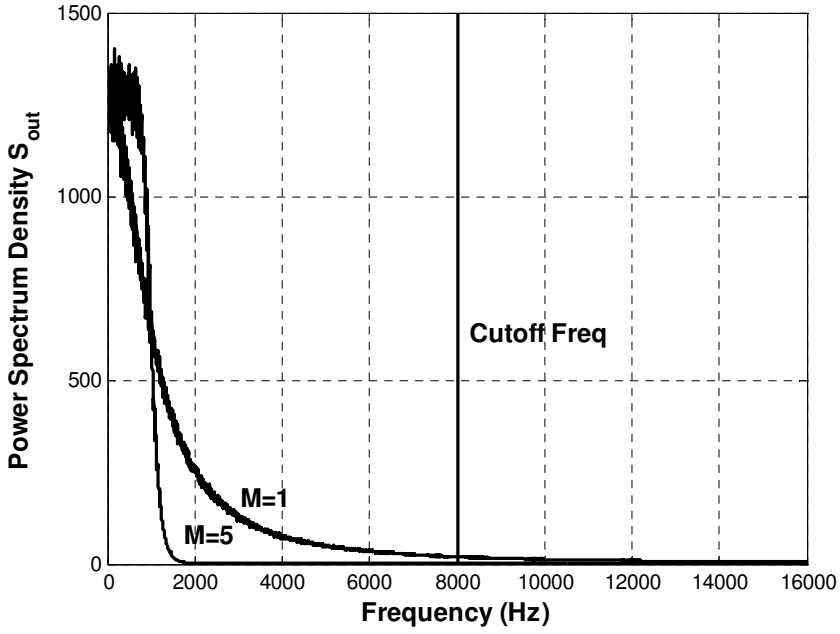

Figure A.18: PSD of Output Band-limited Noise

Theoretically, for an nth-order Butterworth LPF defined by

$$\left|H(f)\right| = \frac{1}{\sqrt{1+(f/B)^{2n}}}, \tag{A.16}$$

its NEB is related to the 3-dB bandwidth by

$$B_N = \frac{\pi B}{2n \sin\left(\frac{\pi}{2n}\right)}. \tag{A.17}$$

Hence, $B_N = \frac{\pi}{2} B$ as $n = 1$. When $n \to \infty$, $B_N \to B$.

Appendix B Ultrasonic Transmitter and Receiver Specifications

B.1 Kobitone 400ST16 Ultrasonic Transmitter Specifications

KOBITONE™ AUDIO COMPANY

Ultrasonic Transducers Date: 9/19/06

Dimensions: mm (In.)

Part Number:
255-400ST16-ROX
255-400SR16-ROX

Ultrasonic Transducers

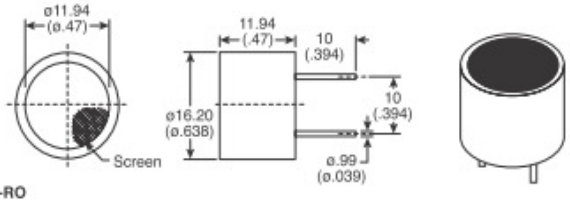

Directivity for 255-400ST160-RO

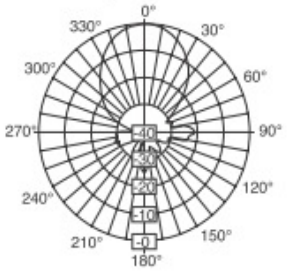

Sensitivity For 255-400SR16-ROX

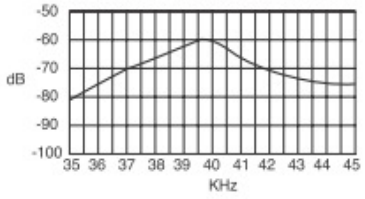

SPL Variation vs. Driving Voltage

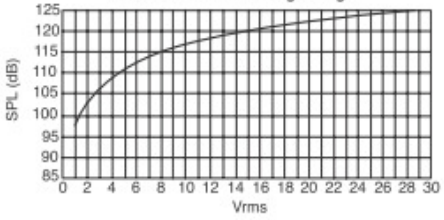

Sound Pressure for 255-400ST16-ROX

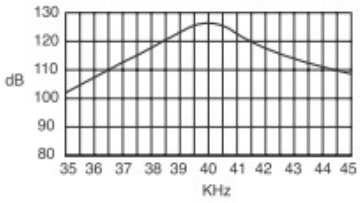

Sensitivity/Sound Pressure Level
Tested under 10Vrms @30cm

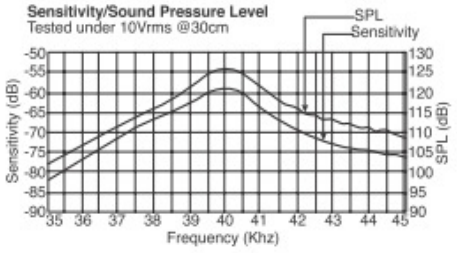

Impedance/Phase Angle vs. Frequency
Tested under 1Vrms Oscillation Level

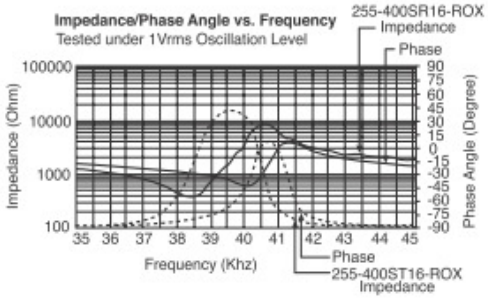

KT-400244

Electrical Specifications:
- Center Frequency (f_0): 40.0KHz±1.0KHz
- SPL @ f_0 for 255-400ST16-RO: 119dB (0dB re 0.0002μ bar)
- Sensitivity @ f_0 for 255-400SR16-ROX: -65dB (0dB=1V/μ bar)
- Bandwidth (-6dB): 255-400ST16-ROX - 2KHz; 255-400SR16-RO - 2.5KHz
- Allowable Input Power: 0.2W
- Capacitance: 2,400pF±20% @ 1KHz

Mechanical Specifications:
- Type: Transmitter - 255-400ST16-ROX; Receiver - 255-400SR16-ROX
- Operating Temperature: -30°C ~ +85°C
- Storage Temperature: -40°C ~ +100°C

Note:
- RoHS Compliant by Exemption

Available from Mouser Electronics www.mouser.com (800) 346-6873

Specifications are subject to change without notice. No liability or warranty implied by this information. Environmental compliance based on producer documentation.

B.2 Kobitone 400SR12 Ultrasonic Receiver Specifications

KOBITONE™ AUDIO COMPANY

Ultrasonic Transducers Date: 6/14/05

Dimensions: mm (In.)

Part Number:

255-400ST12 255-400SR12

Ultrasonic Transducers

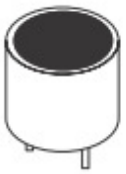

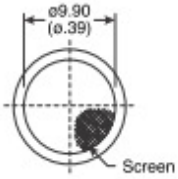

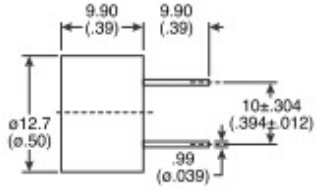

Directivity
(255-400ST12)

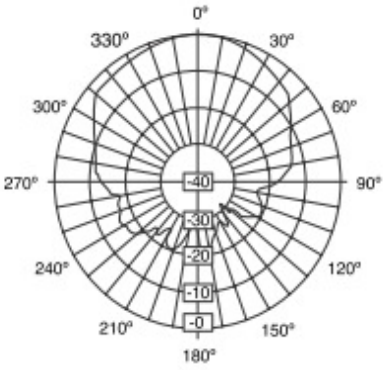

Sensitivity (255-400SR12)

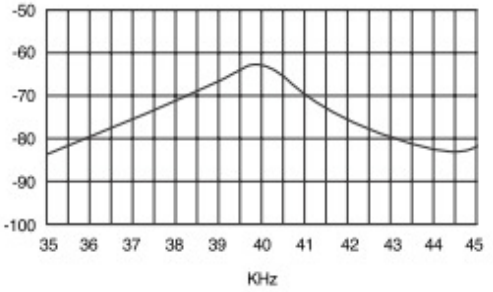

Sound Pressure (255-400ST12)

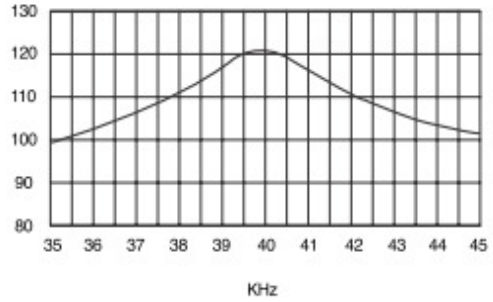

KT-400050

Electrical Specifications:

- Center frequency (f_0): 40.0KHz ± 1.0KHz
- SPL @ f_0: 255-400ST12 = 115dB (0dB re 0.0002 μ bar)
- Sensitivity @ f_0: 255-400SR12 = -67dB (0dB = 1V/μ bar)
- Driving voltage: 1V min., 20V max.
- Bandwidth (-6dB): 2KHz
- Allowable input power: .2W
- Capacitance @ 1KHz: 2,400pF ± 20%

Mechanical Specifications:

- Type: Transmitter: 255-400ST12
  Receiver: 255-400SR12
- Operating temperature: -30°C ~ +85°C
- Storage temperature: -40°C ~ +100°C

Available from Mouser Electronics www.mouser.com (800) 346-6873

Appendix C PHONIC Helix Board 12 Plus A/D Device Specifications

Inputs	
Total channels	6
Balanced Mono Mic/Line channel	4
Balanced Stereo Line Channel	2
AUX Return	2 Stereo
2T Input	Stereo RCA
Outputs	
Main L/R Stereo	2 x 1/4" TRS, Bal.
ALT 3-4	2 x 1/4" TRS, Bal.
Rec Out with trim control	Stereo RCA
CTRL RM L/R	2 x 1/4" TS
Phones	1
USB 2.0 Interface	10 in & 2 out, 24-bit / 96 kHz 8 in & 2 out, 24-bit / 192 kHz
Channel Strips	6
Insert Points	2
AUX Send	2
Pan/Balance Control	Yes
Volume Controls	Rotary
Master Section	
Stereo AUX Returns	2
Effects Return to Monitor	1
Control Room/Phones Level Control	Yes
Faders	Main L/R, 60mm fader
Metering	
Number of Channels	2
Segments	8
Phantom Power Supply	+48VDC
Switches	Master
Effect Processor	100 programs plus tap delay; foot switch (effect on/off, tap)
Frequency Response (Mic input to any output)	
20Hz ~ 60KHz	+0/-1 dB
20Hz ~ 100KHz	+0/-3 dB
Crosstalk (1KHz @ 0dBu, 20Hz to 20KHz bandwidth, channel in to main L/R outputs)	
Channel fader down, other channels at unity	<-90 dB
Noise (20Hz~20KHz; measured at main output, Channels 1-4 unit gain; EQ flat; all channels on main mix; channels 1/3 as far left as possible, channels 2/4 as far right as possible. Reference=+6dBu)	
Master @ unity, channel fader down	-86.5 dBu
Master @ unity, channel fader @ unity	-84 dBu
S/N ration, ref to +4	>90 dB

Microphone Preamp E.I.N. (150 ohms terminated, max gain)	<-129.5 dBm
THD (Any output, 1KHz @ +14dBu, 20Hz to 20KHz, channel inputs)	<0.005%
CMRR (1 KHz @ -60dBu, Gain at maximum)	80 dB
Maximum Level	
Mic preamp input	+10 dBu
All other input	+22 dBu
Balanced output	+28 dBu
Impedance	
Mic preamp input	2 K ohms
All other inputs (except insert)	10 K ohms
RCA 2T output	1.1 K ohms
Equalization	3-band, +/-15 dB
Low EQ	80 Hz
Mid EQ	2.5 KHz
Hi EQ	12 KHz
Low cut filter	75Hz (-18dB/oct)
Power Requirement (external power supply, depends on region)	100VAC, 120VAC, 220~240VAC, 50/60Hz
Physical	
Net Weight	2.9 kg (6.4 lbs)
Dimensions (WxHxD)	245.4 x 86 x 271.3 mm (9.7" x 3.4" x 10.7")

Figure C.1: Phonic Helix Board 12 Plus USB 2.0 12-Channel Mixer

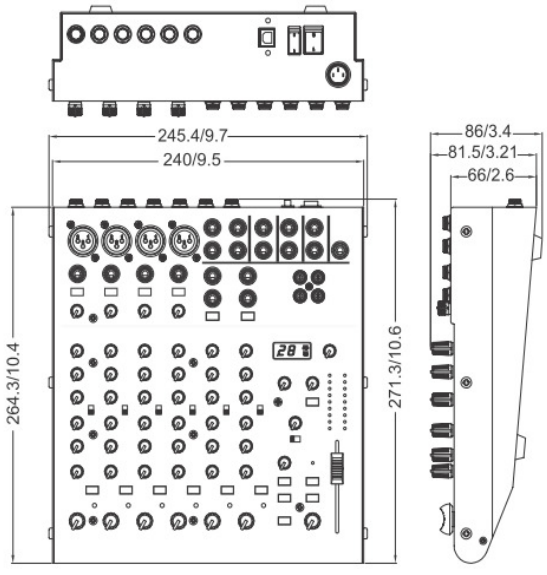

Figure C.2: Dimensions (measurement are shown in mm/inches)